

AD-A242 450



2

# NAVAL POSTGRADUATE SCHOOL

## Monterey, California



DTIC  
ELECTE  
NOV 14 1991  
S B D

# THESIS

PROFILE SAMPLING DEPENDENCE  
OF THE  
MLAYER PROGRAM

by

Chang Ting-Hsun

March 1991

Thesis Advisor:

Hung-Mou Lee

Approved for public release; distribution is unlimited

91-15193

REPORT DOCUMENTATION PAGE				Form Approved OMB No. 0704-0188	
1a. REPORT SECURITY CLASSIFICATION <b>UNCLASSIFIED</b>			1b. RESTRICTIVE MARKINGS		
2a. SECURITY CLASSIFICATION AUTHORITY <b>UNCLASSIFIED</b>			3. DISTRIBUTION/AVAILABILITY OF REPORT Approved for public release; distribution is unlimited		
2b. DECLASSIFICATION/DOWNGRADING SCHEDULE					
4. PERFORMING ORGANIZATION REPORT NUMBER(S)			5. MONITORING ORGANIZATION REPORT NUMBER(S)		
6a. NAME OF PERFORMING ORGANIZATION Naval Postgraduate School		6b. OFFICE SYMBOL (If applicable) EC	7a. NAME OF MONITORING ORGANIZATION Naval Postgraduate School		
6c. ADDRESS (City, State, and ZIP Code) Monterey, CA 93943-5000			7b. ADDRESS (City, State, and ZIP Code) Monterey, CA 93943-5000		
8a. NAME OF FUNDING/SPONSORING ORGANIZATION		8b. OFFICE SYMBOL (If applicable)	9. PROCUREMENT INSTRUMENT IDENTIFICATION NUMBER		
8c. ADDRESS (City, State, and ZIP Code)			10. SOURCE OF FUNDING NUMBERS		
			PROGRAM ELEMENT NO.	PROJECT NO.	TASK NO.
					WORK UNIT ACCESSION NO.
11. TITLE (Include Security Classification) PROFILE SAMPLING DEPENDENCE OF THE MLAYER PROGRAM					
12. PERSONAL AUTHOR(S) CHANG Ting-Hsun					
13a. TYPE OF REPORT Master's Thesis		13b. TIME COVERED FROM _____ TO _____		14. DATE OF REPORT (Year, Month, Day) 1991 March	
15. PAGE COUNT 99					
16. SUPPLEMENTARY NOTATION The views expressed in this thesis are those of the author and do not reflect the official policy or position of the Department of Defense or the US Government.					
17. COSATI CODES			18. SUBJECT TERMS (Continue on reverse if necessary and identify by block number)		
FIELD	GROUP	SUB-GROUP	Evaporation duct propagation		
19. ABSTRACT (Continue on reverse if necessary and identify by block number) The dependence of the predictions of the MLAYER program on the set of heights at which the refractive index value are sampled from a fixed reference profile are analyzed. A refractivity profile with a four-meter evaporation duct is adopted as a reference. Two variable piecewise linear profiles of four and five segments, respectively, are used to approximate the reference profile for MLAYER computations. The sensitivities of the waveguide mode location, the range attenuation rate, and the height-gain function to the changes of the piecewise linear profiles are investigated at the frequencies 3, 6, 10, and 15 GHz. The frequency dependence of the dominant mode for one profile is also studied to investigate the fact that the sensitivity to changes in sampling point location is lower at 6 GHz than at other frequencies. A general rule-of-thumb for the change in range attenuation rate due to a slight change in refractivity is suggested.					
20. DISTRIBUTION/AVAILABILITY OF ABSTRACT <input checked="" type="checkbox"/> UNCLASSIFIED/UNLIMITED <input type="checkbox"/> SAME AS RPT <input type="checkbox"/> DTIC USERS			21. ABSTRACT SECURITY CLASSIFICATION <b>UNCLASSIFIED</b>		
22a. NAME OF RESPONSIBLE INDIVIDUAL LEE, Hung-Mou			22b. TELEPHONE (Include Area Code) 408-646-2846		22c. OFFICE SYMBOL EC/Lh

Approved for public release; distribution is unlimited.

Profile Sampling Dependence  
of the  
MLAYER Program

by

Chang Ting-Hsun  
Lieutenant, Taiwan Navy  
B.S., Chinese Naval Academy, 1984

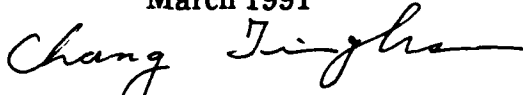
Submitted in partial fulfillment  
of the requirements for the degree of

MASTER OF SCIENCE IN ELECTRICAL ENGINEERING

from the

NAVAL POSTGRADUATE SCHOOL  
March 1991

Author:



Chang Ting-Hsun

Approved by:



Hung-Mou Lee, Thesis Advisor



R. Clark Robertson, Second Reader



Michael A. Morgan, Chairman

Department of Electrical and Computer Engineering

## ABSTRACT

The dependence of the predictions of the MLAYER program on the set of heights at which the refractive index value are sampled from a fixed reference profile are analyzed. A refractivity profile with a four-meter evaporation duct is adopted as a reference. Two variable piecewise linear profiles of four and five segments, respectively, are used to approximate the reference profile for MLAYER computations. The sensitivities of the waveguide mode location, the range attenuation rate, and the height-gain function to the changes of the piecewise linear profiles are investigated at the frequencies 3, 6, 10, and 15 GHz. The frequency dependence of the dominant mode for one profile is also studied to investigate the fact that the sensitivity to changes in sampling point location is lower at 6 GHz than at other frequencies. A general rule-of-thumb for the change in range attenuation rate due to a slight change in refractivity is suggested.

Accession For	
NTIS GRA&I	<input checked="checked" type="checkbox"/>
DTIC TAB	<input type="checkbox"/>
Unannounced	<input type="checkbox"/>
Justification	
By	
Distribution/	
Availability Codes	
Dist	Avail and/or Special
A-1	

## TABLE OF CONTENTS

I.	INTRODUCTION .....	1
A.	BACKGROUND .....	1
B.	MLAYER PROGRAM OVERVIEW .....	4
C.	OBJECTIVE .....	8
D.	APPROACH .....	10
II.	PROFILE SAMPLING DEPENDENCE .....	14
A.	INTRODUCTION .....	14
B.	FOUR-LINEAR-SEGMENT APPROXIMATION .....	17
1.	15 GHz .....	17
a.	Path Loss Analysis .....	19
(1)	Class One .....	19
(2)	Class Two .....	19
(3)	Discussion .....	24
b.	Attenuation Rate Analysis .....	25
c.	Mode Location Analysis .....	25
2.	10 GHz .....	28
a.	Path Loss Analysis .....	28

(1) Class One .....	28
(2) Class Two .....	28
(3) Discussion .....	33
b. Attenuation Rate Analysis .....	34
c. Mode Location Analysis .....	34
3. 6 GHz .....	37
a. Path Loss Analysis .....	37
(1) Class One .....	37
(2) Class Two .....	37
(3) Discussion .....	40
b. Attenuation Rate Analysis .....	40
c. Mode Location Analysis .....	42
4. 3 GHz .....	44
a. Path Loss Analysis .....	44
(1) Class One .....	44
(2) Class Two .....	44
(3) Discussion .....	44
b. Attenuation Rate Analysis .....	47
c. Mode Location Analysis .....	47
C. FIVE-LINEAR-SEGMENT APPROXIMATION .....	50
1. 15 GHz .....	50
a. Path Loss Analysis .....	50

(1) Class One .....	50
(2) Class Two .....	52
(3) Discussion .....	57
b. Attenuation Rate Analysis .....	57
c. Mode Location Analysis .....	59
2. 10 GHz .....	61
a. Path Loss Analysis .....	61
(1) Class One .....	61
(2) Class Two .....	61
(3) Discussion .....	61
b. Attenuation Rate Analysis .....	66
c. Mode Location Analysis .....	68
3. 6 GHz .....	70
a. Path Loss Analysis .....	70
(1) Class One .....	70
(2) Class Two .....	70
(3) Discussion .....	70
b. Attenuation Rate Analysis .....	73
c. Mode Location Analysis .....	73
4. 3 GHz .....	76
a. Path Loss Analysis .....	76
(1) Class One .....	76

(2) Class Two .....	79
(3) Discussion .....	79
b. Attenuation Rate Analysis .....	79
c. Mode Location Analysis .....	81
III. DISCUSSIONS AND SUGGESTIONS .....	83
A. FREQUENCY DEPENDENCE .....	83
B. REFRACTIVITY DEPENDENCE .....	85
C. ROOT-FINDING .....	87
LIST OF REFERENCES .....	88
INITIAL DISTRIBUTION LIST .....	90



## I. INTRODUCTION

### A. BACKGROUND

The atmosphere of the earth is a mixture of many gases together with suspended particles of liquids and solids which significantly affect electromagnetic wave propagation. The two regions of the atmosphere that are of importance for their effects on the propagation of radio waves are the troposphere and the ionosphere. The troposphere is the non-ionized region extending from the surface of the earth up to about 15 km. The complex nature of this medium affects the propagation of electromagnetic waves in many ways such as the bending of the waves due to changes in the refractive index under various climatic conditions and the absorption and scattering of the waves by the gases of the atmosphere. At most radar frequencies, the troposphere is by far the most important region affecting electromagnetic propagation and is of interest in this thesis.

Weather conditions can result in the attenuation of radio wave transmissions through the absorption or scattering of energy by gases or rain. Under certain meteorological conditions, an enhancement in field strength may be realized at large distances from the source. This enhancement in field strength is caused by an unusually significant bending of the direction of wave propagation due to the inversion of the modified refractive index profile (*M*-profile). This bending results in the trapping of electromagnetic energy within the inversion region which is known

as a duct or a tropospheric waveguide. The radio wave is confined to this region, with a fraction of its energy leaking out of the duct whenever the wave is reflected back in from the boundary of the inversion layer.

There are three types of ducts: surface-based, elevated, and evaporation. The third type, which has a typical height below 40 m, is called the evaporation duct because it is formed adjacent to the sea surface where rapid humidity decrease occurs due to evaporation. It is usually very thin compared to the other two types of ducts and has its base at the surface of the water. This duct almost always occurs, to some degree, over the ocean and is of particular importance for over-the-horizon radar coverage. The evaporation duct height is defined as the height of the minimum value of the  $M$ -profile. Electromagnetic wave trapping may occur below this height. The higher the duct is, the stronger the propagation in the duct becomes. The modified refractivity is denoted as  $M$  in this thesis. More detailed discussions about this quantity are given later in this section.

A FORTRAN program MLAYER is available for studying propagation in the troposphere with a spherically stratified refractive index profile. This program, originally developed by Naval Ocean Systems Center (NOSC), was recently reviewed and documented [REF. 1] by NPS and is being investigated for improvement. In the mathematical formulation of MLAYER, the earth-flattening approximation using the concept of modified index of refraction of the atmosphere is adopted. In a uniform atmosphere with constant index of refraction, electromagnetic waves travel in straight lines, or rays, over the curved surface of the earth. The earth can be considered as

flat and the rays as curved if the relative curvatures between the earth and the rays are preserved. The modified index of refraction is then given by:

$$m(z) = n + \frac{z}{a}, \quad (1)$$

where  $n$  is the index of refraction,  $z$  is the height above the surface of the earth, and  $a$  is the radius of the earth. In Eq. (1),  $n$  is replaced with  $n(z)$  because in a stratified atmosphere the properties of the atmosphere vary only with height. In this case, the equation for modified index of refraction is given by:

$$m(z) = n(z) + \frac{z}{a}. \quad (2)$$

With the earth-flattening approximation, electromagnetic wave propagation over a spherical earth can be reduced to that of wave propagation over a flat earth if the index of refraction is replaced with the modified index of refraction. The accuracy of this approximation was investigated by Pekeris [Ref. 2]. For the standard atmosphere, the fractional error in the height-gain function which provides the height variation of the electric fields [Ref. 1] is approximately:

$$\Delta = 2 \pi \frac{\sqrt{6}}{5} \frac{z^{5/2}}{\lambda a^{3/2}}. \quad (3)$$

As can be seen from Eq. (3), the accuracy of the earth-flattening approximation depends upon the frequency of the electromagnetic wave and the height above the surface of the earth at which the signal is measured. This approximation breaks down as the frequency and the height above the surface of the earth increase. The

work of Pekeris also indicates that this approximation is valid to within two percent for ranges up to about one half of the radius of the earth [Ref. 2].

Since the modified index of refraction of the atmosphere is very close to one, with the difference on the order of  $10^{-3}$ , it is convenient to introduce the modified refractivity for the mathematical formulation of tropospheric ducts. In this thesis the modified refractivity, written as  $M$ , is defined by:

$$M(z) = [m(z) - 1] \times 10^6. \quad (4)$$

## B. MLAYER PROGRAM OVERVIEW

MLAYER was developed by the NOSC. It approximates the refractive index with a continuous, piecewise linear profile and computes the propagation of electromagnetic waves in each layer. It was originally developed by Baumgartner under the name XWVG [Ref. 3] and then by Pappert [Ref. 4]. Many changes were introduced over the years. Up-to-date documentation was completed by Yeoh in 1990 [Ref. 1].

MLAYER calculates the signal level of over-the-horizon propagation under the tropospheric environment over seawater by locating all waveguide modes having an attenuation rate below a specified value. Like XWVG, the program by Baumgartner, MLAYER uses the complex root-finding program developed by Shellman and Morfitt to find the waveguide modes in which waves can propagate in the tropospheric duct. This root-finding program is discussed later in this section. XWVG utilizes three linear segments to model the  $M$ -profile of the troposphere. In

MLAYER, the number of piecewise linear segments for approximating the  $M$ -profile is variable. Each linear segment is defined by the values of the  $M$ -profile at its end points and is considered a layer of the troposphere. With  $M_i(z)$ , the  $M$ -value in the  $i$ -th layer, the  $M$ -profile in this layer is given by:

$$M_i(z) = M(z_i) + \frac{dM_i}{dz}(z - z_i), \text{ for } z_i \leq z \leq z_{i+1}. \quad (5)$$

MLAYER has one main program, twenty-six subroutine subprograms, four function subprograms, and six supporting programs. Main, the controlling program in MLAYER, calls appropriate subroutines to find the modes, to sum up individual mode contributions, to calculate path loss, and to locate the radar horizon. The main program also calls the subroutine 'wvgstdin' to read data from an input file and to open three output files. MLAYER also incorporates the effects of surface roughness, atmospheric absorption, and the complex index of refraction of seawater as a function of frequency, salinity, and temperature. Overflow problems commonly encountered in the evaluation of the modal functions are avoided by performing numerical computations with extended complex arithmetic.

In MLAYER the cylindrical coordinate system  $(r, \phi, z)$  is utilized and both horizontally and vertically polarized sources can be selected. Since the  $M$ -profile of the troposphere is approximated with layers of linear  $M$ -profile, the altitude dependence of the fields can be given in terms of Airy functions. Thus, for the  $i$ -th layer, the field is described as a linear combination of Airy functions of two different types with the coefficients  $A_i$  and  $B_i$ , respectively. From the boundary conditions of

each layer, a system of linear equations can be formed which is used to solve for the coefficients  $A_i$  and  $B_i$ . This system of linear equations is written in matrix notation. Setting the determinant of this matrix to zero leads to the modal equation. The propagation constants which correspond to the solutions of the modal equation determine the waveguide modes in which electromagnetic waves are trapped in the multilayer tropospheric environment. These zeroes in the MLAYER program are called eigenvalues.

The zeroes of the modal equation are located by the Shellman-Morfitt root-finding program. This program initially sets up a search rectangle on the complex wave-number plane according the 'aloss' variable and some other preset parameters of the program. 'Aloss' is the maximum attenuation in dB/km of modes to be found. The root-finding routine follows the same phase line to locate all zeroes in this rectangle. It then sets up a neighboring search rectangle and repeats the process. The program follows the same procedures until the number of zeroes located are greater than the maximum number of zeroes requested in the MLAYER program or until all search rectangles have been covered.

As is usually encountered in the evaluation of the radiated fields, a contour integral in the complex wave number plane has to be evaluated. This integral can be broken into two parts: a branch cut integral which represents the reflected and the surface waves, and the sum of residues of the poles located at the zeroes of the modal equations which represents the trapped propagation in the tropospheric waveguide. In MLAYER, only contributions from the waveguide modes are retained

since the reflected ray and the surface waves are insignificant in over-the-horizon situations. Therefore, the results of MLAYER applies only in the diffraction region.

The quantities associated with the analysis are introduced in the rest of this section. The radiation of a horizontally polarized source is of interest. This source is approximated as a radiating magnetic dipole which is oriented in the  $z$  direction and located at  $r=0$  and  $z=z_T$ . Relative to the broadside field strength in free-space, the coherent mode sum of the electric field,  $ECMS$ , is given in decibels by [Ref. 1]:

$$ECMS = 10 \log \left| \frac{E_\phi}{E_{\phi FS}} \right|^2, \quad (6)$$

$$= 10 \log \left( \frac{2\pi r^2}{k^2 a \sin(\frac{r}{a})} \left| \sum_m \rho_m^{1/2} g_m(z) g_m(z_T) e^{-j\rho_m r} \right|^2 \right),$$

where  $k$  is the wave number,  $a$  is the radius of the earth,  $r$  is the range in km between transmitter and receiver,  $\rho_m$  is the guide wavenumber of the  $m$ -th waveguide mode,  $z$  is the height where the field is measured,  $z_T$  is the height at which the transmitter is located, and  $g_m(z)$  is the normalized height-gain function.

The coherent path loss is the field strength, relative to that in free space, for a receiver which is located at a certain range and height. It is given in decibels by [Ref. 1]:

$$Coherent \ path \ loss = 32.45 + 20 \log r + 20 \log f - ECMS, \quad (7)$$

where  $r$  is the range in km and  $f$  is the frequency in MHz.

The guide wavenumber along the radial direction,  $k\beta$ , is given by [Ref. 1]:

$$\beta = \frac{\rho}{k}, \quad (8)$$

$$= \left( m^2(z_1) - q_{11} \left( \frac{\alpha_1}{k} \right)^{\frac{2}{3}} \right)^{1/2},$$

where  $q_{11}$  is a zero of the modal equation found using the root-finding program and  $k$  is the free space wavenumber. The quantity  $\beta-1$  is used in this thesis for presenting the locations of the modes of propagation.

The range attenuation rate of each mode, in dB/km, is an indicator of the strength of the waveguide mode. It is given as [Ref. 1]:

$$\text{Attenuation rate} = -20 \log_{10}(e) k \operatorname{Im}[\beta] \times 10^{-3}. \quad (9)$$

In this thesis only the range attenuation rate is of interest. Therefore, the range attenuation rate from this point on is referred to simply as the attenuation rate.

### C. OBJECTIVE

MLAYER is a useful research tool for conducting case studies of propagation effects over a wide range of frequencies. It is the program from which faster but less accurate programs, IREPS [Ref. 5] and EREPS [Ref. 6], are constructed. In this thesis, the sensitivity of MLAYER in relation to the piecewise linear approximation of the evaporation duct  $M$ -profile is analyzed. The particular evaporation duct profile adopted for the analysis is discussed in the following section.



The evaporation duct is usually the dominant propagation mechanism for waves reaching the diffraction region. To determine the characteristics of a duct, the  $M$ -profile must be determined. The  $M$ -value at the absolute temperature,  $T$ , and pressure,  $p$ , is given by [Ref. 7]:

$$M = \frac{A}{T} \left( p + B \frac{e}{T} \right) + \frac{z}{a} \times 10^6, \quad (10)$$

where  $e$  is the partial pressure of the water vapor,  $A = 79^\circ \text{K/mb}$ , and  $B = 4800^\circ \text{K}$ .

The  $M$ -value depends on humidity more critically than on temperature.

The best instrument for measuring  $M$  in the atmosphere is a microwave refractometer. It must be carried on an aircraft or a balloon for vertical profiling and is relatively costly and complex. The most commonly used instrument is the radiosonde. It measures temperature and humidity as a function of pressure. The  $M$ -profile can be deduced from those values using Eq. (10).

Since MLAYER uses piecewise linear segments to approximate the atmospheric  $M$ -profile, it is interesting to examine the best way to carry out this approximation. In practice, if the  $M$ -profile is known to be approximately based on environmental parameters such as the air-sea temperature difference, it would be desirable to take radiosonde data at the particular heights which will provide the best approximate  $M$ -profile. Furthermore, increasing the number of linear segments models the  $M$ -profile more accurately, but this results in a longer MLAYER execution time. The objective of this thesis is to study how to reduce the number of sampling points on the actual

*M*-profile while retaining the accuracy of the program. As a result of this investigation, the variations of the attenuation rates and the locations of the waveguide modes as a function of the propagation frequency have been found. Modifications to the program such as changing the order to select the zeroes in the root-finding program are also suggested.

#### D. APPROACH

In the MLAYER program, the source is assumed to be horizontally polarized and located at a height of 25 m. The *M*-profile is set to zero on the sea surface. Sea-water temperature and salinity are set at 15 degree Celsius and 35 gram/kg, respectively. The roughness height of the sea surface is set to 0.25 m. The atmospheric absorption in dB/km at each layer boundary is set to zero. The evaporation duct profile utilized for the sensitivity analysis of this thesis is discussed in the following paragraph.

A four-meter high evaporation duct is adopted in this thesis to analyze the propagation problem. It is defined as:

$$M(z) = 0.197 - 0.796 \ln(z + 0.0488) - 2.4044, \quad (11)$$

*for*  $0 \leq z \leq 10$ ,

$$M(z) = 0.118 z - 3.451, \text{ for } z \geq 10, \quad (12)$$

$$\lim_{z \rightarrow 10^-} \frac{d M(z)}{d z} = \lim_{z \rightarrow 10^-} \frac{d M(z)}{d z} = 0.118 , \quad (13)$$

$$\lim_{z \rightarrow 4} \frac{d M(z)}{d z} = 0 . \quad (14)$$

This  $M$ -profile assumes a constant standard gradient, 0.118, above 10 m. This number is equivalent to a four-thirds effective earth radius; i.e., the  $M$ -profile above 10 m is defined to be the standard atmosphere. Below 10 m, the refractive index profile follows the wind-speed variation which is logarithmic. This  $M$ -profile is called the reference  $M$ -profile in this thesis and is shown in Figs. 1 and 2. In Fig. 2, the linear portion above 10 m is not plotted so that the variation below 10 m can be examined. Since this thesis focuses only on the evaporation duct, the evaporation duct will subsequently be referred to simply as 'the duct'. To investigate the propagation problem utilizing MLAYER, the reference  $M$ -profile is approximated with either four or five continuous piecewise linear segments. These two approximate  $M$ -profiles are designated as the 4-L-S and the 5-L-S, respectively.

In Chapter II, the effects of approximating the reference  $M$ -profile using the 4-L-S and the 5-L-S are investigated, respectively. To specify the 4-L-S case, a set of five endpoints which consist of four fixed points and one test point are needed. The 5-L-S case utilizes six endpoints composed of five fixed points and one test point. To investigate the effects of the different approximations, the test point is varied in two

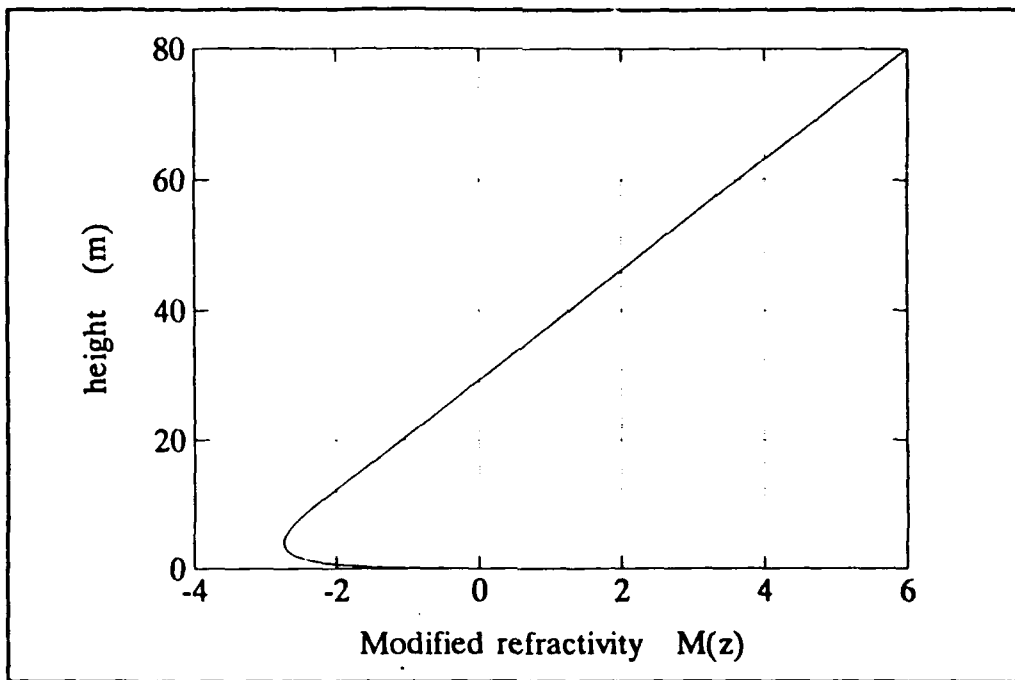


**Figure 1.** Evaporation duct profile.

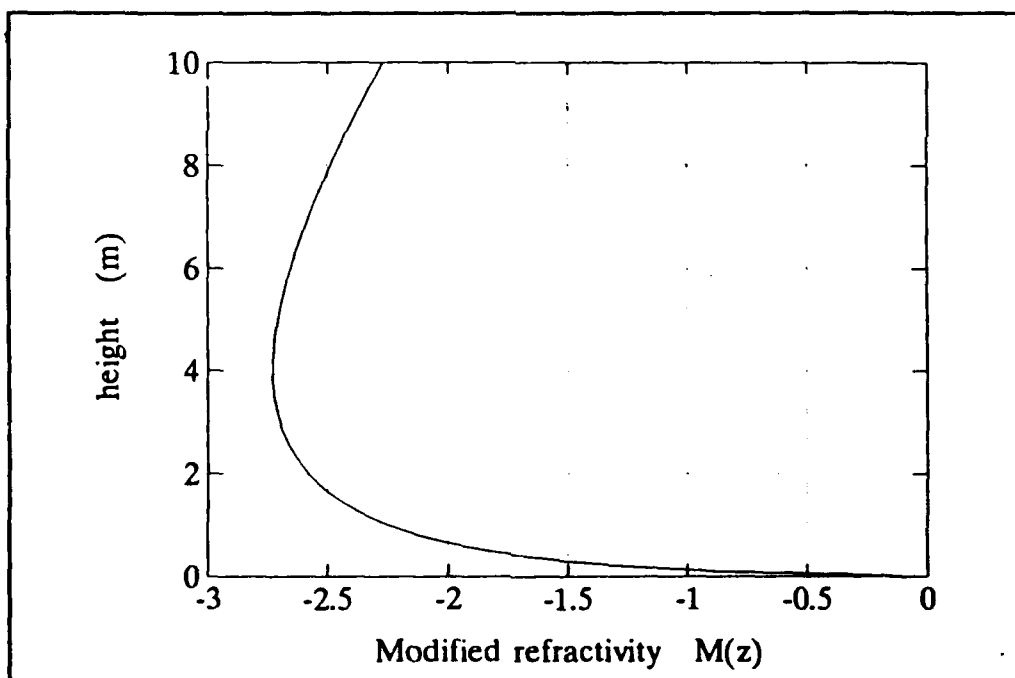


**Figure 2.** Evaporation duct profile, below 4 meter height.

ranges of height on the reference  $M$ -profile: below 4 m, the duct height, or between 4 m and 10 m. At each sampling height, the  $M$ -value on the reference profile is used.

To investigate the effects of different approximate  $M$ -profiles on propagation, three items are computed: path loss, attenuation rate, and the location of each mode. The modes are found with the maximum admissible attenuation rate set at 5 dB/km and plotted on the  $\beta$ -1 complex plane. Since  $\beta$  deviates only slightly from 1,  $\beta$ -1 is utilized for the examination of the variation of mode locations.

In Chapter III, the variation of attenuation rate of each mode with propagation frequency is discussed. The approximate  $M$ -profile used is the 4-L-S with the test point fixed on the reference  $M$ -profile at a height of 0.5 m. The propagation frequency is varied from 1 GHz to 25 GHz. The modes are found with the maximum admissible attenuation rate set at 5 dB/km. The zero-selection priorities in the root-finding program are also discussed.

## II. PROFILE SAMPLING DEPENDENCE

### A. INTRODUCTION

In this chapter, the reference  $M$ -profile of a duct of four meters height, given by Eqs. (11) through (14), is employed to analyze the propagation effects predicted by MLAYER. The reference  $M$ -profile is approximated with either four or five continuous piecewise linear segments, denoted as the cases 4-L-S and 5-L-S, respectively.

Four fixed points and one test point are employed to form the 4-L-S. Five fixed points and one test point are used for the 5-L-S. In both cases, the test point can be selected from between sea surface and 3.5 m and between 4.5 m and 10 m. No test point is sampled between 3.5 m and 4.5 m, because within this region the  $M$ -values are so close to the minimum that the program will not complete the computation due to floating-point error. No test point is selected between 10 m and 80 m, because the profile is a straight line above 10 m.

In Sections B and C of this chapter, the effects of varying the test points are discussed. Effects discussed include changes in the path loss, the modal attenuation rate, and the mode location. Four propagation frequencies are utilized in the analysis: 3 GHz, 6 GHz, 10 GHz, and 15 GHz.

Investigation in this thesis shows that for both the 4-L-S and the 5-L-S approximate  $M$ -profiles, a single mode dominates the propagation at the four

frequencies considered. Only this mode contributes significantly to the field strength at the ranges of interest. It is called the dominant mode in this thesis.

For single mode propagation, the coherent mode sum, defined by Eq. (6), reduces to a single term. The path loss, given by Eq. (7), is also determined by the dominant mode only. Thus, the modal attenuation with range is a single exponent given by Eq. (6) as  $e^{j\rho_m r}$ . The attenuation rate is the imaginary part of  $\rho_m$ . At a fixed range, the path loss with height is proportional to the height-gain function,  $g_m$ .

The path loss in dB is calculated for a receiver at ranges of 60 km and 120 km from the transmitter and at heights varying from 1 m to 35 m at 0.1 m increments. As the propagation is single mode, the path loss curves for these two ranges are similar. Results obtained for receiver range of 60 km and 120 km are presented, and a detailed discussion of the 60 km range results is given.

For the 4-L-S and the 5-L-S approximate  $M$ -profiles, the effect on path losses as a result of varying the test point is examined for two classes; *class one* refers to the cases when the test point lies within the duct, and *class two* refers to the cases when the test point lies above the duct. Hence, for *class one* the height of the test point is smaller than the duct height of 4 m, while the *class two* test point height is greater than the duct height.

A difference in dB values of two path losses is called the path loss ratio. When it is calculated by subtracting the path loss computed using a lower test point from that using a higher one, the path loss ratio gives an indication of the sensitivity of the height-gain function as a result of varying the test point from the lower to the higher

height. The larger the magnitude of the path loss ratio over a change in unit height, the greater is the sensitivity.

In MLAYER, the zero with the smallest real part is used to determine the waveguide mode first. Therefore, in this thesis, the modes are listed by the size of the real part and are in the same order that the program finds them.

The modal attenuation rate as a function of sampling height of the test point is obtained. The scale used for the sampling height is linear for one set of plots and logarithmic for the other set. The logarithmic scale allows the change in the attenuation rate for test points below 1 m to be easily read. From these figures, the effect of different approximate *M*-profiles with varying test points on the field strength in the radial direction can be visualized. The modal attenuation rate depends on the duct *M*-profile only. It does not vary with the heights and ranges of the transmitter and receiver.

For each frequency considered, the mode locations on the  $\beta$ -1 complex plane at different sampling heights of the test points are plotted. Since the propagation is single mode, the location of the dominant mode which has the least negative imaginary part of all modes found is important for the field strength. This is plotted in a separate figure. From these figures, the effect of varying test point height on each mode location and on the field strength can be determined.



## B. FOUR-LINEAR-SEGMENT APPROXIMATION

In this section the reference  $M$ -profile shown in Figs. 1 and 2 is approximated with 4-L-S. This approximate  $M$ -profile has five endpoints consisting of one variable test point and four fixed points at the heights of 0, 4, 10 and 80 m. Two typical 4-L-S approximate  $M$ -profiles for *class one* and *class two* are shown in Figs. 3 and 4, respectively. In these figures, points marked with '\*' are the fixed points and those marked with 'o' are the test points. Solid lines represent the approximate  $M$ -profile. Dashed lines represent the reference  $M$ -profile on which points are sampled. The linear portion of the  $M$ -profile above 15 m are not shown in the figures. The point at 4 m has the minimum  $M$ -value on the reference  $M$ -profile and this determines the duct height. The approximate profile and the reference  $M$ -profile above 10 m are identical.

### 1. 15 GHz

This subsection investigates the effect of sampling the test point for 15 GHz propagation. The height of the receiver is varied from 1 m to 35 m at 0.1 m increments at a range of either 60 km or 120 km from the transmitter. For these ranges and heights, the receiver is located well into the diffraction region. These same parameters are also utilized at the other three frequencies and will not be further mentioned.

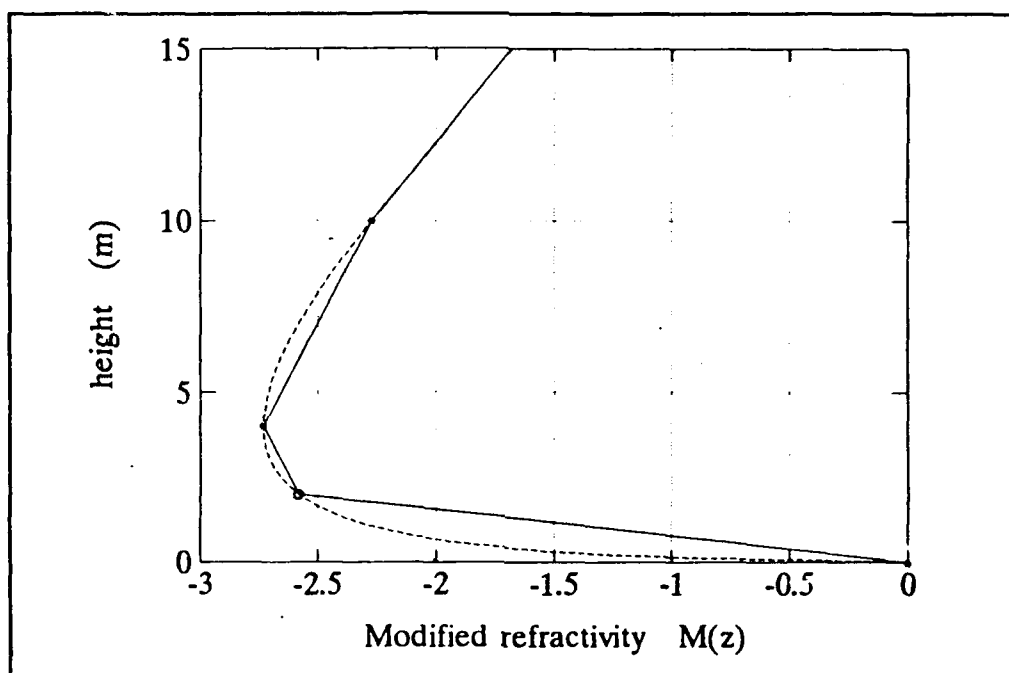


Figure 3. 4-L-S profile, test point within the duct (*class one*).

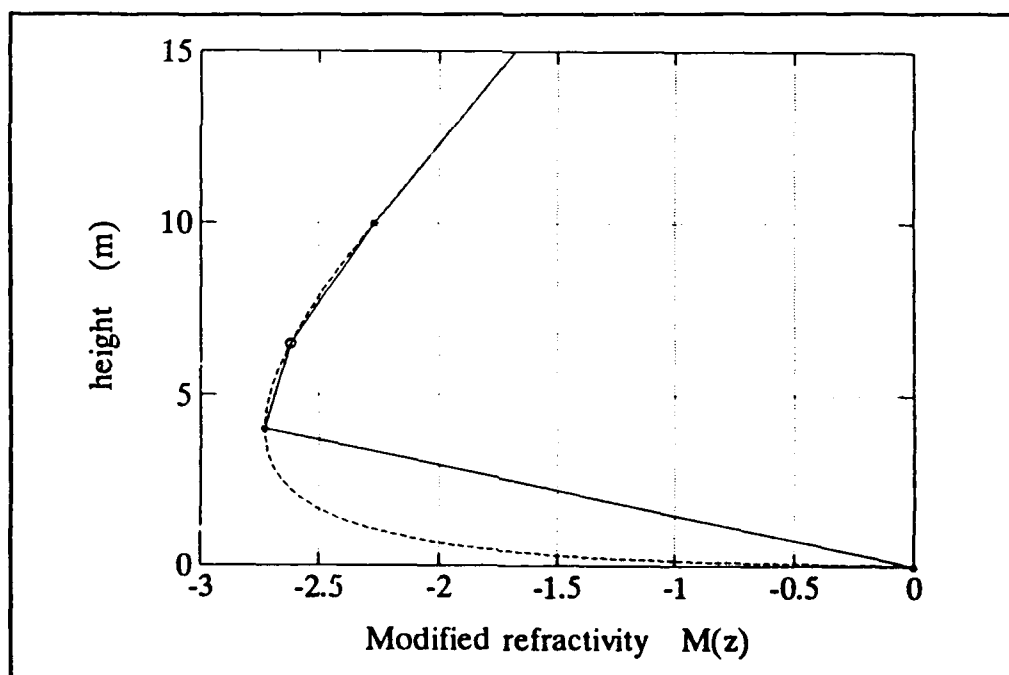


Figure 4. 4-L-S profile, test point above the duct (*class two*).

### *a. Path Loss Analysis*

(1) *Class One.* In Fig. 5 through Fig. 8, the receiver range is fixed at 60 km; and in Fig. 9 through Fig. 12, the receiver range is fixed at 120 km. The path loss as a function of receiver height when the test points at 0.1 m and at 3.5 m is shown in Fig. 29. The resulting path loss curves are representative of the path loss curves of *class one*; i.e., they are all of similar shapes. This observation is also true for propagation at the other three frequencies. In Fig. 5, it is seen that the path loss increases with decreasing receiver height. The rate of increase is higher when the receiver is located in the duct. Hence, the field strength in the duct is weaker.

The difference in path losses is shown in Fig. 6. It is clear that this difference decreases with increasing receiver height. Hence, when the test point is moved from 0.1 m to 3.5 m, the sensitivity of the height-gain function is greater when the receiver is lower.

(2) *Class Two.* The path losses when the test point is selected at 4.5 m and at 9.5 m are shown in Fig. 7. These are representative of all path loss curves for which the test point is sampled above the duct. This observation is also true for propagation at the other three frequencies. The path loss in *class two*, in contrast to that of *class one*, is not a monotonic function of receiver height. As the receiver moves up from within the duct, the signal strength increases rapidly at a rate of about 2 dB/m until it reaches a maximum (minimum path loss) just below the upper

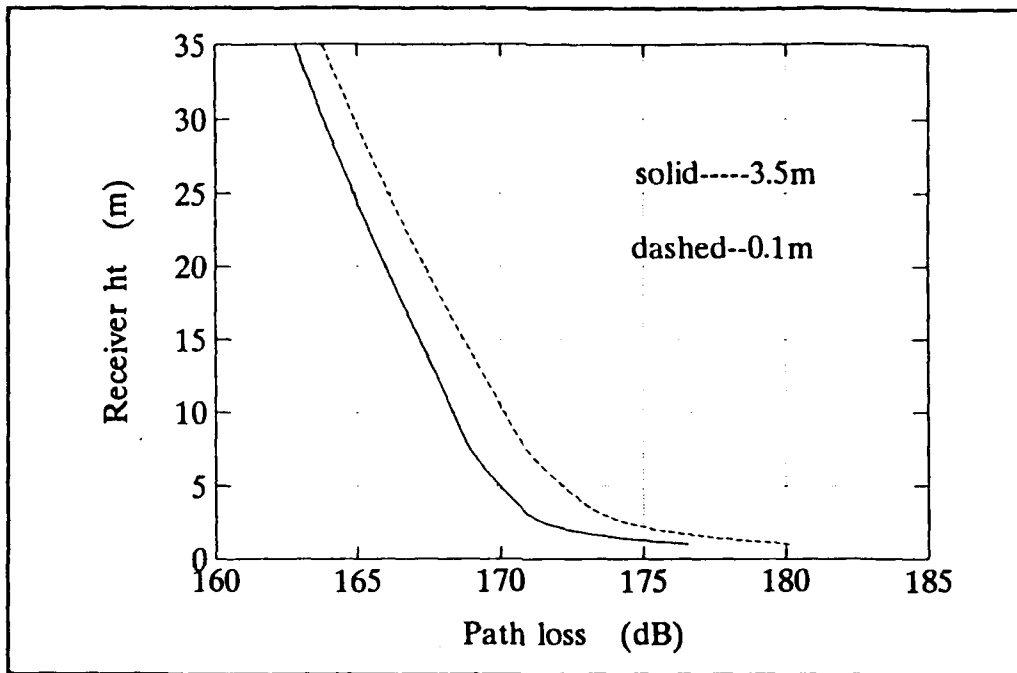


Figure 5. Path loss for 4-L-S, test points at 0.1 m and 3.5 m ( $f = 15$  GHz,  $r = 60$  km).

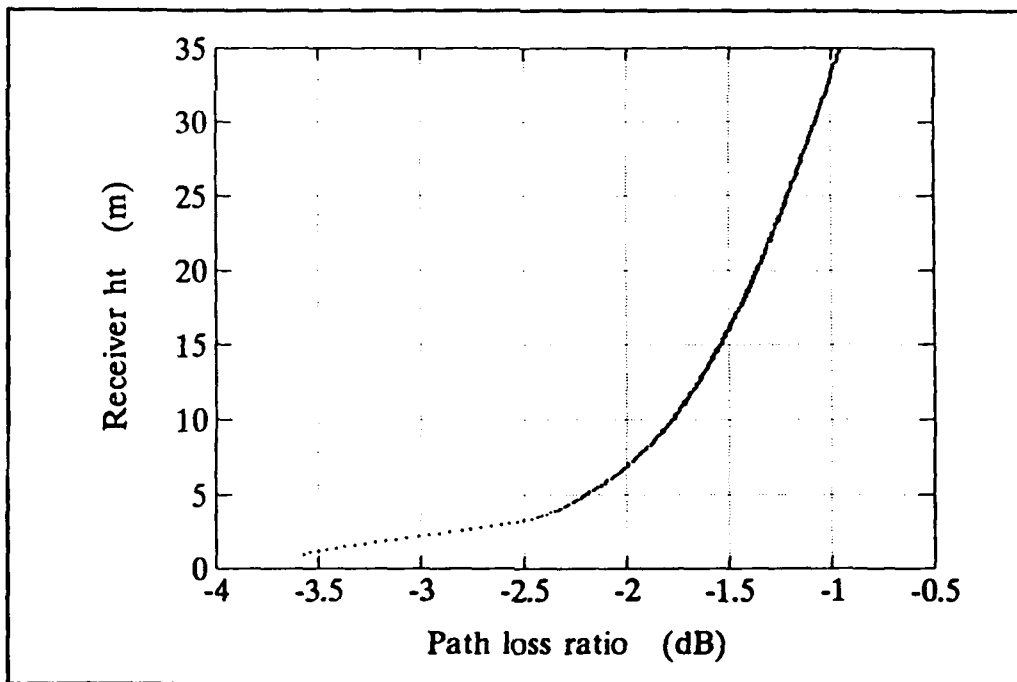


Figure 6. Path loss ratio.

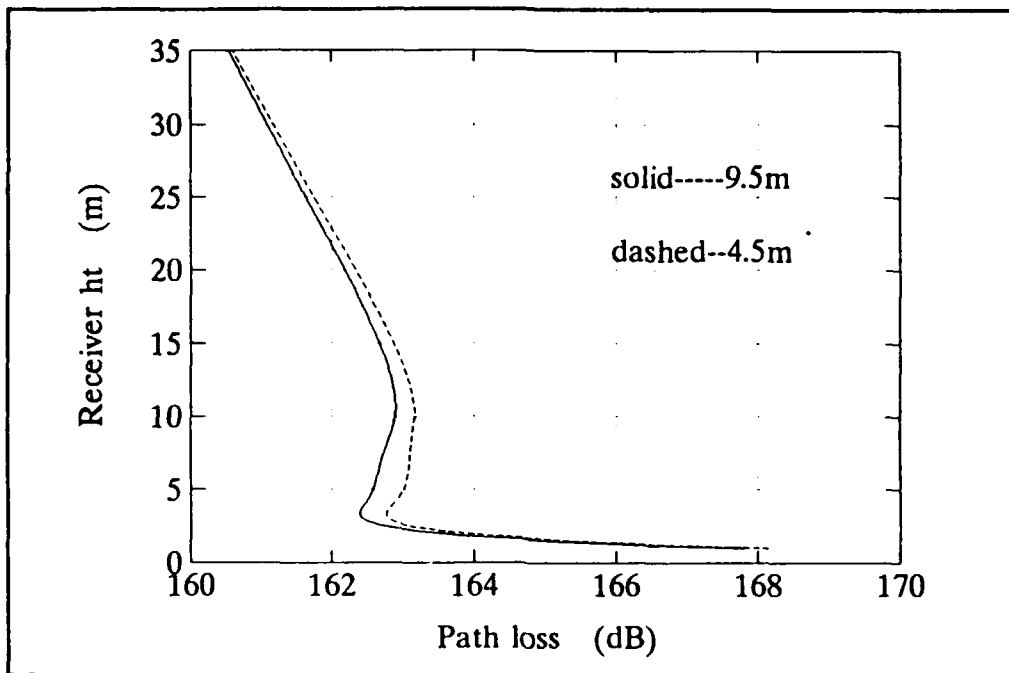


Figure 7. Path loss for 4-L-S, test points at 4.5 m and 9.5 m ( $f = 15$  GHz,  $r = 60$  km).

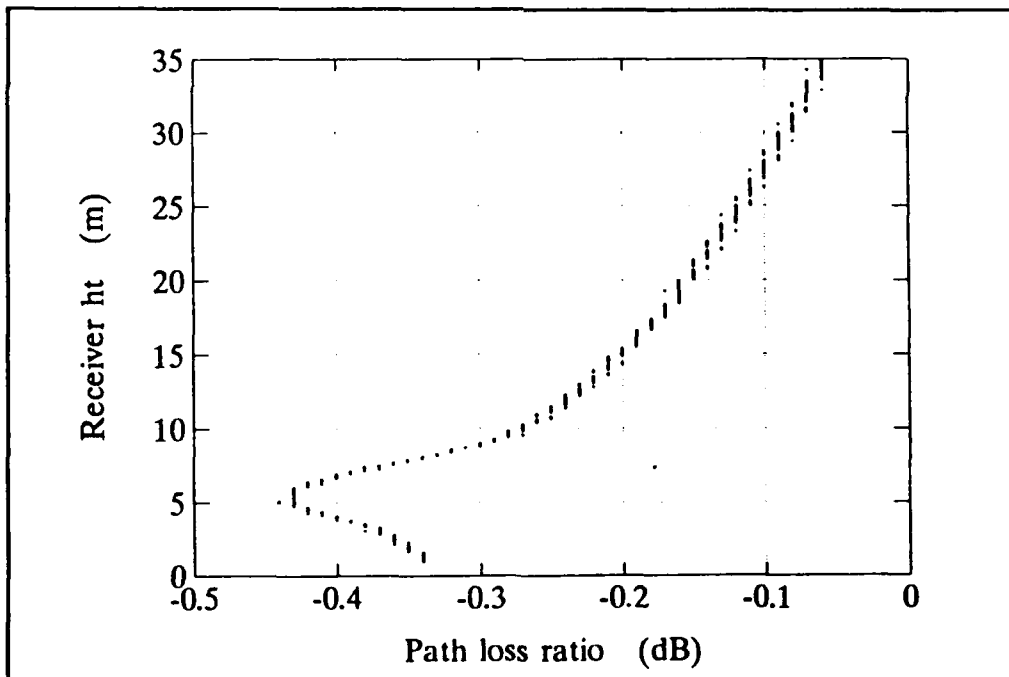


Figure 8. Path loss ratio.

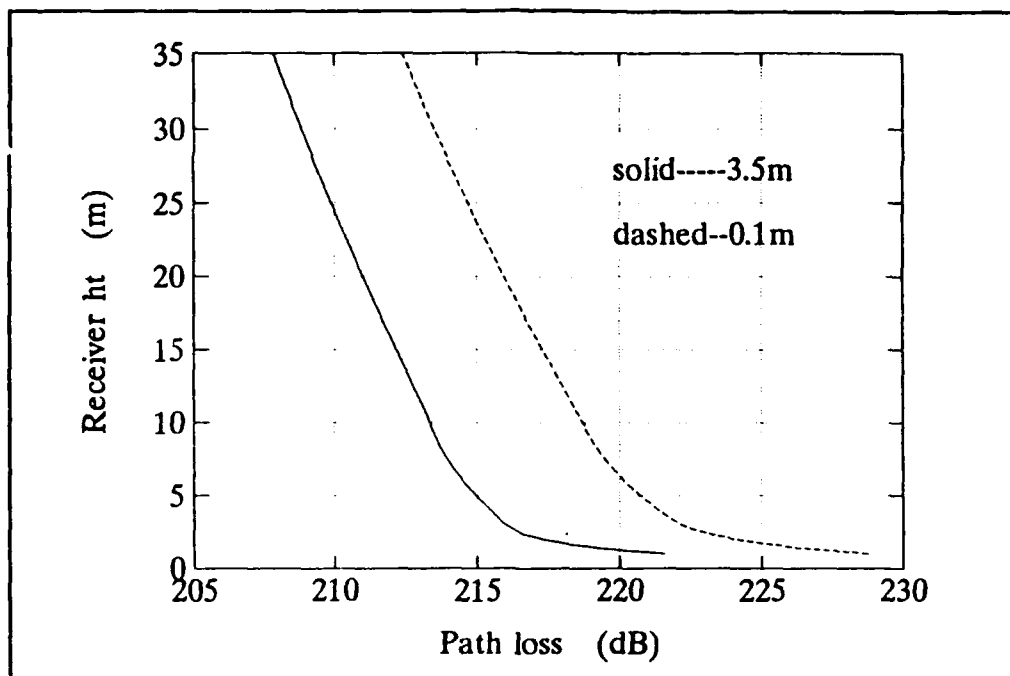


Figure 9. Path loss for 4-L-S, test points at 0.1 m and 3.5 m ( $f = 15$  GHz,  $r = 120$  km).

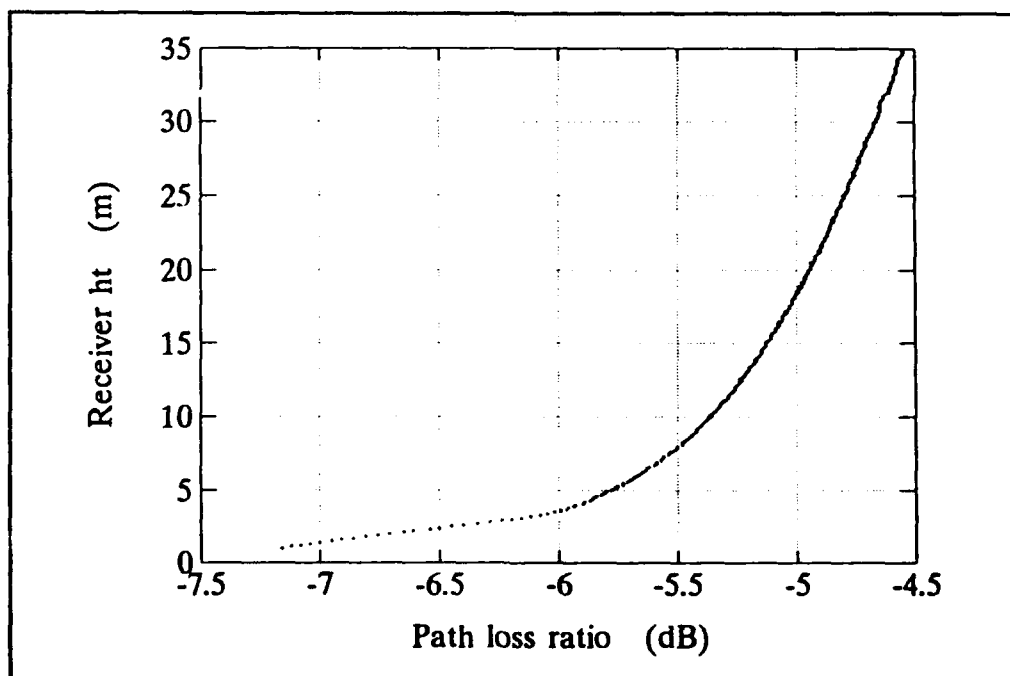


Figure 10. Path loss ratio.

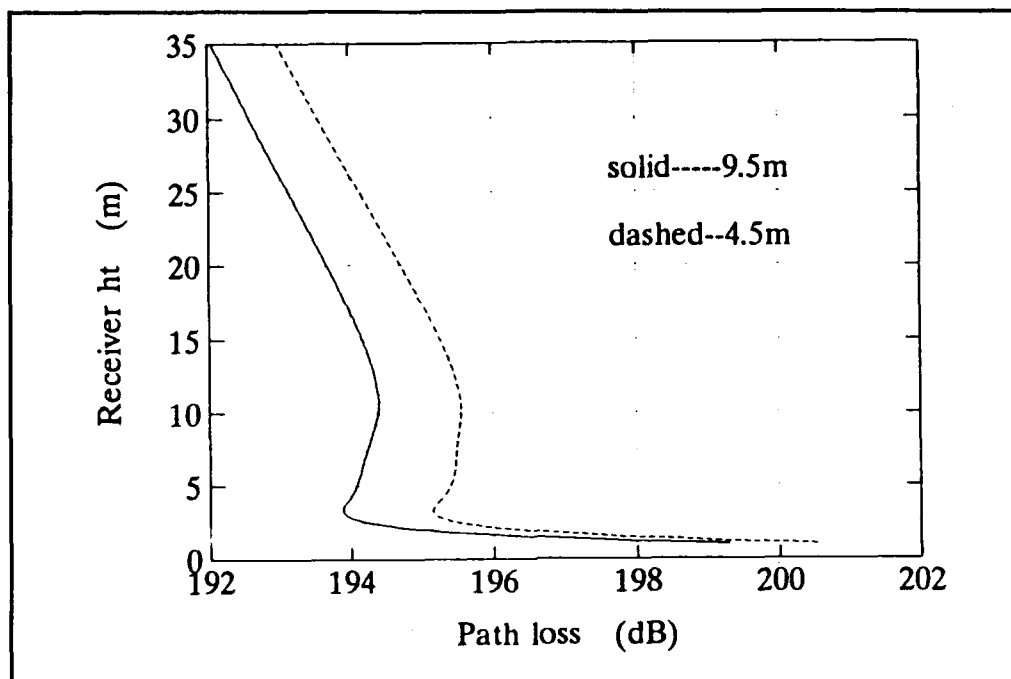


Figure 11. Path loss for 4-L-S, test points at 4.5 m and 9.5 m ( $f = 15$  GHz,  $r = 120$  km).

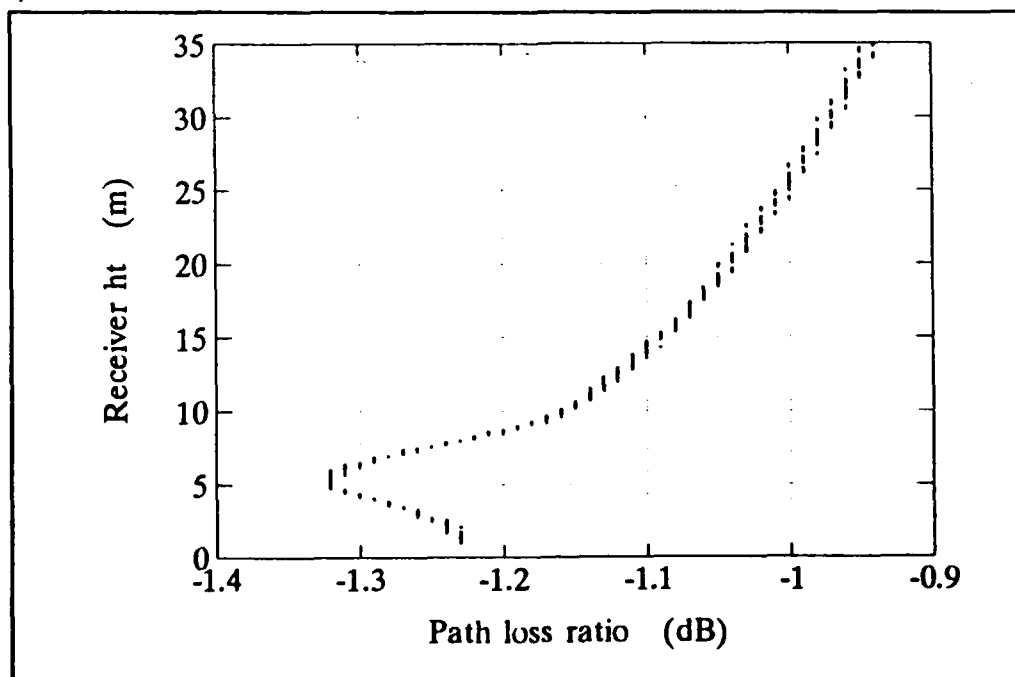


Figure 12. Path loss ratio.

boundary of the duct. Then it starts to decrease. The signal strength continues to decrease until the receiver is about 10 m high. Thereafter, it resumes increasing.

The difference in path losses is shown in Fig. 8. It can be seen that the path loss ratio has a maximum at 5 m which is just above the duct. An interesting feature observed is that the variation of this curve with receiver height is quite different when the receiver is located in the duct than when it is located above the duct. The gradient of the path loss ratio curve has different signs below 5 m and above 5 m. The difference increases as the receiver height increases when the receiver is below 5 m, and decreases with increasing height when the receiver is above 5 m. This means that when the test point is moved from 4.5 to 9.5 m, the sensitivity of the height-gain function is smaller for greater receiver heights unless the receiver is lower than 5 m.

(3) *Discussion.* From Figs. 5 and 6, it is seen that the field strength is stronger at every receiver height when the test point is at 3.5 m than when it is at 0.1 m. Also, by comparing Fig. 5 to Fig. 7, it is seen that, using the 4-L-S approximate *M*-profile, the field strength is weaker when the test point is sampled at either 0.1 m or 3.5 m than when the test point is sampled at either 4.5 m or 9.5 m. Amongst these four particular situations, the strongest field occurs when the test point is located at 9.5 m.



### ***b. Attenuation Rate Analysis***

Three modes are found with attenuation rates lower than 5 dB/km (Figs. 13 and 14). The dominant mode is mode b. It has a smaller attenuation rate than the other two modes by at least 2 dB/km for every sampling height. Thus, at 60 km, the path loss of this dominant mode is at least 120 dB less than the other two modes. The attenuation rate of mode b deviates by 0.7 dB/km for *class one* but remains almost a constant for *class two*. At a sampling height of 1.5 m, the attenuation rate of mode b reaches a maximum. Thus, for 15 GHz propagation, the field strength is more sensitive to test point variation in *class one* than in *class two*.

### ***c. Mode Location Analysis***

As can be seen in Fig. 15, the imaginary part of mode b is consistently the least negative of the three modes. This implies that mode b is the strongest mode having the smallest range attenuation rate. In Fig. 15, the number following the location identification is the sampling height of the test point. For example, 'x -- 9.5 m' indicates that the mode location marked with 'x' is obtained when the test point is sampled at 9.5 m. Mode a generally has the strongest attenuation. However, the modal strength of mode c becomes the weakest for some heights of the test point in *class two*. This can also be seen in Figs. 13 and 14, where the attenuation rate of mode c becomes greater than that of mode a when the test point is located at a height between 7.6 m and 8.6 m.

The variation of mode b only is shown in Fig. 16. It can be seen that when the test point height is varied from 0.1 m to 3.5 m the imaginary part of

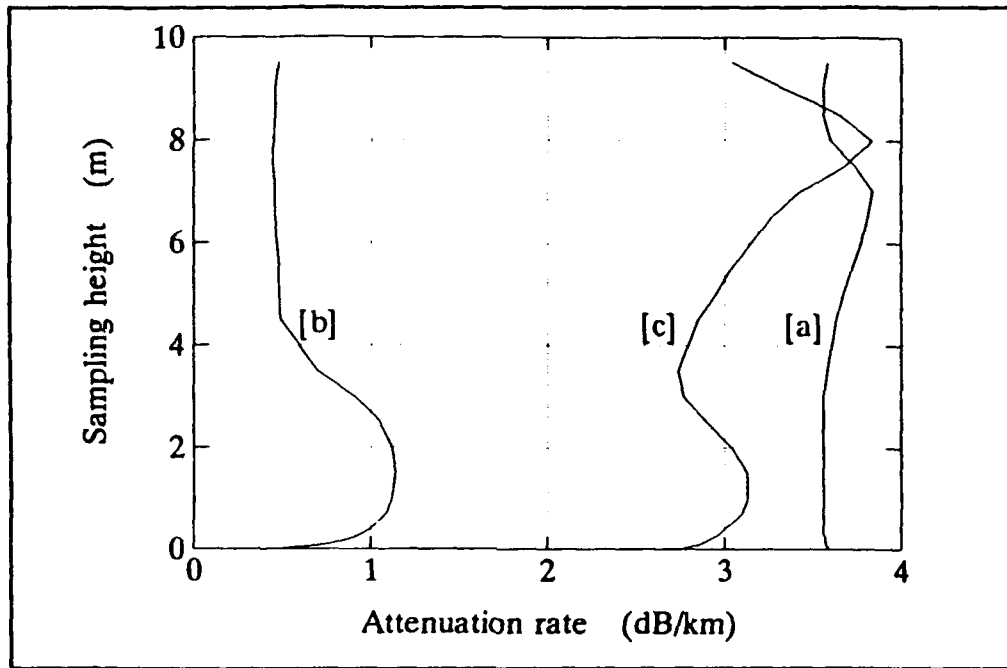


Figure 13. Modal attenuation rate for 4-L-S ( $f = 15$  GHz).

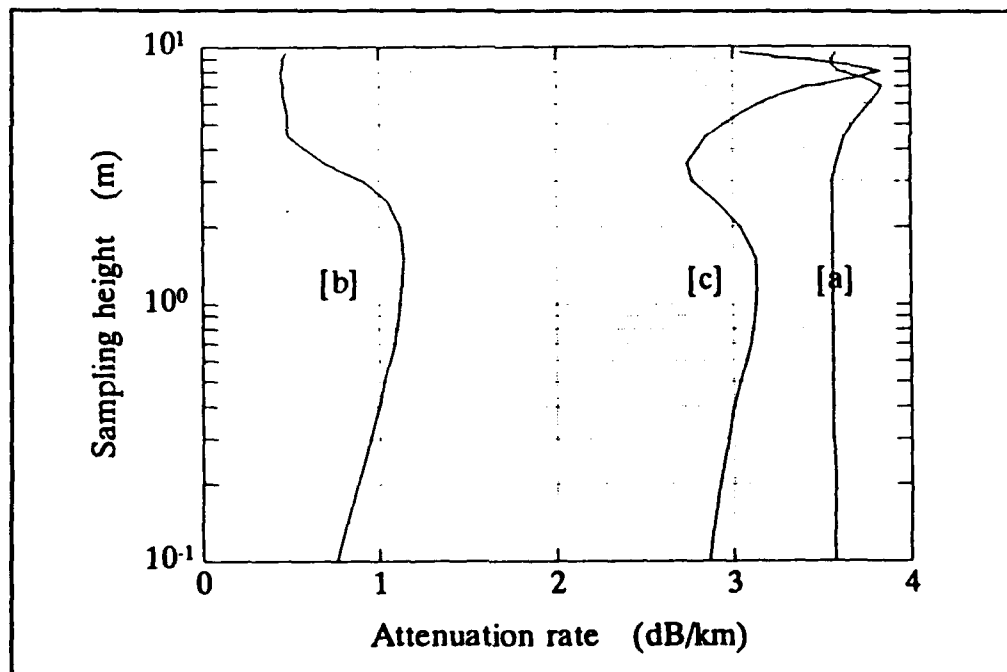


Figure 14. Modal attenuation rate for 4-L-S, sampling height in logarithmic scale ( $f = 15$  GHz).

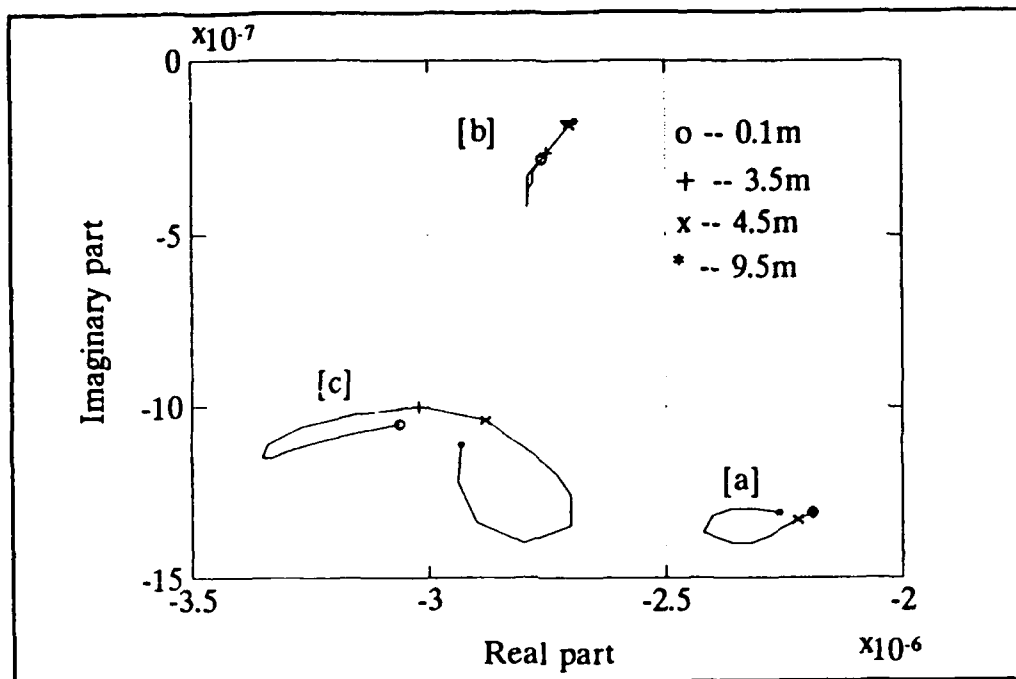


Figure 15. Mode location on the  $\beta-1$  complex plane for 4-L-S ( $f = 15$  GHz).

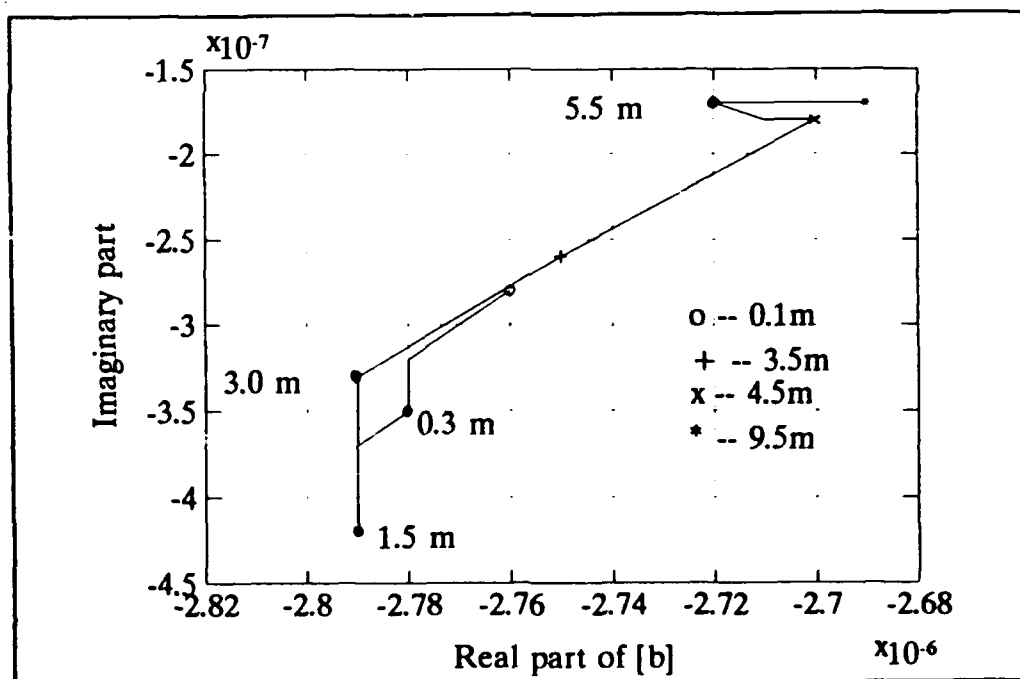


Figure 16. Dominant mode location on the  $\beta-1$  complex plane for 4-L-S ( $f = 15$  GHz).

this mode varies much more than when the test point height is varied from 4.5 m to 9.5 m. Thus, the sensitivity of the field strength is greater for *class one* than *class two*. This can also be observed in Figs. 13 and 14.

## 2. 10 GHz

### a. Path Loss Analysis

(1) *Class One*. In Fig. 17 through Fig. 20, the receiver range is fixed at 60 km; and in Fig. 21 through Fig. 24, the receiver range is fixed at 120 km. The path loss as a function of receiver height when the test point is located at 0.1 m and at 3.5 m is shown in Fig. 17. The path loss curves are similar to those for *class one* at 15 GHz. The only difference is that the curves for 10 GHz propagation are smoother. The difference in path losses is shown in Fig. 18. It has features similar to that of *class one* at 15 GHz.

(2) *Class Two*. The path losses when the test point is selected at 4.5 m and at 9.5 m are shown in Fig. 19. The path loss curves are similar to those for *class one* at 15 GHz. Earlier, it was observed that *class two* at 15 GHz results in a change in sign of the gradient in the path loss curve. This phenomenon does not occur at 10 GHz.

The difference in path losses is shown in Fig. 20. This difference remains almost constant when the receiver is located in the duct and decreases with increasing receiver height when the receiver is located above the duct. This means that the sensitivity of the height-gain function when the test point is moved from 4.5 m

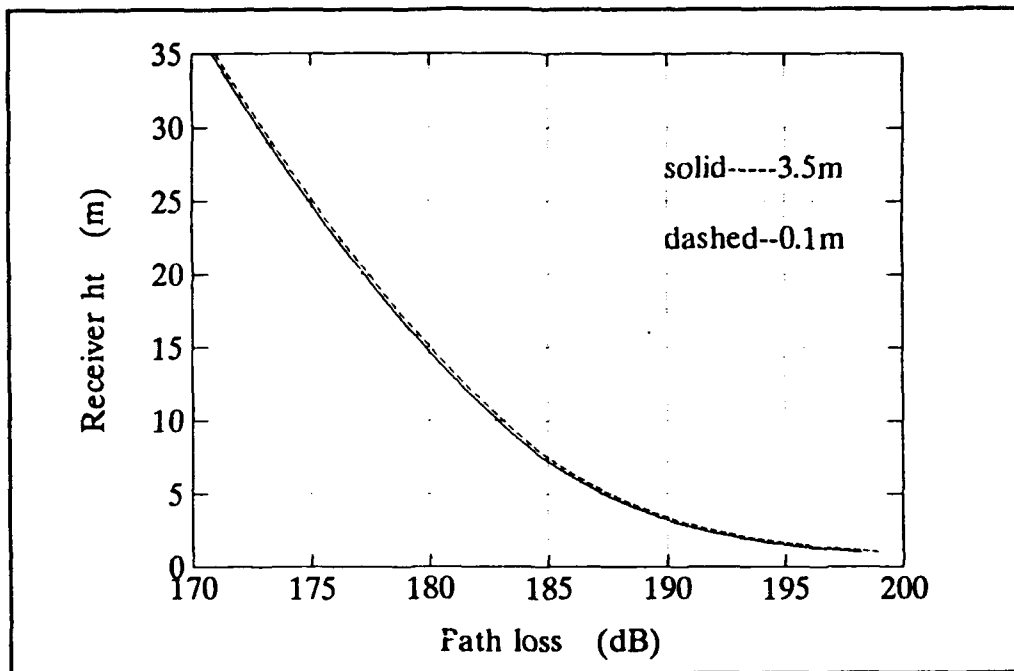


Figure 17. Path loss for 4-L-S, test points at 0.1 m and 3.5 m ( $f = 10$  GHz,  $r = 60$  km).

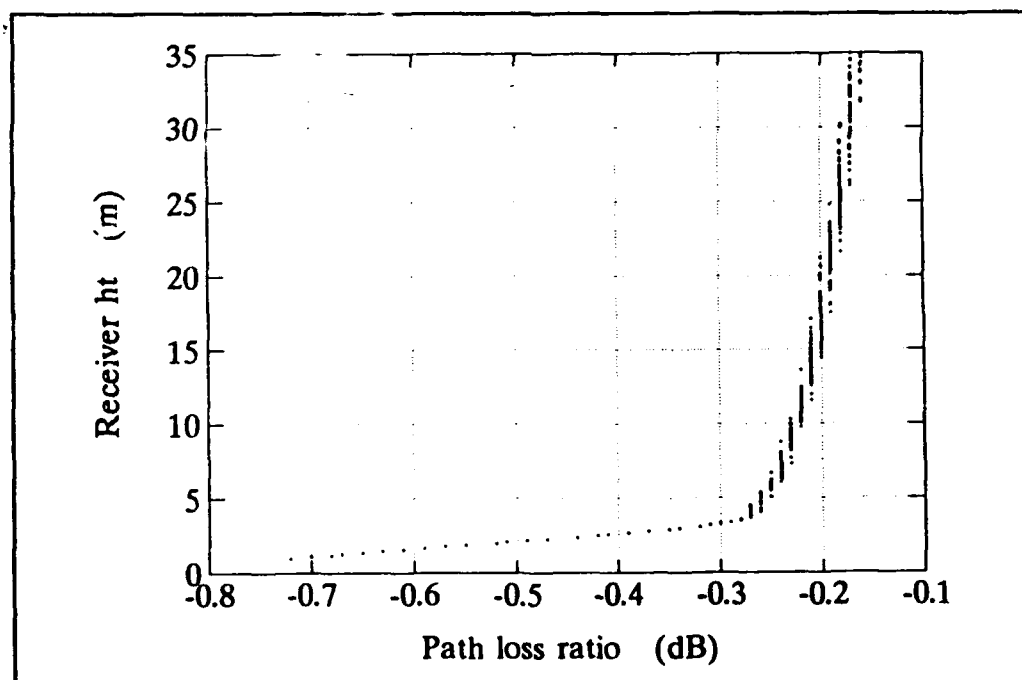


Figure 18. Path loss ratio.

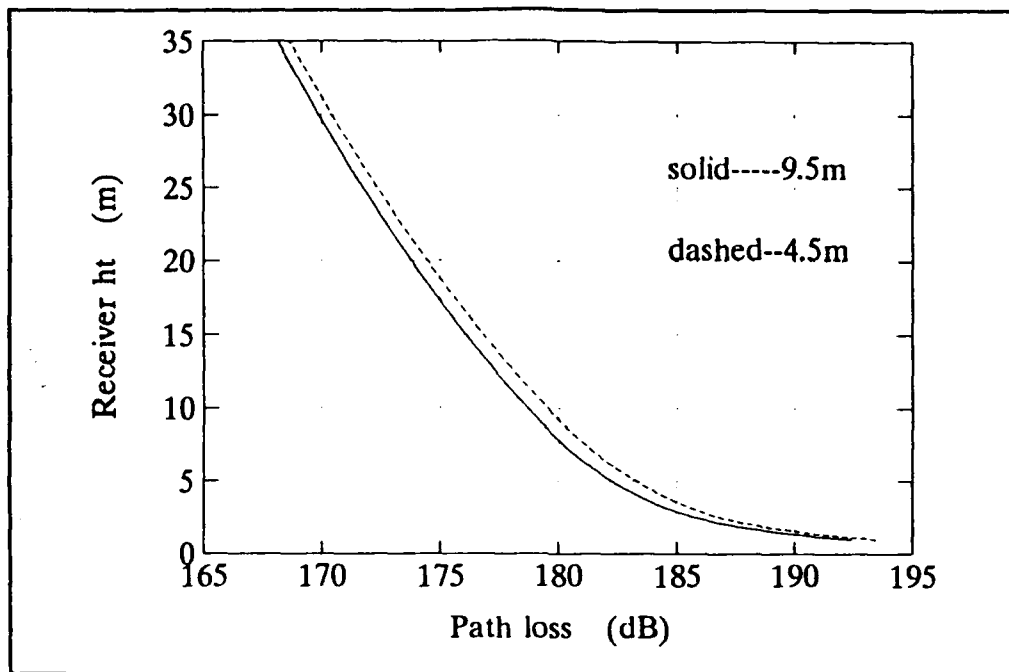


Figure 19. - Path loss for 4-L-S, test points at 4.5 m and 9.5 m ( $f = 10$  GHz,  $r = 60$  km).

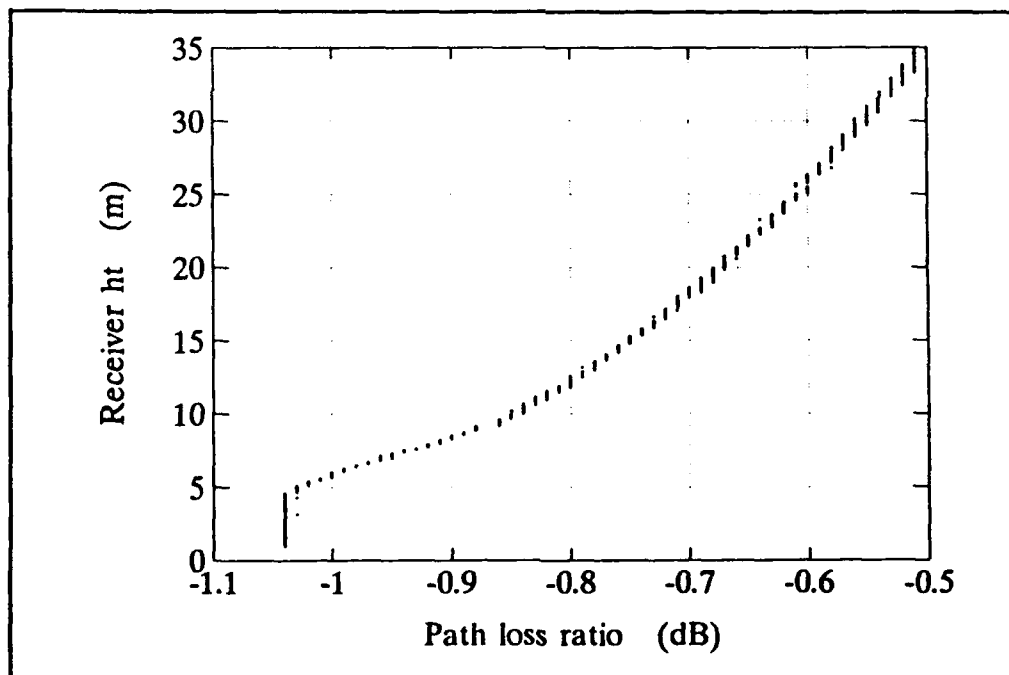


Figure 20. Path loss ratio.

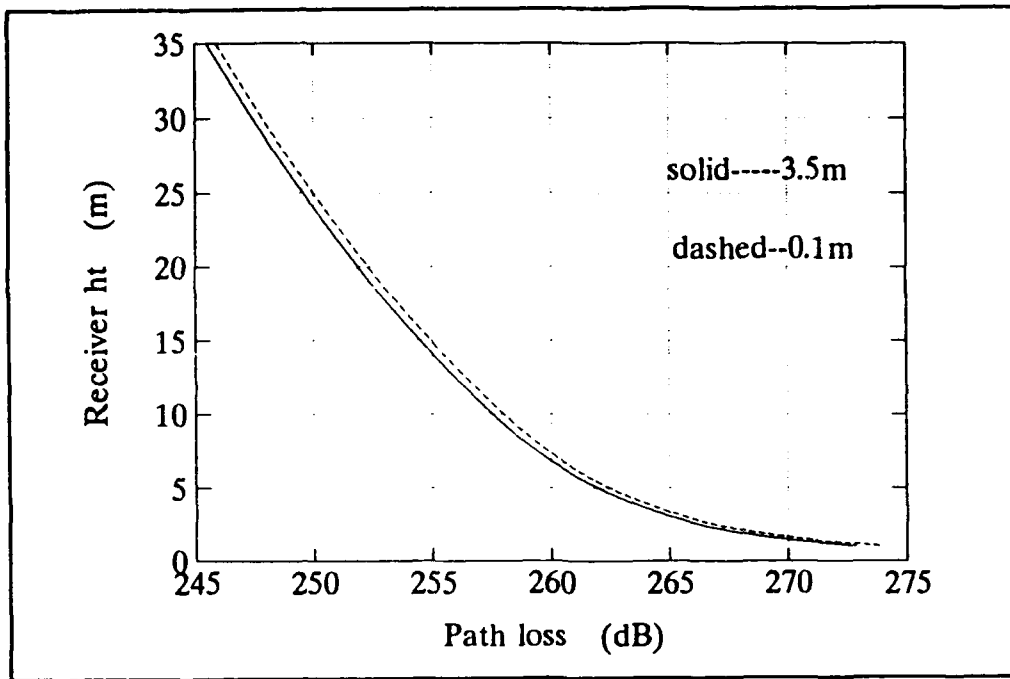


Figure 21. Path loss for 4-L-S, test points at 0.1 m and 3.5 m ( $f = 10$  GHz,  $r = 120$  km).

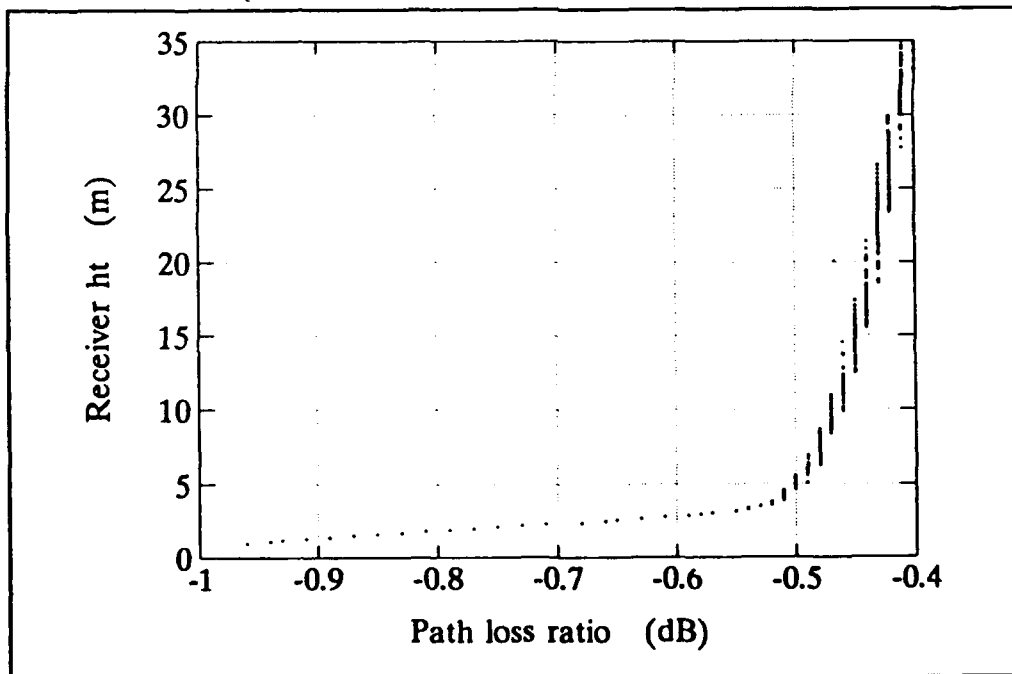


Figure 22. Path loss ratio.

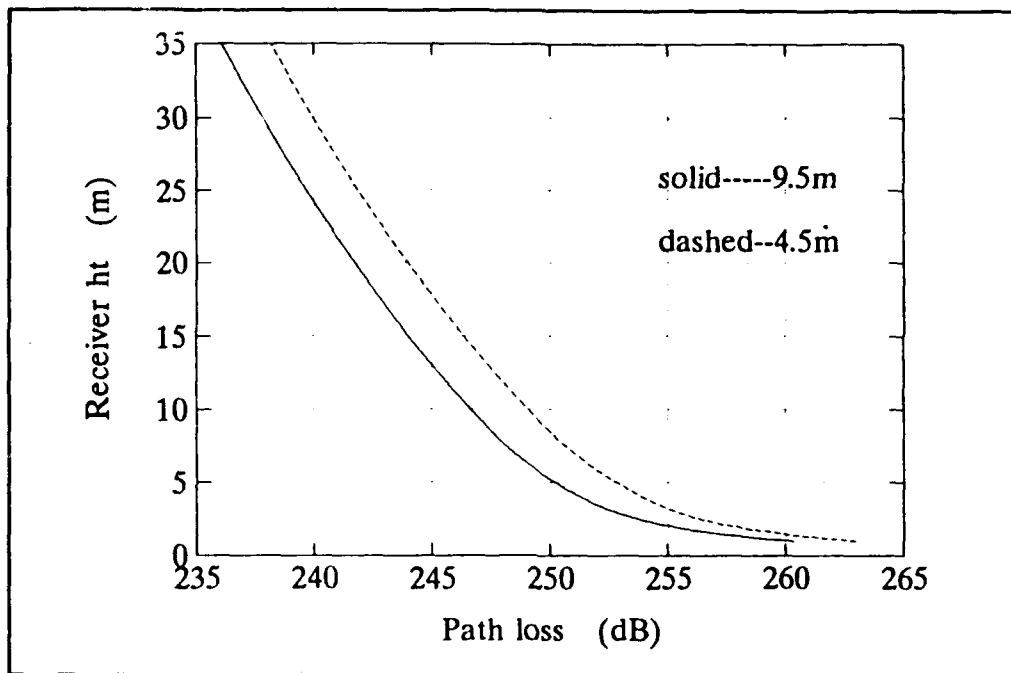


Figure 23. Path loss for 4-L-S, test points at 4.5 m and 9.5 m ( $f = 10$  GHz,  $r = 120$  km).

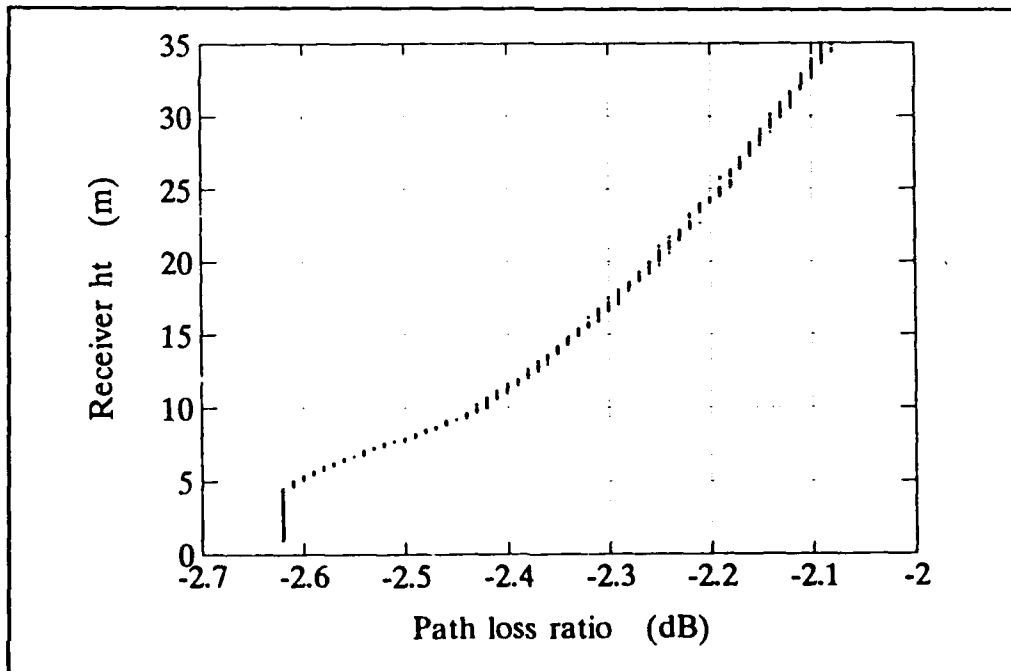


Figure 24. Path loss ratio.



to 9.5 m is smaller for a higher receiver and is almost constant when the receiver is located in the duct. This relationship is different from that obtained at 15 GHz.

(3) *Discussion.* The variation in field strength with respect to the choice of one of the four particular test point location at 10 GHz is similar to the variation observed at 15 GHz.

When the test point is located at any of the four heights, the path loss for a 10 GHz signal is larger than that for a 15 GHz signal at every receiver height. This can be seen by comparing Fig. 5 with Fig. 17 and Fig. 7 with Fig. 19. It can, therefore, be concluded that the higher the propagation frequency, the greater the enhancement of the field strength by the duct.

When the test point is moved from 0.1 m to 3.5 m, the path loss for 10 GHz propagation varies by 0.72 dB for a 1 m receiver height and by 0.16 dB for 35 m (see Fig. 18). For propagation at 15 GHz, the variations of path loss are 3.6 and 0.9 dB, respectively, at the same two heights as shown in Fig. 6. From these figures, it can be concluded that when the test point is moved from 0.1 m to 3.5 m the path loss ratio (i.e., the variation in path loss) for 15 GHz propagation is greater than that for 10 GHz propagation at every receiver height. When the test point is moved from 4.5 m to 9.5 m, the path loss ratio for 15 GHz propagation is smaller than that for 10 GHz propagation. This can be seen by comparing Fig. 8 with Fig. 20. Consequently, when the test point is moved from 0.1 m to 3.5 m, the sensitivity

of the height-gain function at 10 GHz is lower than that at 15 GHz. When the test point is moved from 4.5 m to 9.5 m, the sensitivity is lower at 15 GHz.

*b. Attenuation Rate Analysis*

Three modes are found with attenuation rates lower than 5 dB/km (Figs. 25 and 26). The dominant mode is mode c. It has an attenuation rate smaller than those of the other two modes by at least 1.6 dB/km at every sampling height. With the test point sampled at 1.5 m, the attenuation rate of mode c reaches a maximum. The situation at 15 GHz is similar. The attenuation rate of the dominant mode c changes about 0.3 dB/km for *class one* and remains almost a constant for *class two*. Thus, for 10 GHz propagation, the field strength is more sensitive to a change of test point height in *class one* than in *class two*.

A comparison of the variation of the attenuation rate of the dominant modes for 10 GHz and 15 GHz propagation shows that the sensitivity of field strength to a change of test point height is higher for 15 GHz propagation.

*c. Mode Location Analysis*

It can be seen from Fig. 27 that the imaginary part of mode c is the least negative of the three modes. This means that the field strength of mode c is the strongest. The modal attenuation rate increases from mode c to b to a for every sampling height (Figs. 25 and 26).

It can be seen from Fig. 28 that when the test point height is varied from 0.1 m to 3.5 m the imaginary part of this mode varies much more than

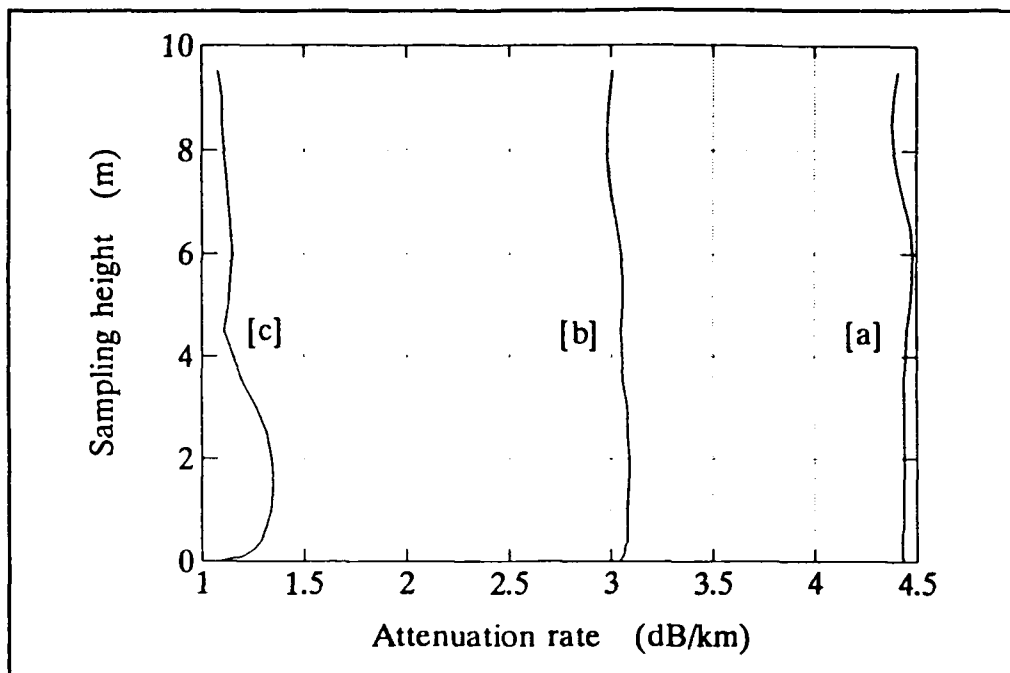


Figure 25. Modal attenuation rate for 4-L-S ( $f = 10$  GHz).

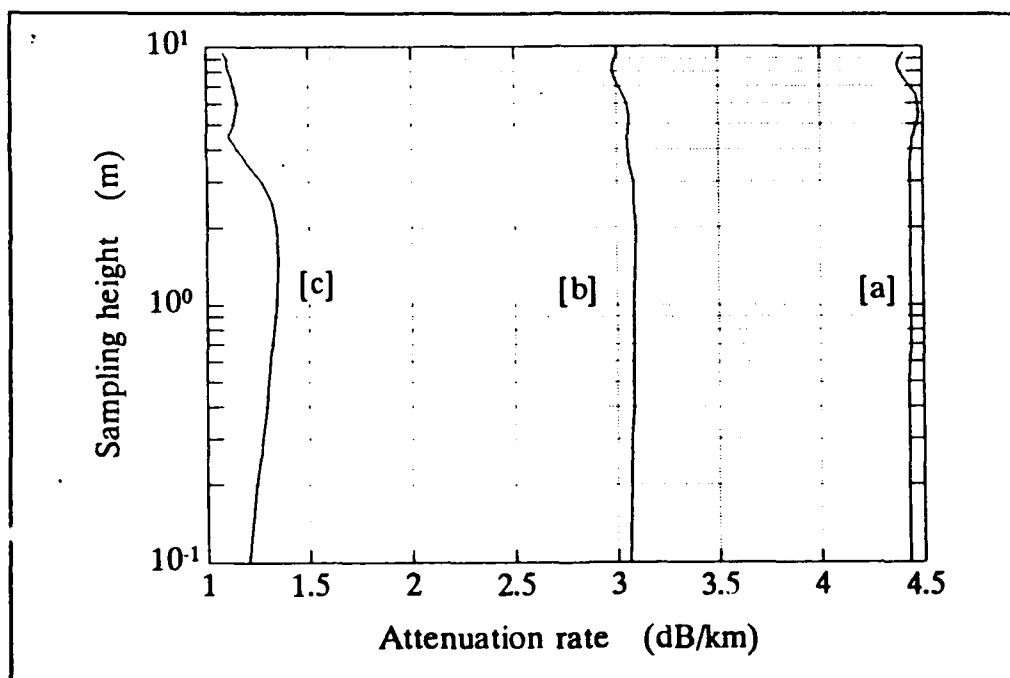


Figure 26. Modal attenuation rate for 4-L-S, sampling height in logarithmic scale ( $f = 10$  GHz).

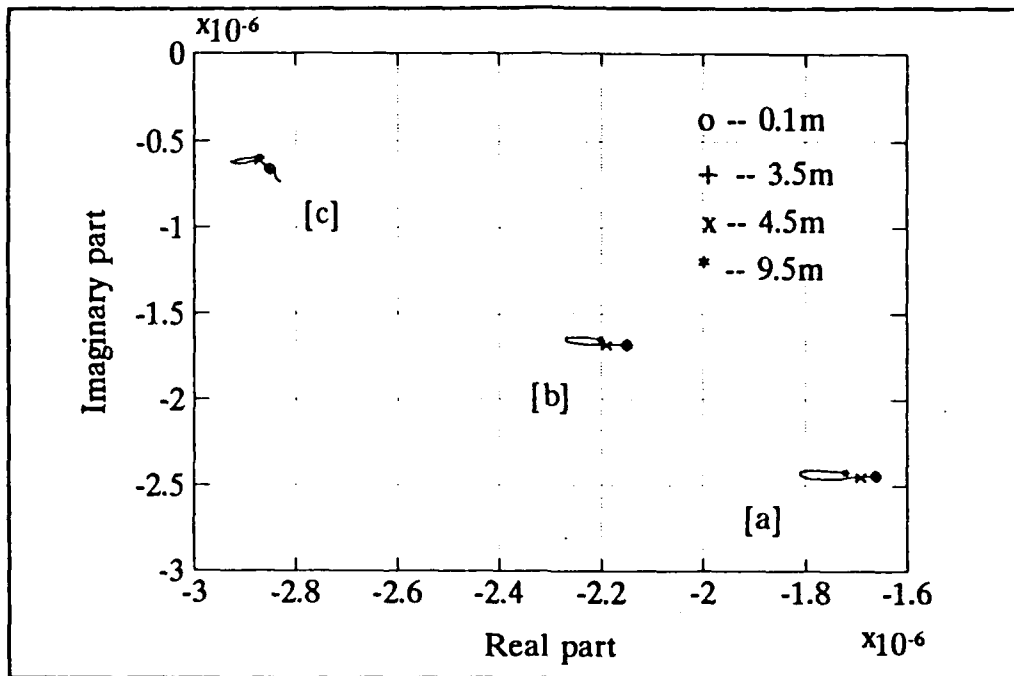


Figure 27. Mode location on the  $\beta-1$  complex plane for 4-L-S ( $f = 10$  GHz).

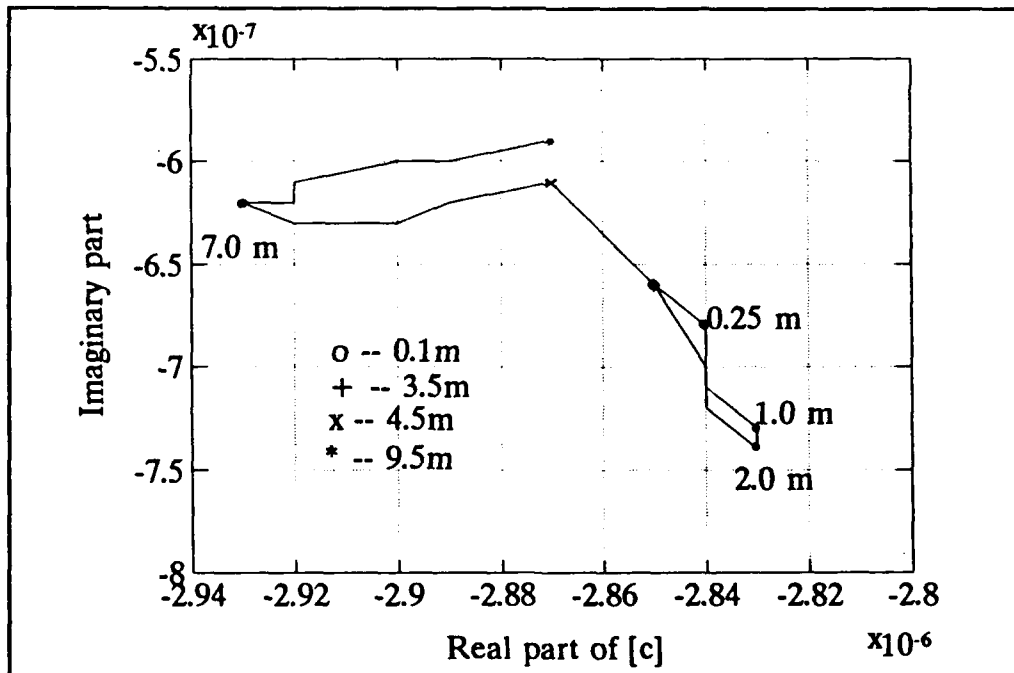


Figure 28. Dominant mode location on the  $\beta-1$  complex plane for 4-L-S ( $f = 10$  GHz).

when the test point height is varied from 4.5 m to 9.5 m. Thus, the sensitivity of the field strength is greater for *class one* than for *class two*, similar to the case of 15 GHz propagation.

By comparing Fig. 15 with Fig. 27, it can be seen that the location of each mode varies more for 15 GHz propagation than for 10 GHz. In general, the higher the propagation frequency, the greater the sensitivity of the mode location to a change of test point height.

### 3. 6 GHz

#### *a. Path Loss Analysis*

(1) *Class One.* In Figs. 29 and 30, the receiver range is fixed at 60 km; and in Figs. 31 and 32, the receiver range is fixed at 120 km. The path loss as a function of the receiver height when the test point is located at 0.1 m and at 3.5 m is shown in Fig. 29. The path loss curves for 6 GHz propagation are similar to those of *class one* at 15 GHz. The only difference is that the two curves for 6 GHz propagation are closer to each other.

(2) *Class Two.* The path losses when the test point is selected at 4.5 and at 9.5 m are shown in Fig. 30. The path loss curves are similar to those for *class one* at 15 GHz propagation. Again, the difference is that the curves for 6 GHz propagation are closer. The path loss ratios for 6 GHz propagation are not plotted because they are too small to be presented accurately.

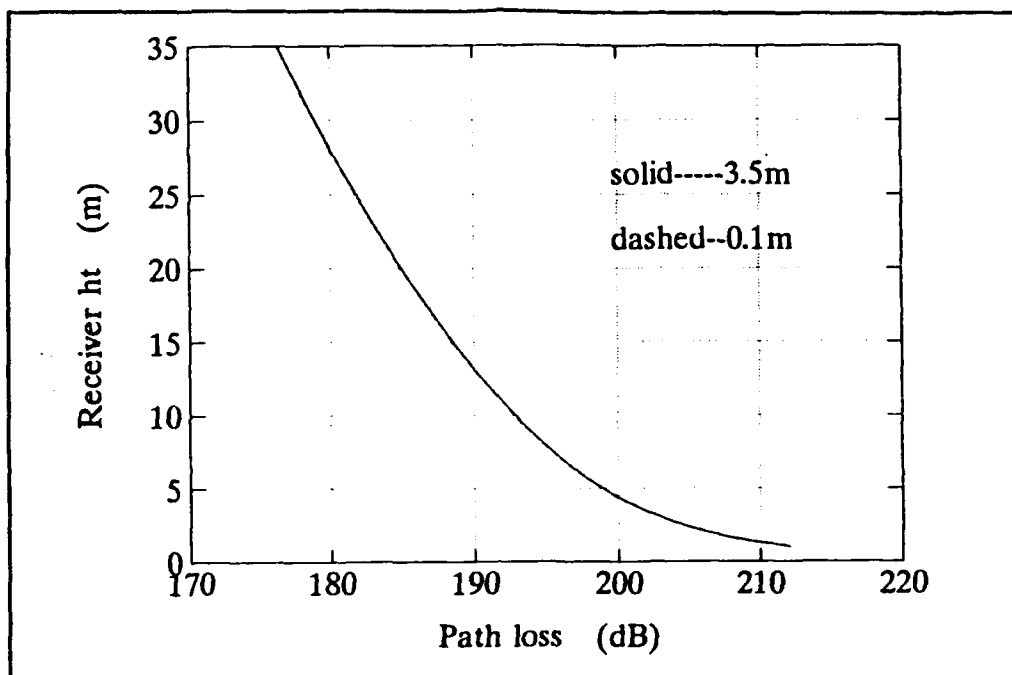


**Figure 29.** Path loss for 4-L-S, test points at 0.1 m and 3.5 m ( $f = 6$  GHz,  $r = 60$  km).

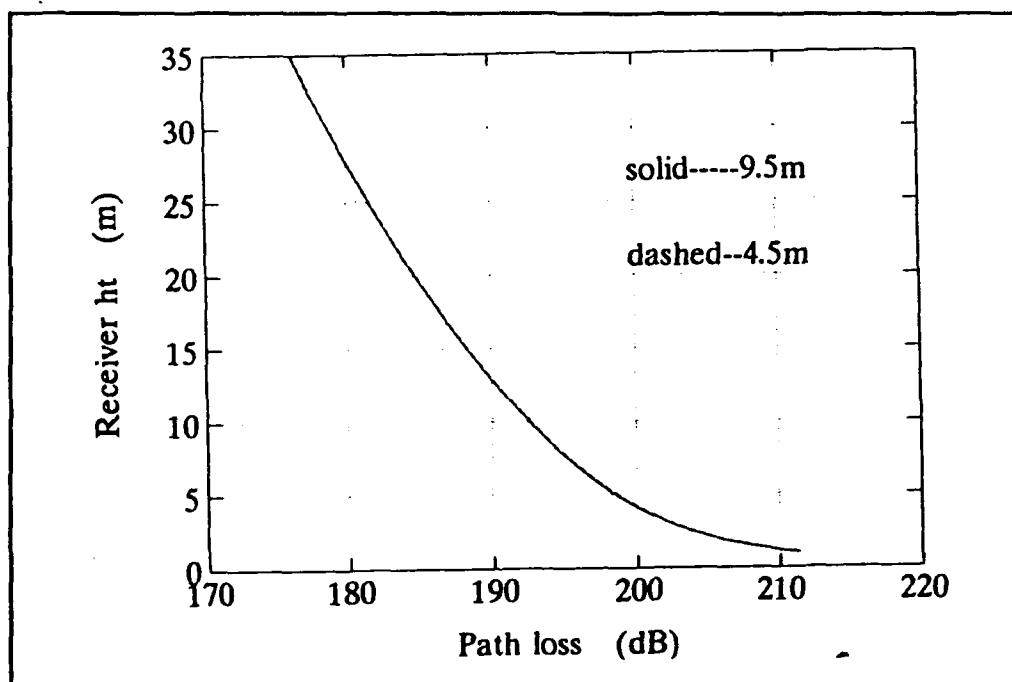


**Figure 30.** Path loss for 4-L-S, test points at 4.5 m and 9.5 m ( $f = 6$  GHz,  $r = 60$  km).

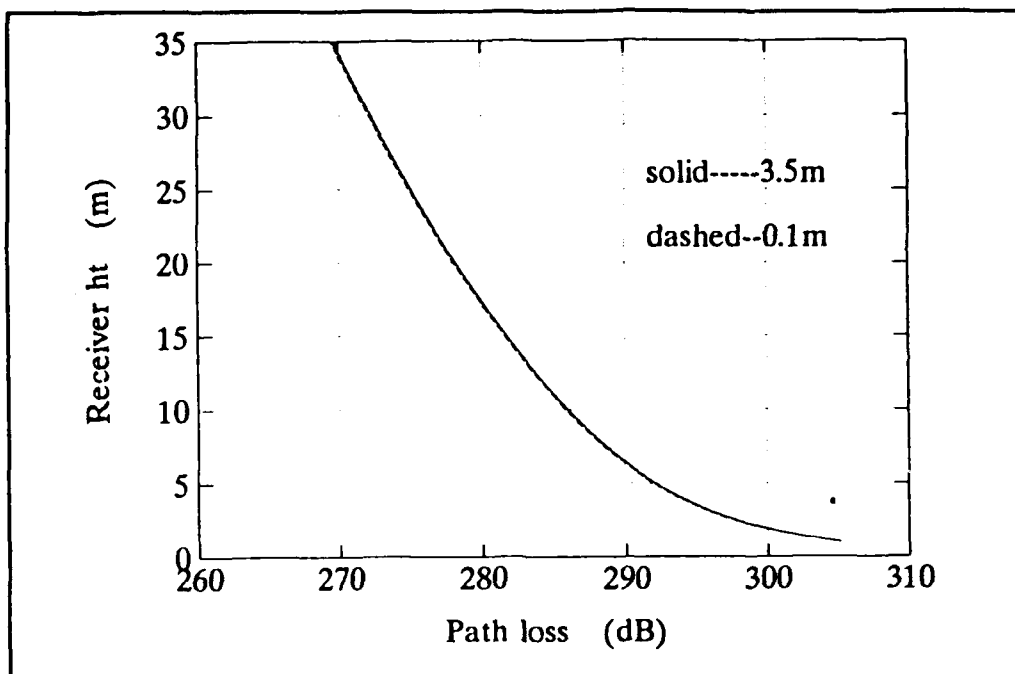


Figure 31. Path loss for 4-L-S, test points at 0.1 m and 3.5 m ( $f = 6$  GHz,  $r = 120$  km).

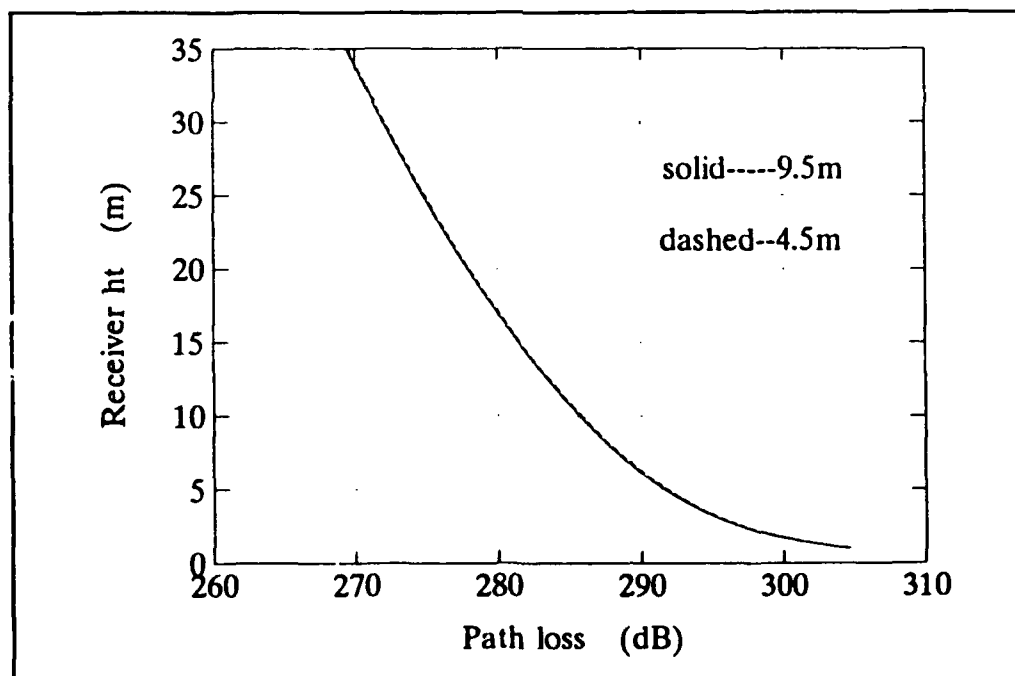


Figure 32. Path loss for 4-L-S, test points at 4.5 m and 9.5 m ( $f = 6$  GHz,  $r = 120$  km).

(3) *Discussion.* When the test point is selected at any of the four locations, the path loss for a 6 GHz signal is larger than that for a 10 GHz signal at every receiver height. This can be seen by comparing Fig. 17 with Fig. 29 and Fig. 19 with Fig. 30. Thus, the higher the propagation frequency, the greater the enhancement of the field strength by the duct. This behavior is similar to that at 10 GHz and at 15 GHz discussed previously.

When the test point is moved from 0.1 m to 3.5 m, the path loss ratio for 6 GHz propagation varies from 0.72 dB at 1 m receiver height to 0.16 dB at 35 m. For 6 GHz propagation, this ratio varies less than 0.1 dB over the same range of receiver height. Therefore, the path loss ratio for 10 GHz propagation is greater than that for 6 GHz propagation. When the test point is moved from 4.5 m to 9.5 m, a similar result is obtained (cf. Figs. 19 and 30). Consequently, when the test point is moved from 0.1 m to 3.5 m and from 4.5 m to 9.5 m, the sensitivity of the height-gain function for propagation at 6 GHz is smaller than that at 10 GHz.

#### *b. Attenuation Rate Analysis*

Four modes are found with an attenuation rate lower than 5 dB/km (Figs. 33 and 34). The dominant mode is mode d. It has the smallest attenuation rate and is at least 1.2 dB/km smaller than any of the other three modes at every sampling height. The attenuation rate of each mode deviates less than 0.1 dB/km between the two sampling classes.



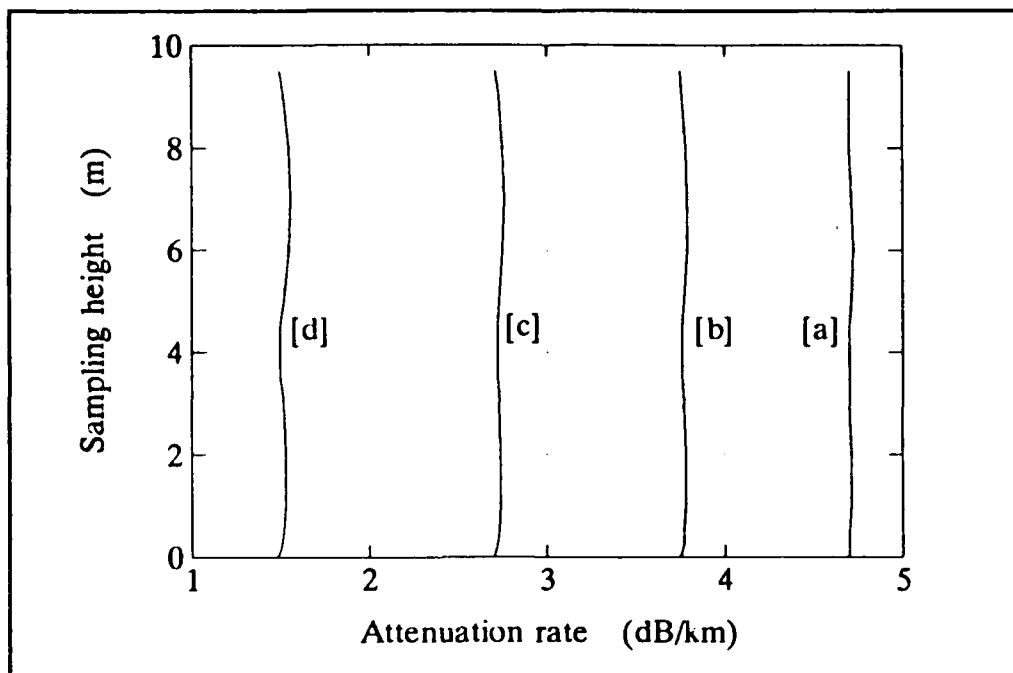


Figure 33. Modal attenuation rate for 4-L-S ( $f = 6$  GHz).

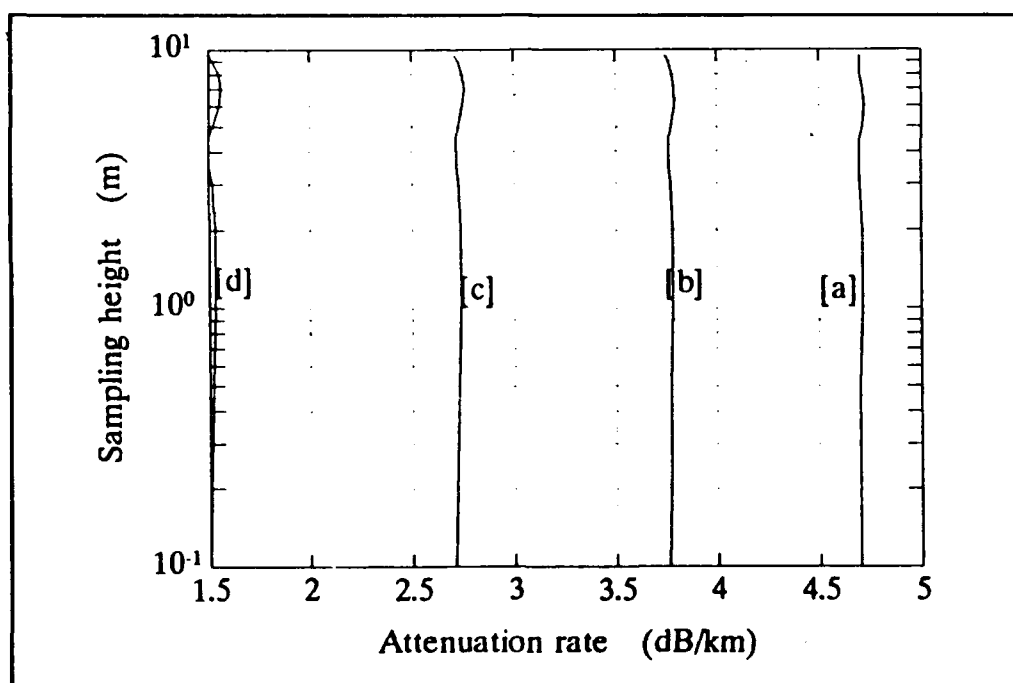


Figure 34. Modal attenuation rate for 4-L-S, sampling height in logarithmic scale ( $f = 6$  GHz).

A comparison of the variation of the attenuation rate of the dominant modes for 6 GHz and 10 GHz propagation shows that the sensitivity of field strength to a change of test point height is greater at the higher frequency.

*c. Mode Location Analysis*

As can be seen from Fig. 35, the imaginary part of mode d is the least negative of the four modes. This means that the field strength of mode d is the strongest. In increasing order, the modal attenuation rate is mode d, c, b, and then a for every sampling height (Figs. 33 and 34). The variation of mode d only is shown in Fig. 36.

By comparing Fig. 27 with Fig. 35, it can be seen that at 10 GHz the variation of each mode location is greater than that at 6 GHz. Thus, the higher the propagation frequency, the higher the sensitivity of the mode location to a change of test point height.

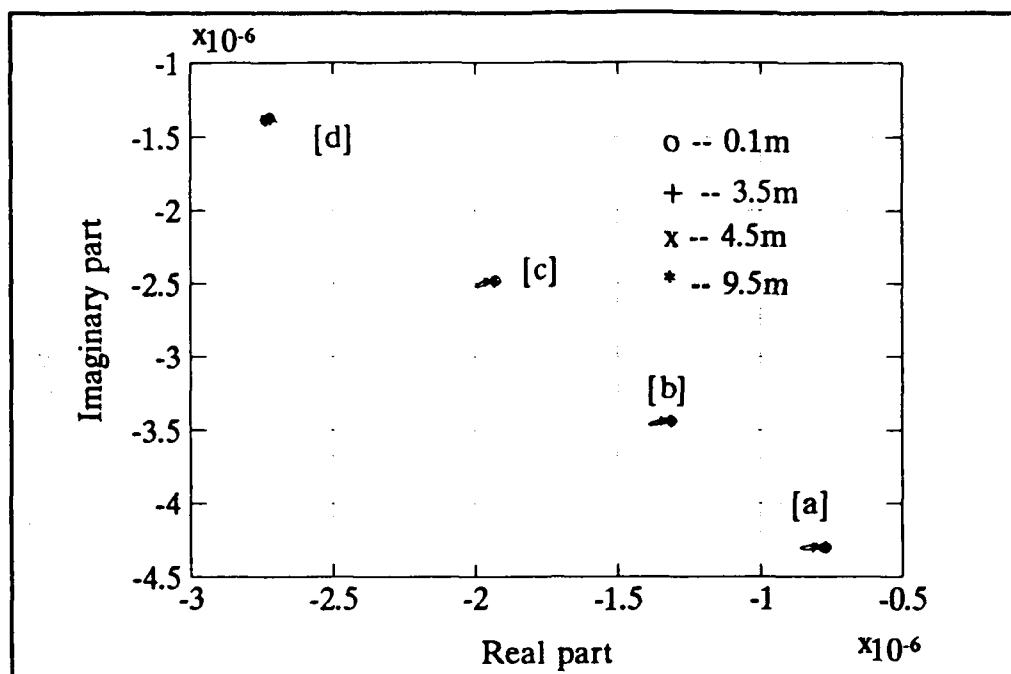


Figure 35. Mode location on the  $\beta-1$  complex plane for 4-L-S ( $f = 6$  GHz).

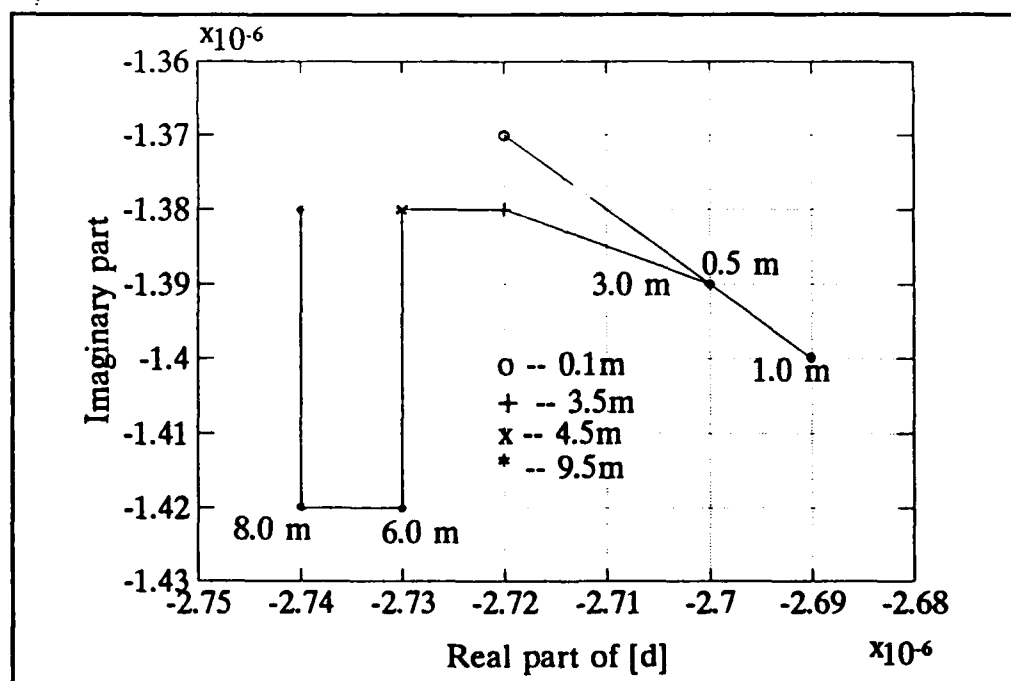


Figure 36. Dominant mode location on the  $\beta-1$  complex plane for 4-L-S ( $f = 6$  GHz).

#### 4. 3 GHz

##### *a. Path Loss Analysis*

(1) *Class One.* In Figs. 37 and 38, the receiver range is fixed at 60 km; and in Figs. 39 and 40, the receiver range is fixed at 120 km. The path loss as a function of the receiver height when the test point is located at 0.1 m and at 3.5 m is shown in Fig. 37. The path loss curves for 3 GHz propagation are similar to those for *class one* at 15 GHz. The two curves for 3 GHz propagation are extremely close to each other.

(2) *Class Two.* The path losses when the test point is selected at 4.5 m and at 9.5 m are shown in Fig. 38. The path loss curves have the same features as those for *class one* at 15 GHz propagation. Again, the difference is that the curves for 3 GHz propagation are closer to each other. The path loss ratios for 3 GHz propagation are not plotted because they are too small to be presented accurately.

(3) *Discussion.* When the test point is selected at any of the four locations, the path loss for a 6 GHz signal is larger than that for a 3 GHz signal at every receiver height. This can be seen by comparing Fig. 29 with Fig. 37 and Fig. 30 with Fig. 38. Thus, between 3 GHz and 6 GHz, the lower the propagation frequency, the greater the enhancement of the field strength by the duct. This is different from the case when the frequency is varied from 6 GHz to 15 GHz. This is explored in Chapter III.

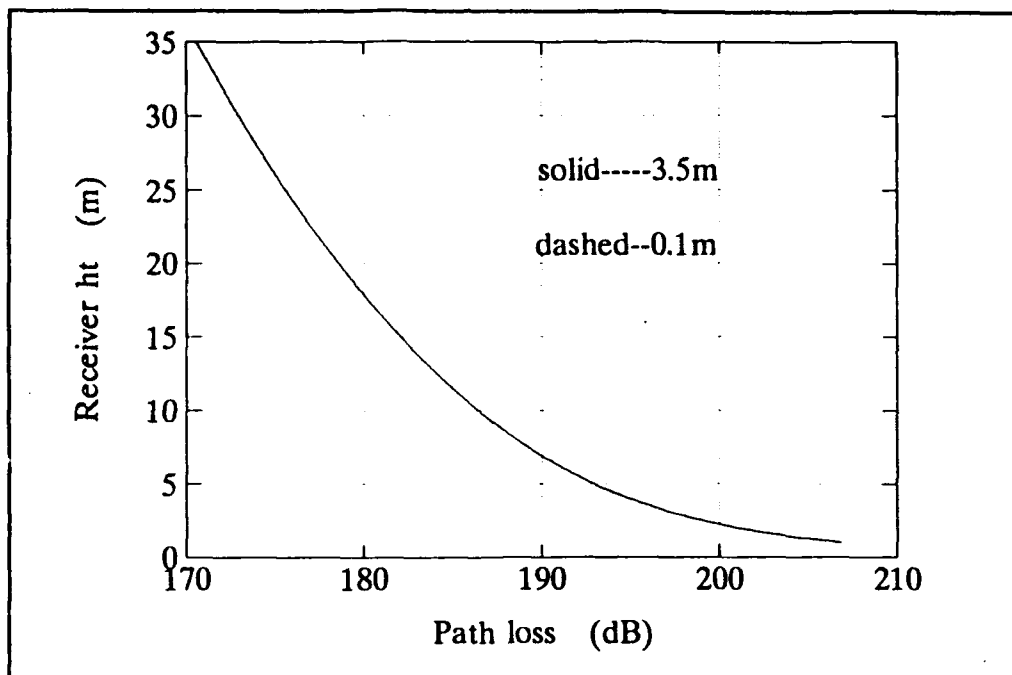


**Figure 37.** Path loss for 4-L-S, test points at 0.1 m and 3.5 m ( $f = 3$  GHz,  $r = 60$  km).

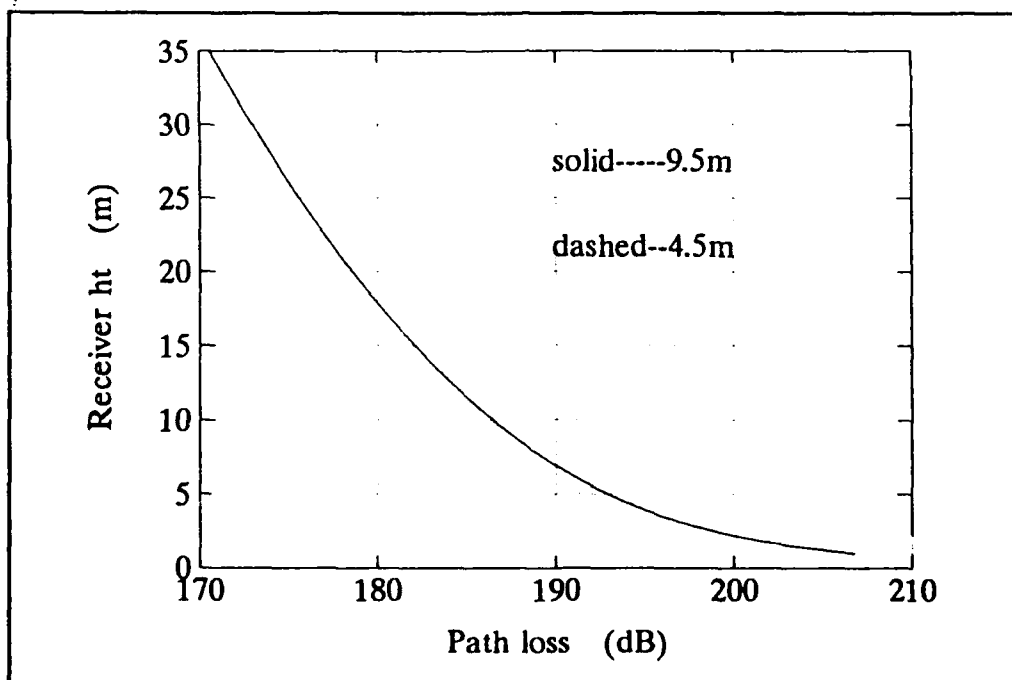


**Figure 38.** Path loss for 4-L-S, test points at 4.5 m and 9.5 m ( $f = 3$  GHz,  $r = 60$  km).

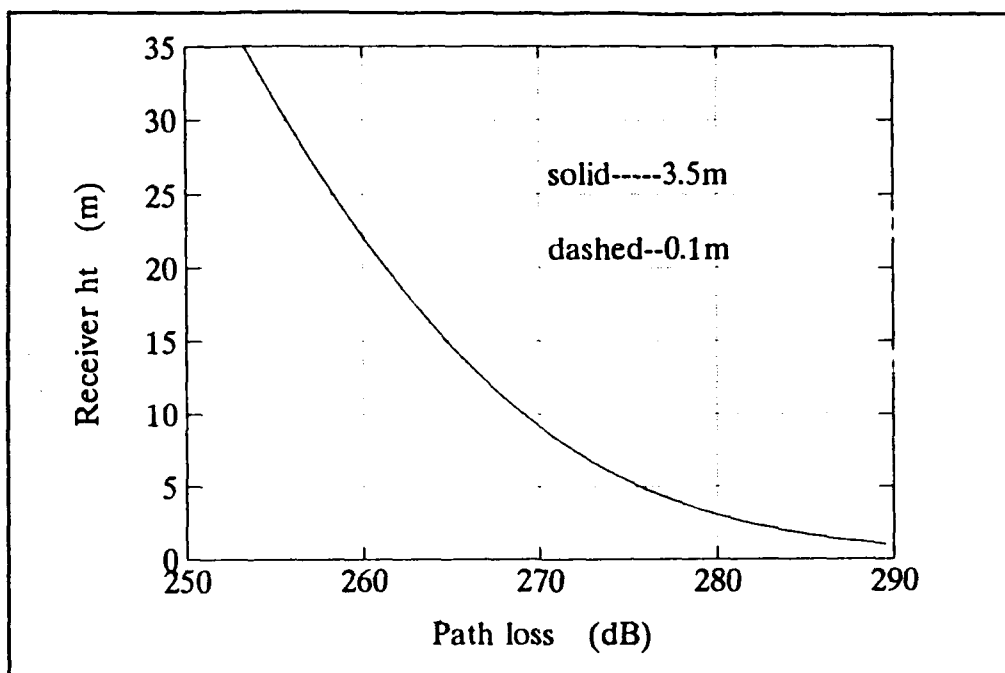


Figure 39. Path loss for 4-L-S, test points at 0.1 m and 3.5 m ( $f = 3$  GHz,  $r = 120$  km).

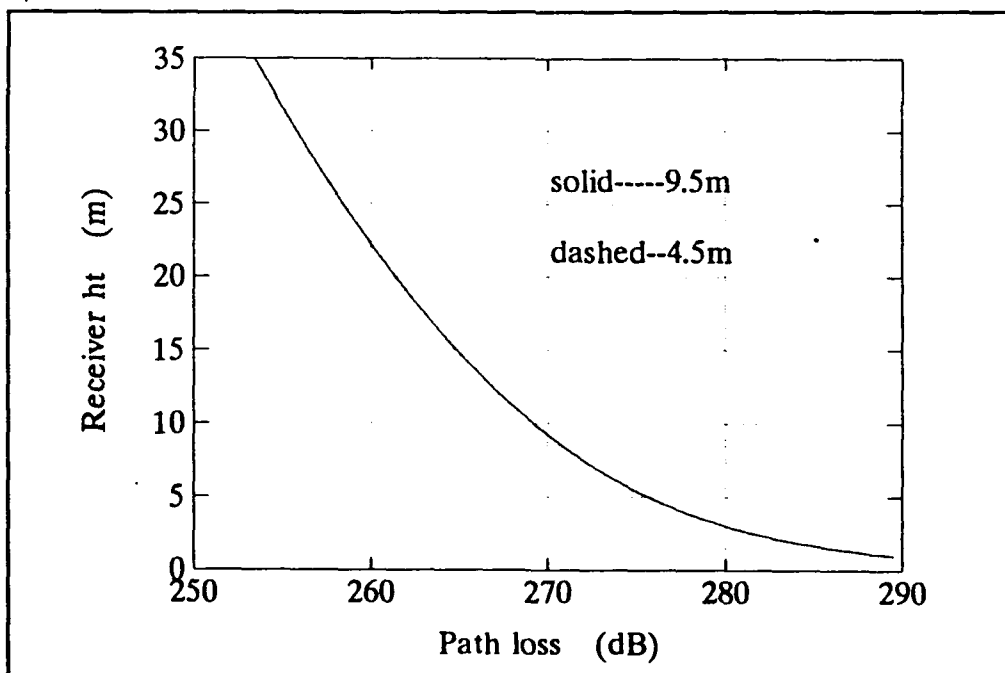


Figure 40. Path loss for 4-L-S, test points at 4.5 m and 9.5 m ( $f = 3$  GHz,  $r = 120$  km).

*b. Attenuation Rate Analysis*

Three modes are found with attenuation rates lower than 5 dB/km (Figs. 41 and 42). The dominant mode is mode c. It has an attenuation rate smaller than those of the other two modes by at least 1 dB/km at every sampling height. The attenuation rate of each mode varies less than 0.05 dB/km between the two sampling classes.

A comparison of the variation of the attenuation rate of the dominant modes for 3 GHz and 6 GHz propagation shows that the sensitivity of field strength to a change of test point height is greater at the higher frequency.

*c. Mode Location Analysis*

As can be seen from Fig. 43, the imaginary part of mode c is the least negative of the three modes. This means that the field strength of mode c is the strongest. The modal attenuation rate increases from mode c to b to a for every sampling height (see Figs. 41 and 42). The variation of mode c only is shown in Fig. 44.

By comparing Fig. 36 with Fig. 43, it can be seen that the variation of each mode location at 6 GHz is greater than that at 3 GHz. Thus, the higher the propagation frequency, the greater the sensitivity of the mode location to a change of test point height.

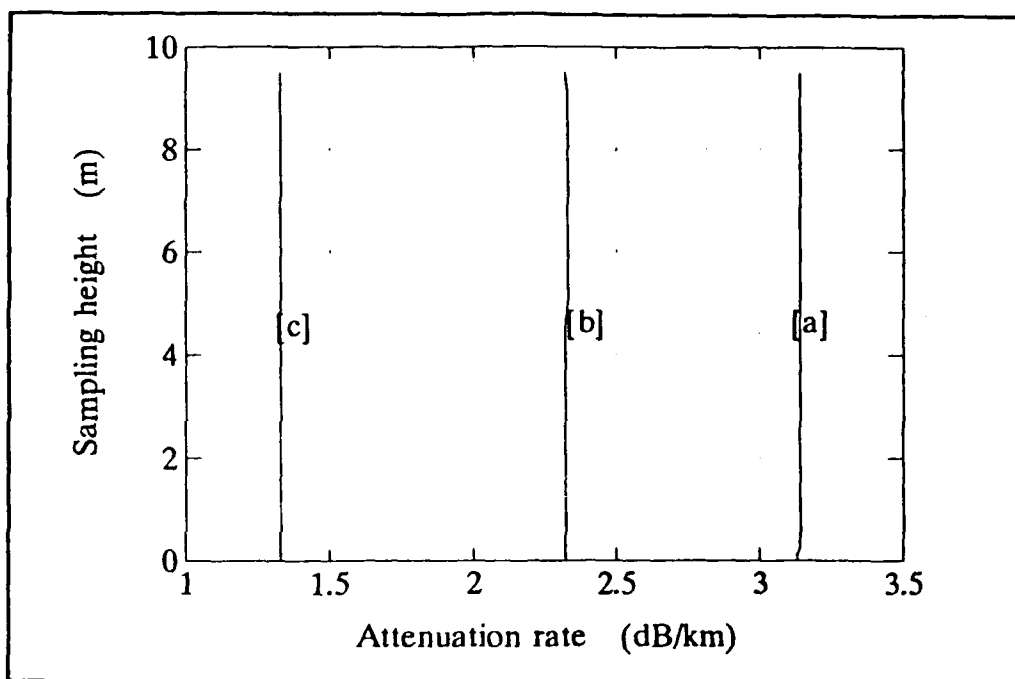


Figure 41. Modal attenuation rate for 4-L-S ( $f = 3$  GHz).

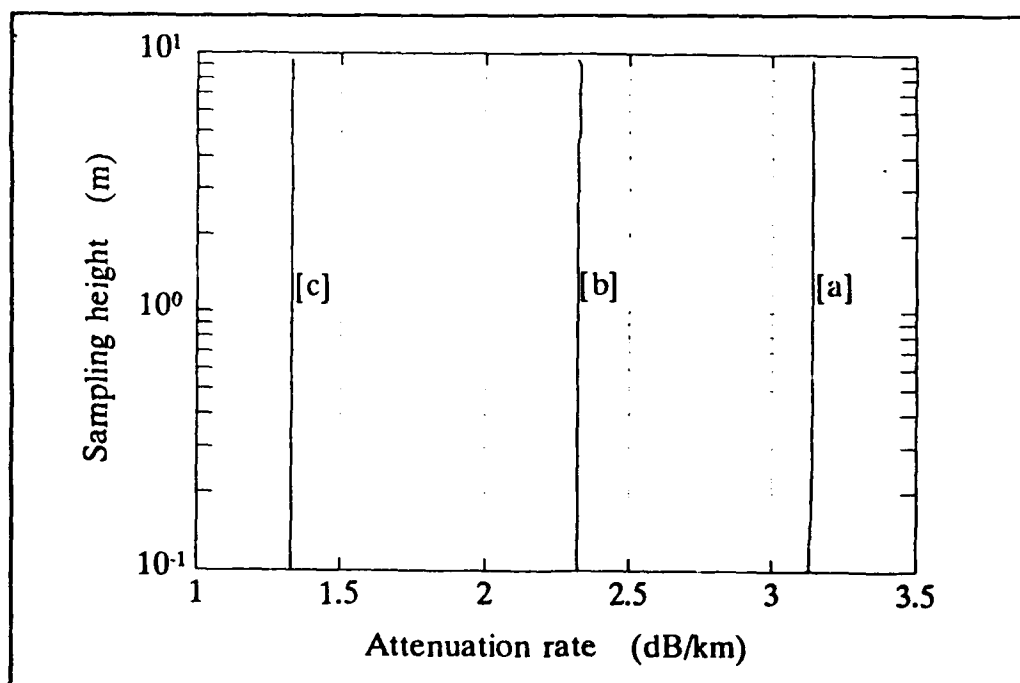


Figure 42. Modal attenuation rate for 4-L-S, sampling height in logarithmic scale ( $f = 3$  GHz).



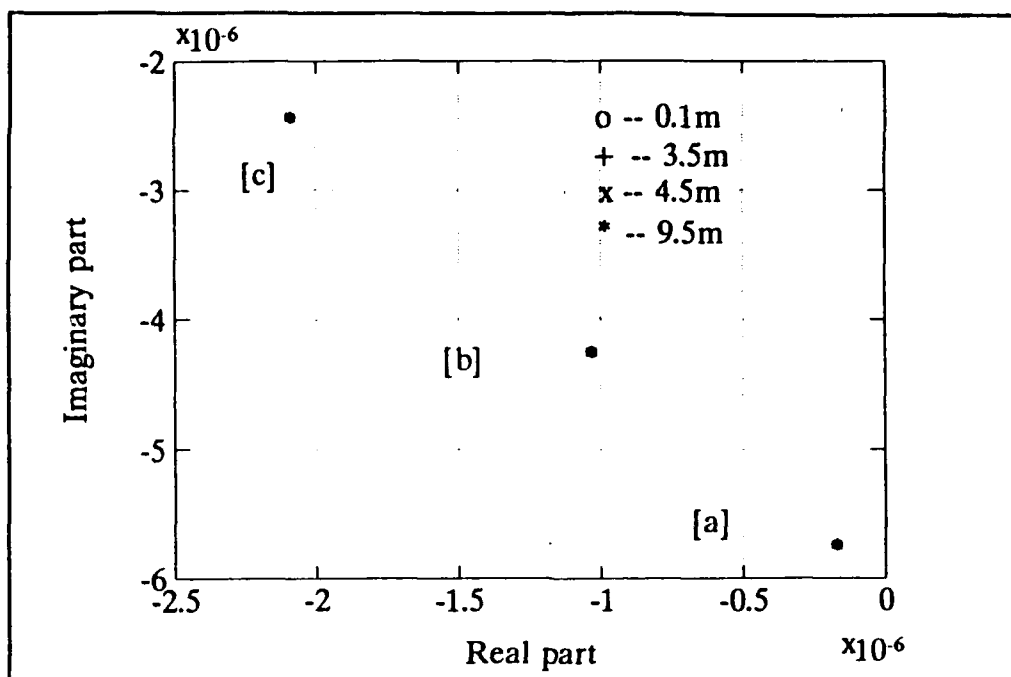


Figure 43. Mode location on the  $\beta-1$  complex plane for 4-L-S ( $f = 3$  GHz).

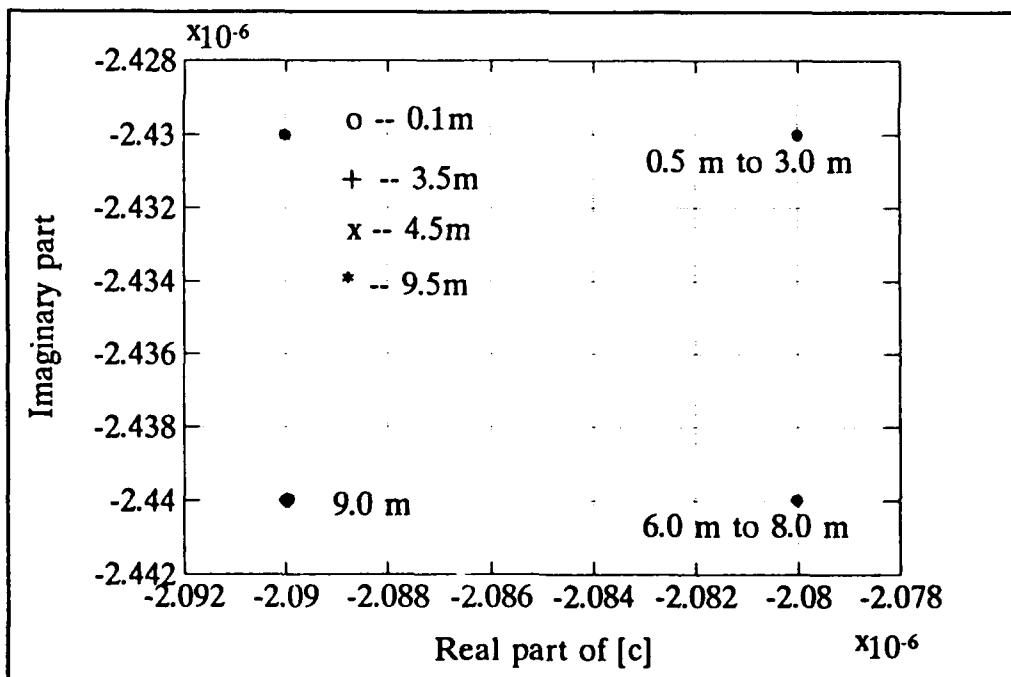


Figure 44. Dominant mode location on the  $\beta-1$  complex plane for 4-L-S ( $f = 3$  GHz).

### C. FIVE-LINEAR-SEGMENT APPROXIMATION

In this section, the reference *M*-profile shown in Figs. 1 and 2 is approximated with 5-L-S. This approximate *M*-profile has six endpoints consisting of one variable test point and five fixed points at the heights of 0, 0.5, 4, 10, and 80 m. The 5-L-S for *class one* and *class two* are shown in Figs. 45 and 46, respectively.

The difference between 4-L-S and 5-L-S is that the latter has one more fixed point than the former. This fixed point is selected at 0.5 m on the reference *M*-profile and is close to the point with the largest curvature (at 1.08 m). With this fixed point, the 5-L-S is a closer approximation to the reference *M*-profile than the 4-L-S. This can be seen by comparing Fig. 3 with Fig. 45 and Fig. 4 with Fig. 46.

#### 1. 15 GHz

This subsection investigates the effect of sampling the test point for 15 GHz propagation. The height of the receiver is varied from 1 m to 35 m at 0.1 m increments at a range of either 60 km or 120 km from the transmitter. For these ranges and heights, the receiver is located well into the diffraction region. These same parameters are also utilized at the other three frequencies and will not be further mentioned.

##### *a. Path Loss Analysis*

(1) *Class One.* In Fig. 47 through Fig. 50, the receiver range is fixed at 60 km; and in Fig. 51 through Fig. 54, the receiver range is fixed at 120 km. The path loss as a function of receiver height when the test point is located at 0.1 m and

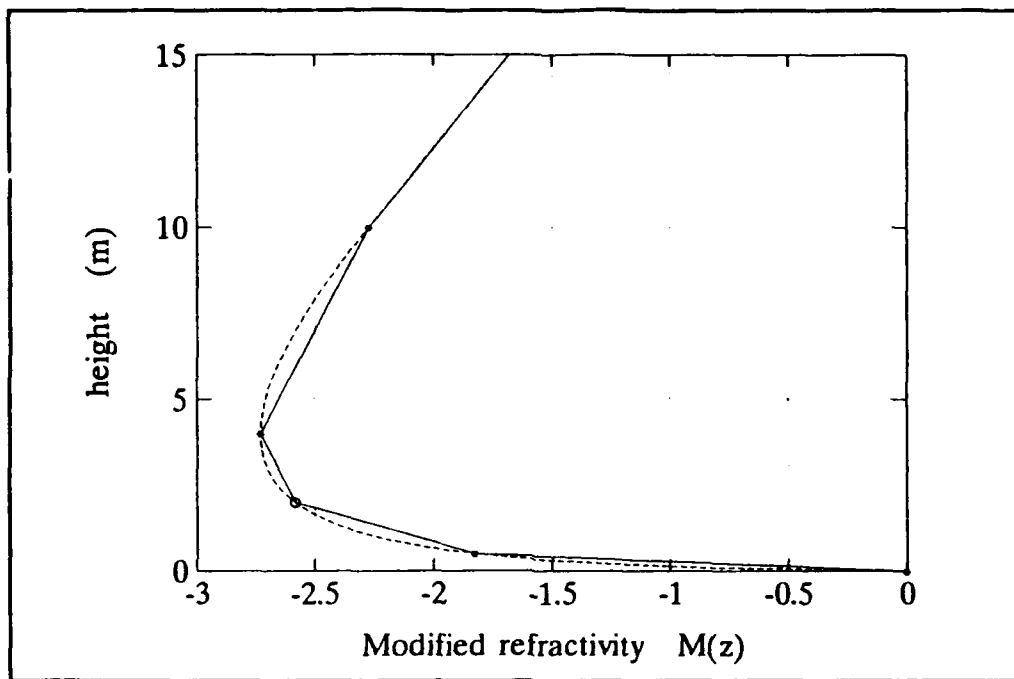


Figure 45. 5-L-S profile, test point within the duct (*class one*).

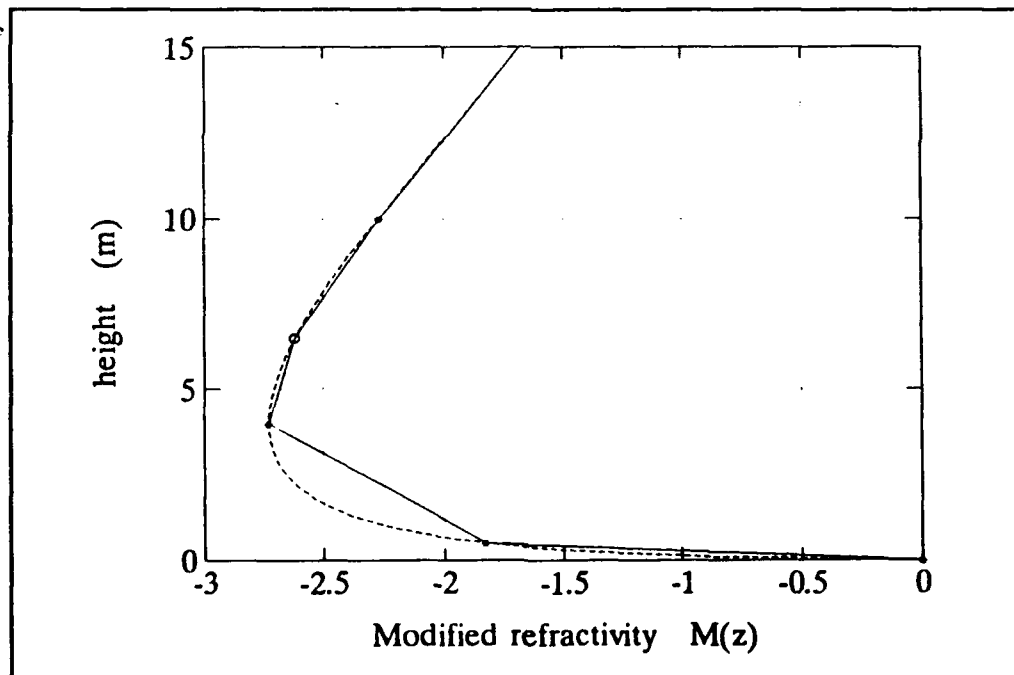


Figure 46. 5-L-S profile, test point above the duct (*class two*).

and at 3.5 m, respectively, is shown in Fig. 47. The resulting path loss curves are representative of the path loss curves of *class one*. This observation is also true for propagation at the other three frequencies. In Fig. 47, it is seen that the path loss increases with decreasing receiver height. The rate of increase is higher when the receiver is located in the duct. Hence, the field strength in the duct is weaker.

The difference in path losses is shown in Fig. 48. It is observed that this difference decreases with increasing receiver height and that the decreasing rate is smaller when the receiver is located in the duct. Hence, when the test point is moved from 0.1 m to 3.5 m, the sensitivity of the height-gain function is greater when the receiver is lower. Note that the sign of the path loss ratio is different from that of the 4-L-S when the test point is moved from 0.1 m to 3.5 m.

(2) *Class Two*. The path losses when the test point is selected at 4.5 m and at 9.5 m are shown in Fig. 49. These are representative of all path loss curves for which the test point is sampled above the duct. This observation is also true for propagation at the other three frequencies. The path loss curves are similar to those of *class one*.

The difference in path losses is shown in Fig. 50 where it can be seen that the path loss ratio has a maximum between 4 m and 5 m which is just above the duct. An interesting feature observed is that the variation of this curve with receiver height is quite different when the receiver is located in the duct than when it is located above the duct. The gradient of the path loss ratio curve has different signs below 4 m and above 5 m. The difference increases as the receiver

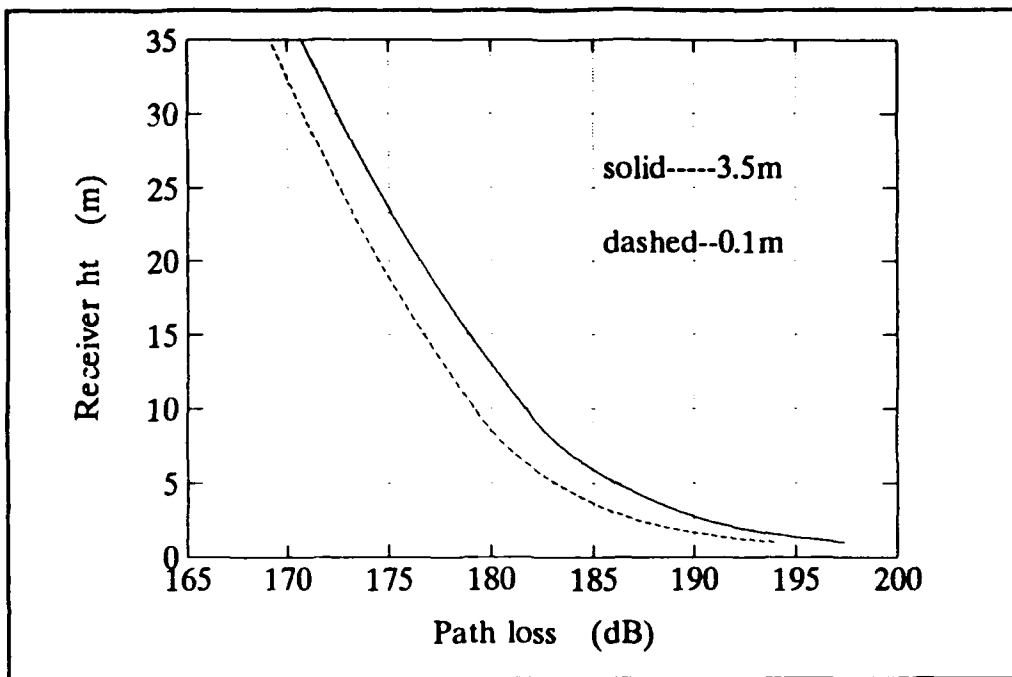


Figure 47. Path loss for 5-L-S, test points at 0.1 m and 3.5 m ( $f = 15$  GHz,  $r = 60$  km).

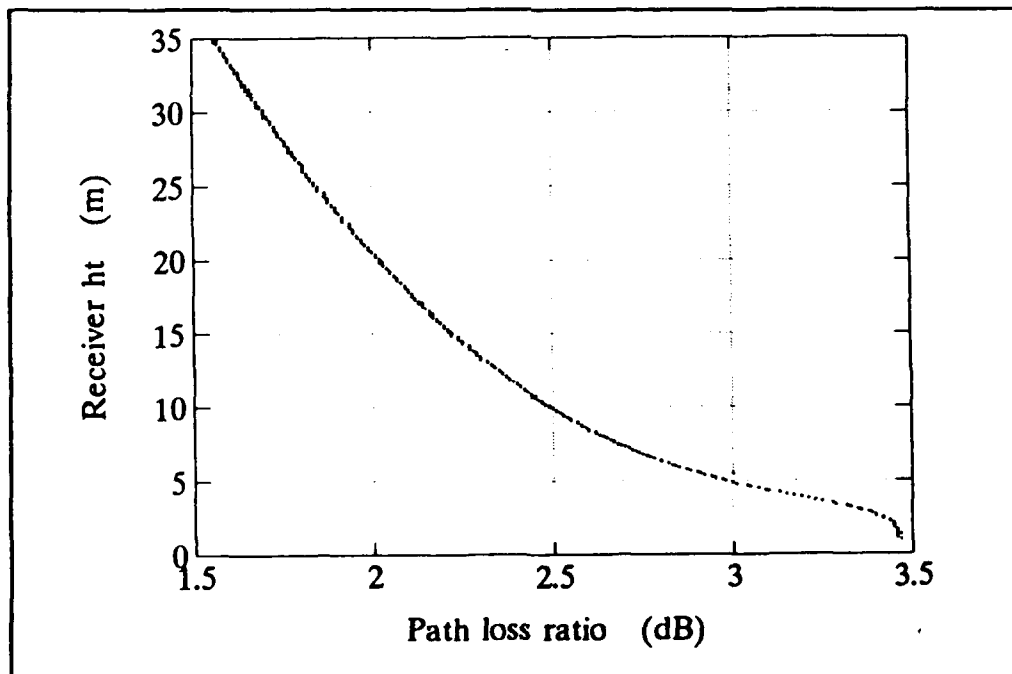


Figure 48. Path loss ratio.

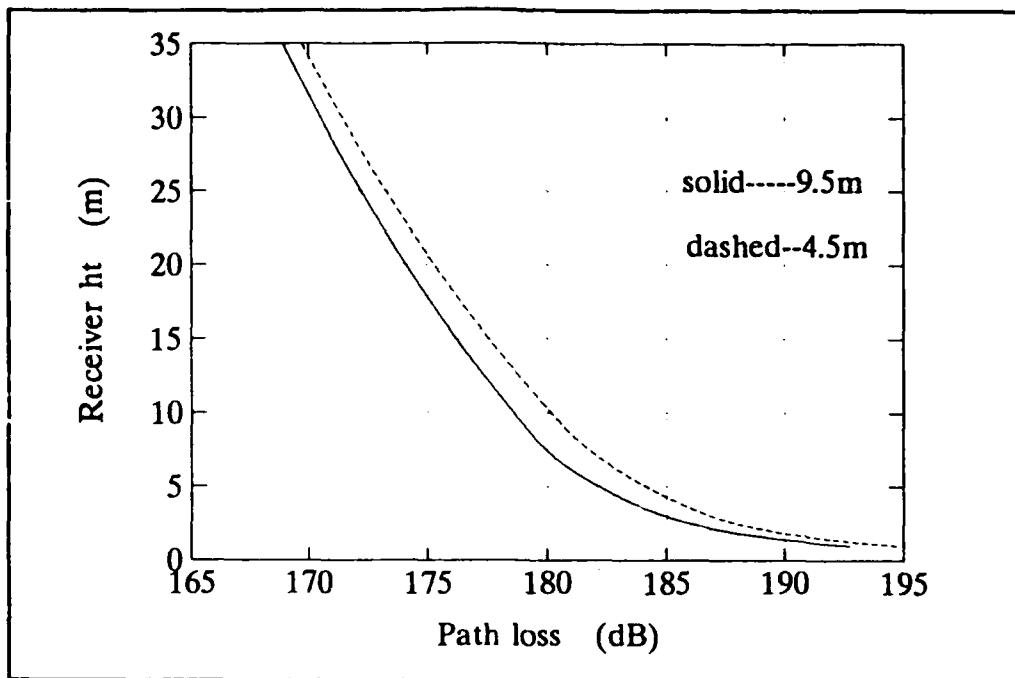


Figure 49. Path loss for 5-L-S, test points at 4.5 m and 9.5 m ( $f = 15$  GHz,  $r = 60$  km).

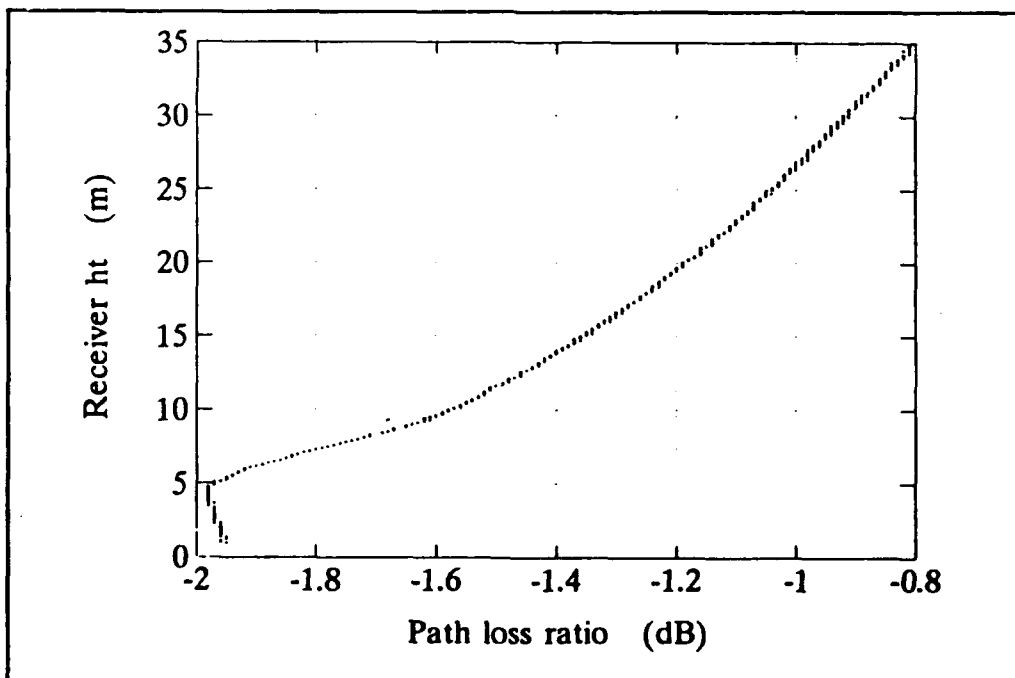


Figure 50. Path loss ratio.

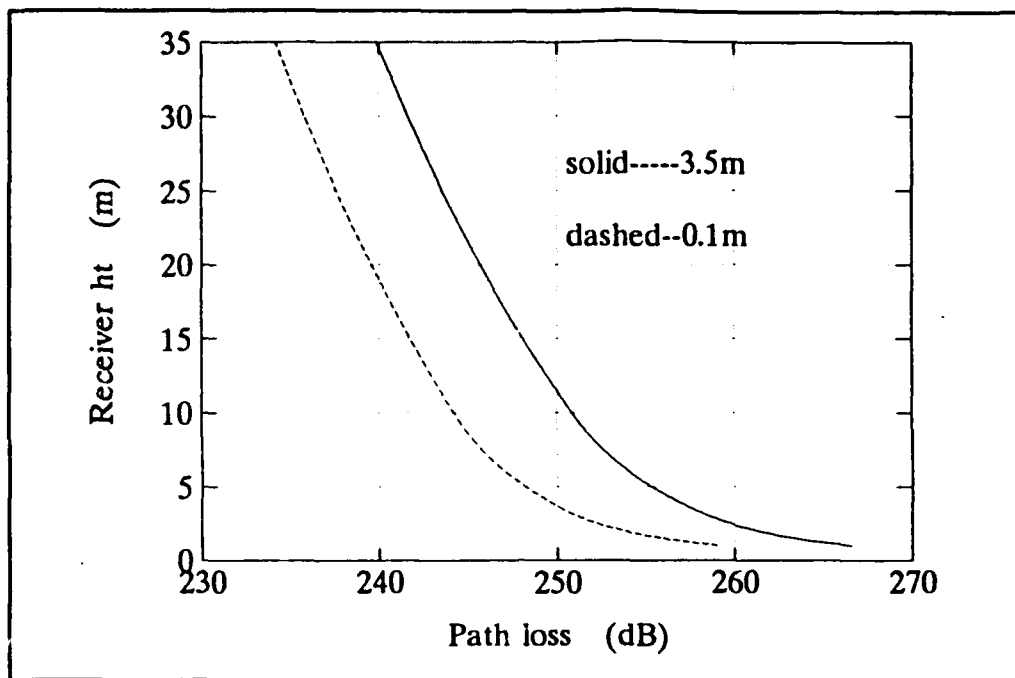


Figure 51. Path loss for 5-L-S, test points at 0.1 m and 3.5 m ( $f = 15$  GHz,  $r = 120$  km).

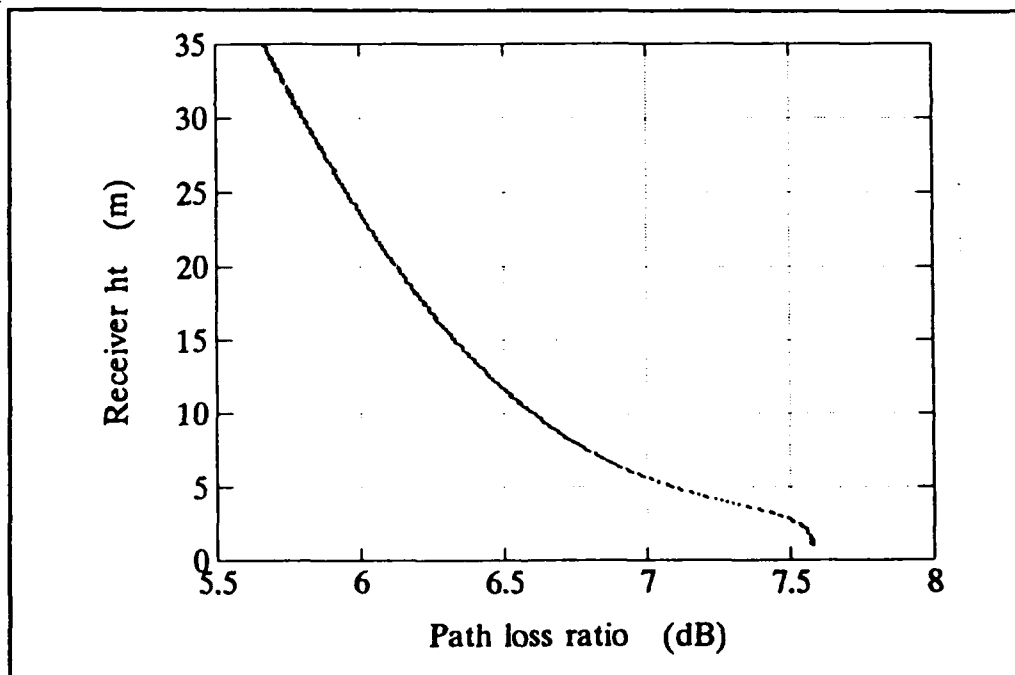


Figure 52. Path loss ratio.

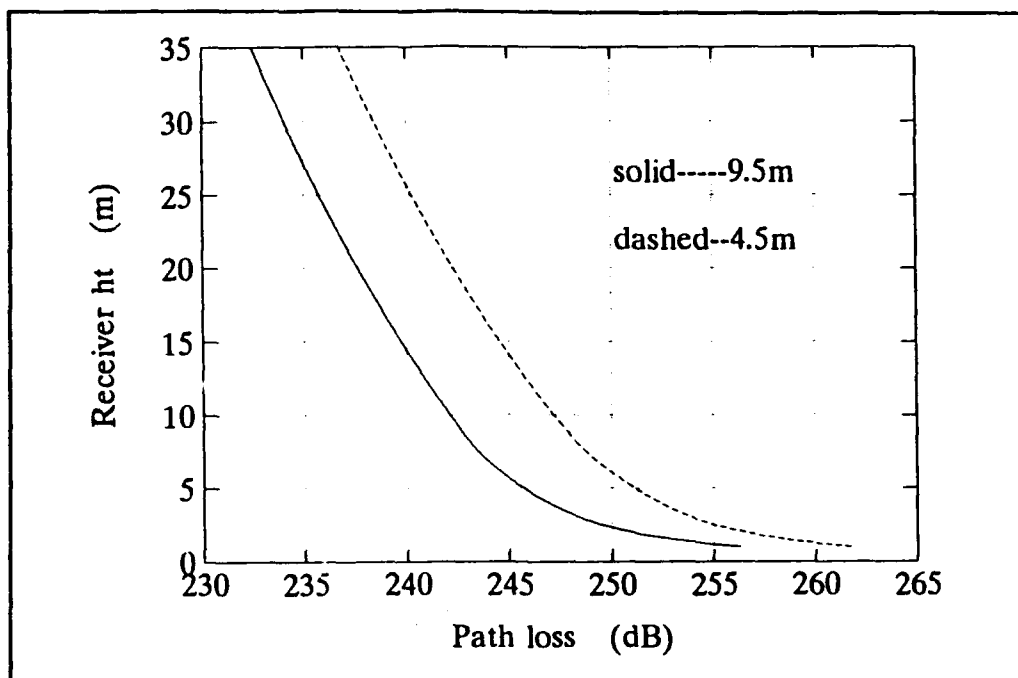


Figure 53. Path loss for 5-L-S, test points at 4.5 m and 9.5 m ( $f = 15$  GHz,  $r = 120$  km).

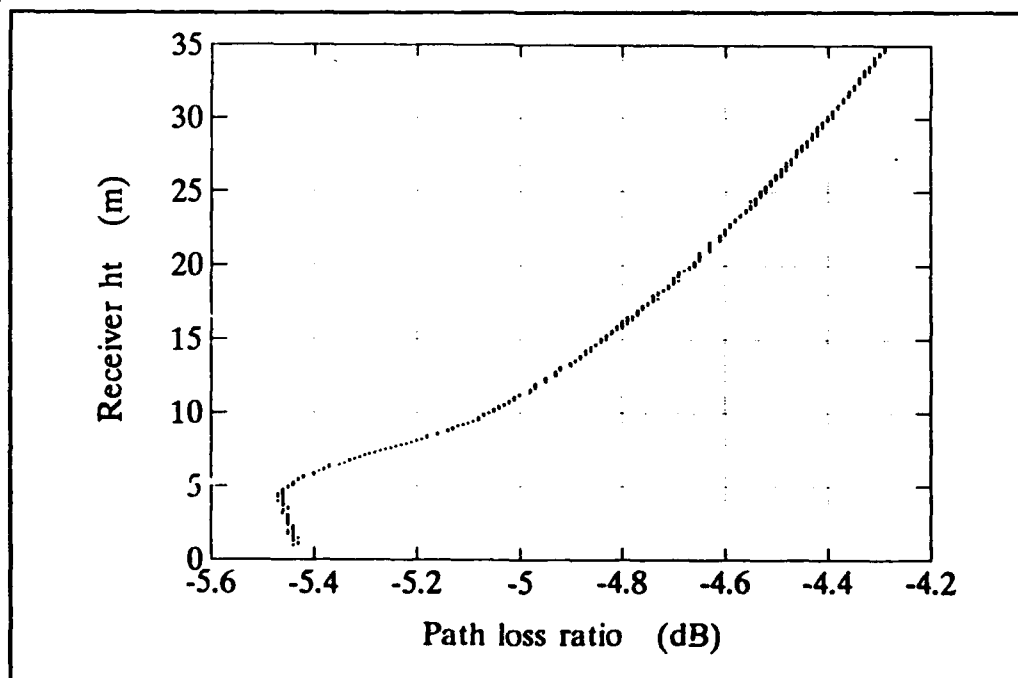


Figure 54. Path loss ratio.



height increases when the receiver is below 4 m. It decreases with increasing height when the receiver is above 5 m. It is almost a constant between 4 m and 5 m. This means that when the test point is moved from 4.5 to 9.5 m the sensitivity of the height-gain function is smaller for greater receiver heights unless the receiver is lower than 5 m.

(3) *Discussion.* From Figs. 47 and 48, it is seen that the field strength is weaker at every height when the test point is at 3.5 m than when it is at 0.1 m. Also, by comparing Fig. 47 to Fig. 49, it is seen that, amongst these four particular situations, the strongest field occurs when the test point is located at 9.5 m. The path losses when the test point is located at 3.5 m and at 4.5 m are so close that they are not compared.

#### *b. Attenuation Rate Analysis*

Three modes are found with attenuation rates lower than 5 dB/km (Figs. 55 and 56). The dominant mode is mode b. It has a smaller attenuation rate than the other two modes by at least 2 dB/km for every sampling height. Thus, at 60 km, the path loss of this dominant mode will be at least 120 dB less than the other two modes. The attenuation rate of mode b fluctuates by 0.2 dB/km for *class one* and fluctuates by 0.1 dB/km for *class two*. Between the sampling height of 1.5 m and 3 m, the attenuation rate of mode b reaches a maximum. Thus, for 15 GHz propagation, the field strength is more sensitive to test point variation in *class one* than in *class two*.

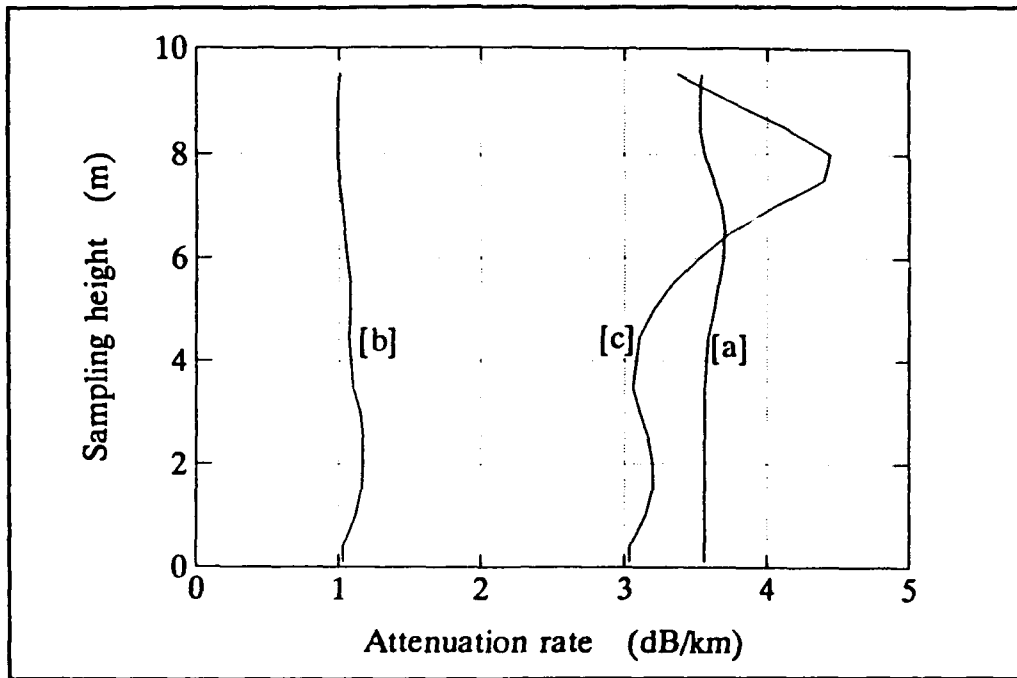


Figure 55. Modal attenuation rate for 5-L-S ( $f = 15$  GHz).

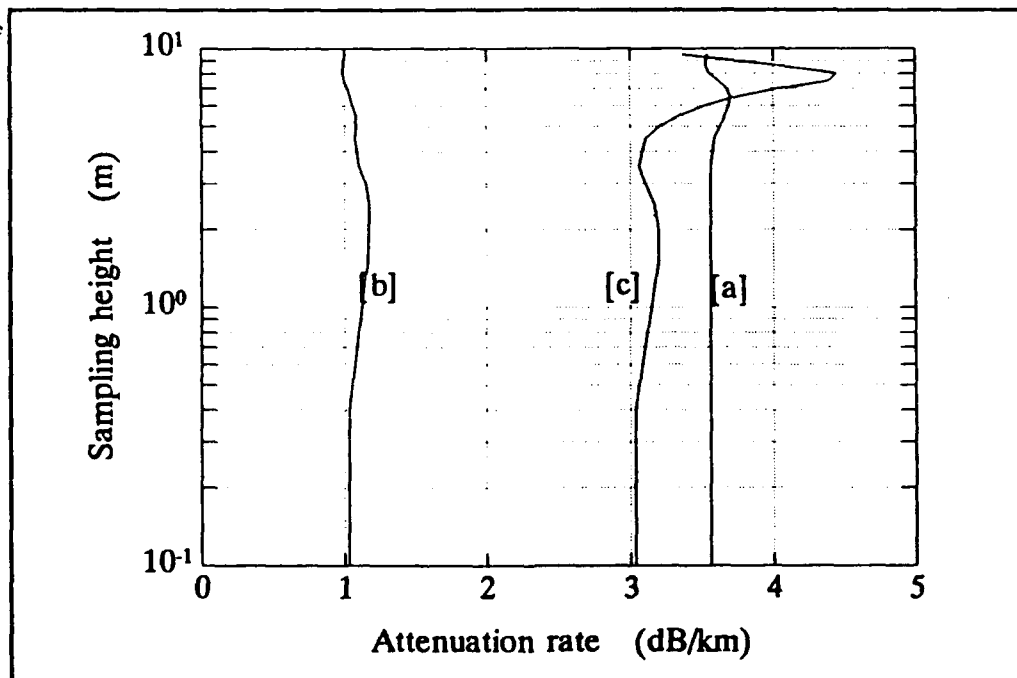


Figure 56. Modal attenuation rate for 5-L-S, sampling height in logarithmic scale ( $f = 15$  GHz).

### *c. Mode Location Analysis*

It can be seen from Fig. 57 that the imaginary part of mode b is consistently the least negative of the three modes. This implies that mode b is the strongest mode having the smallest range attenuation rate. Mode a in general has the strongest attenuation. However, the field strength of mode c becomes the weakest for some heights of the test point in *class two*. This is also apparent in Figs. 55 and 56, where the attenuation rate of mode c becomes greater than that of mode a when the test point is located at a height between 6.4 m and 9.2 m.

The variation of mode b only is shown in Fig. 58. It can be seen that when the test point height is varied from 0.1 m to 3.5 m the imaginary part of this mode varies more than when the test point height is varied from 4.5 m to 9.5 m. Thus, the sensitivity of the field strength is greater for *class one* than *class two*. This can also be observed in Figs. 55 and 56.

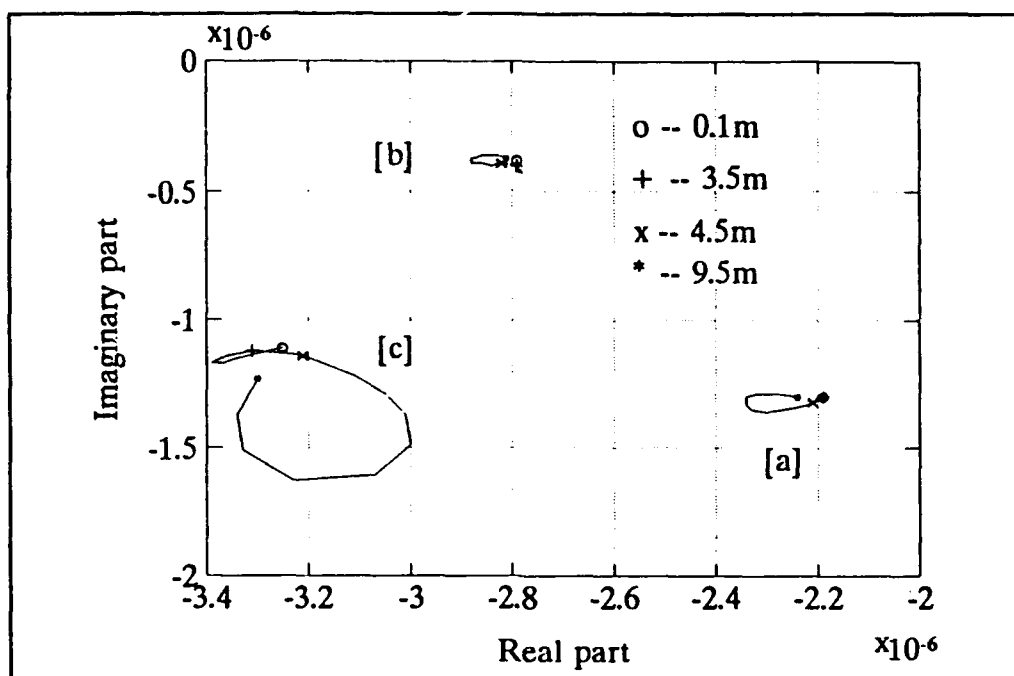


Figure 57. Mode location on the  $\beta-1$  complex plane for 5-L-S ( $f = 15$  GHz).

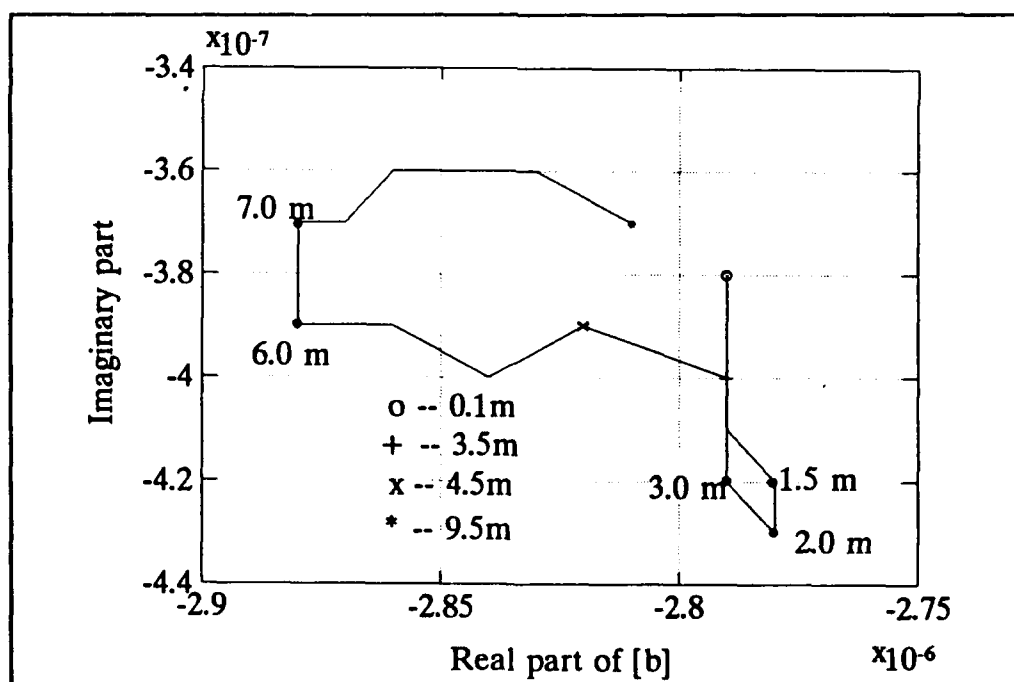


Figure 58. Dominant mode location on the  $\beta-1$  complex plane for 5-L-S ( $f = 15$  GHz).

## 2. 10 GHz

### *a. Path Loss Analysis*

(1) *Class One.* In Fig. 59 through Fig. 62, the receiver range is fixed at 60 km; and in Fig. 63 through Fig. 66, the receiver range is fixed at 120 km. The path loss as a function of receiver height when the test point is located at 0.1 m and at 3.5 m is shown in Fig. 59. The path loss curves are similar to those for *class one* at 15 GHz propagation. The difference in path losses is shown in Fig. 60. It has features similar to that of *class one* at 15 GHz.

(2) *Class Two.* The path losses when the test point is selected at 4.5 m and at 9.5 m are shown in Fig. 61. The path loss curves are similar to those for *class one* at 15 GHz.

The difference in path losses is shown in Fig. 62. This difference remains almost a constant with a less than 0.02 dB deviation when the receiver is located in the duct and decreases with increasing receiver height when the receiver is located above the duct. This means that the sensitivity of the height-gain function when the test point height is varied from 4.5 m to 9.5 m is smaller for a higher receiver and is almost a constant when the receiver is located in the duct. This relationship is different from that observed at 15 GHz.

(3) *Discussion.* The variation in field strength with respect to the choice of one of the four particular test point locations at 10 GHz is similar to the variation observed at 15 GHz.

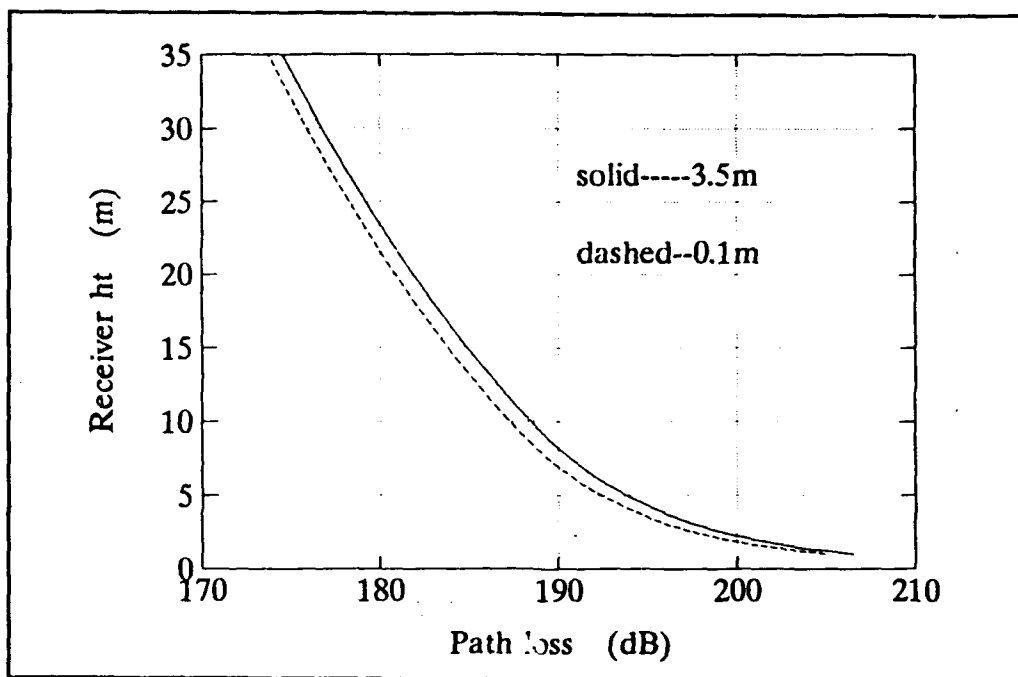


Figure 59. Path loss for 5-L-S, test points at 0.1 m and 3.5 m ( $f = 10$  GHz,  $r = 60$  km).

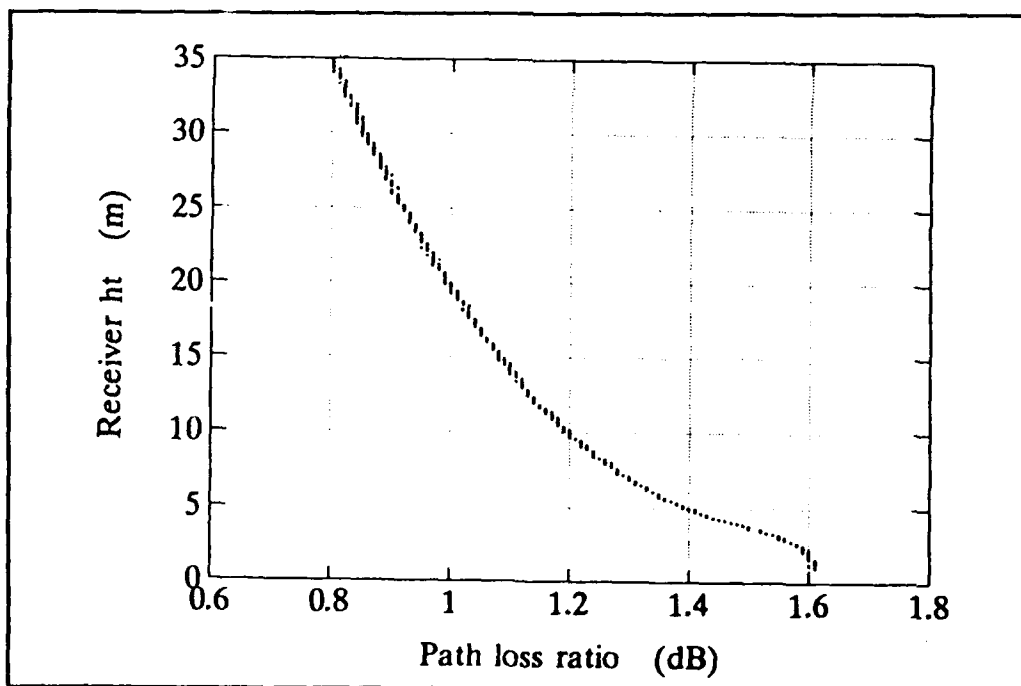
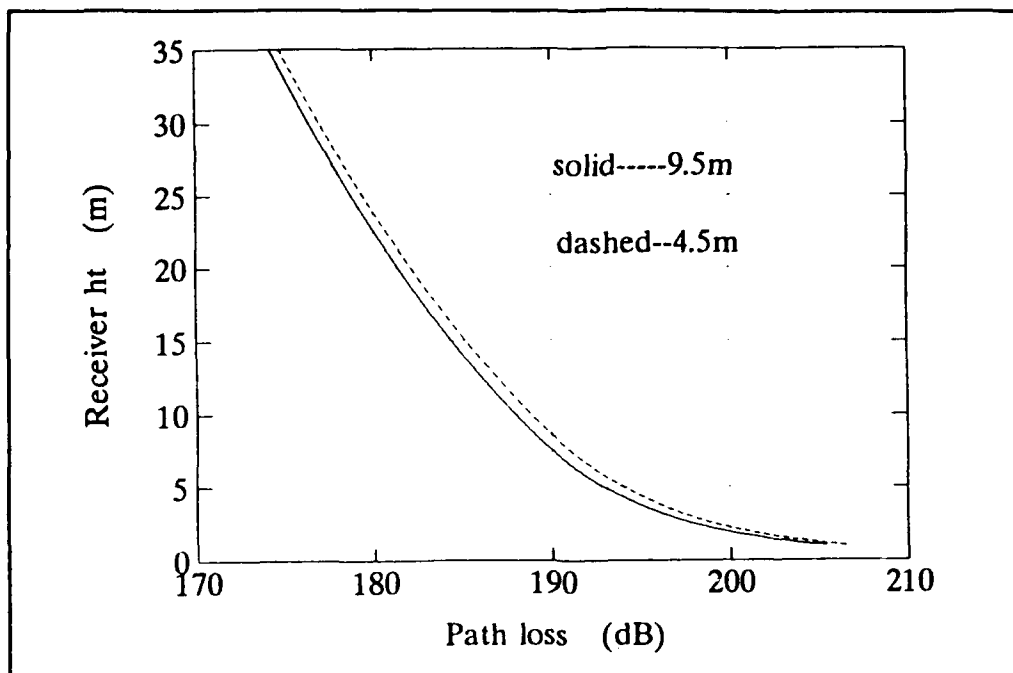
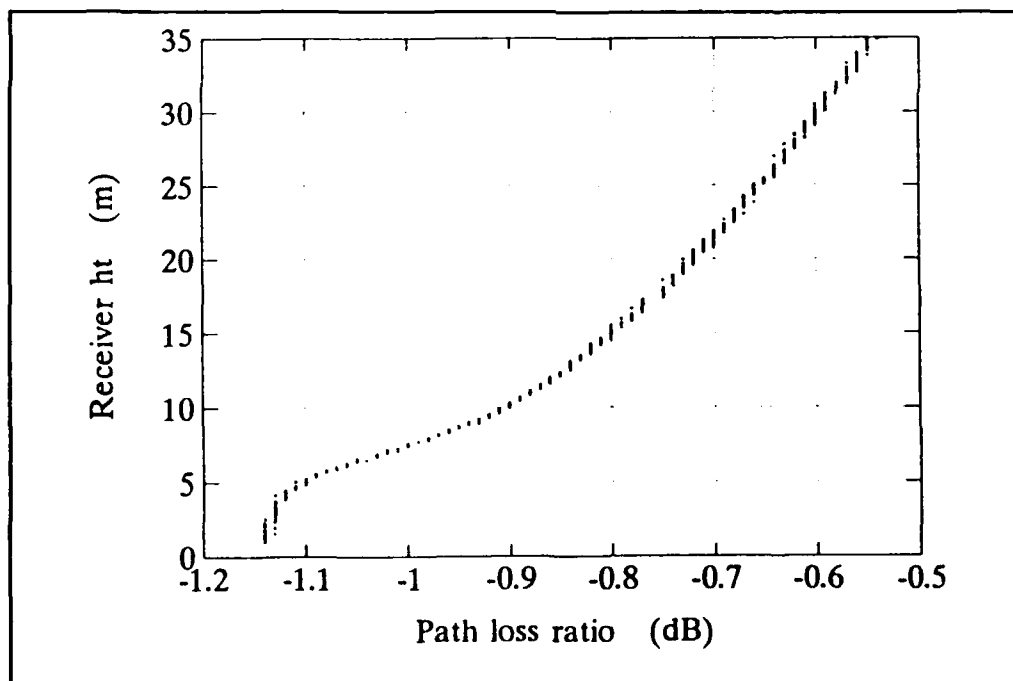


Figure 60. Path loss ratio.



**Figure 61.** Path loss for 5-L-S, test points at 4.5 m and 9.5 m ( $f = 10$  GHz,  $r = 60$  km).



**Figure 62.** Path loss ratio.

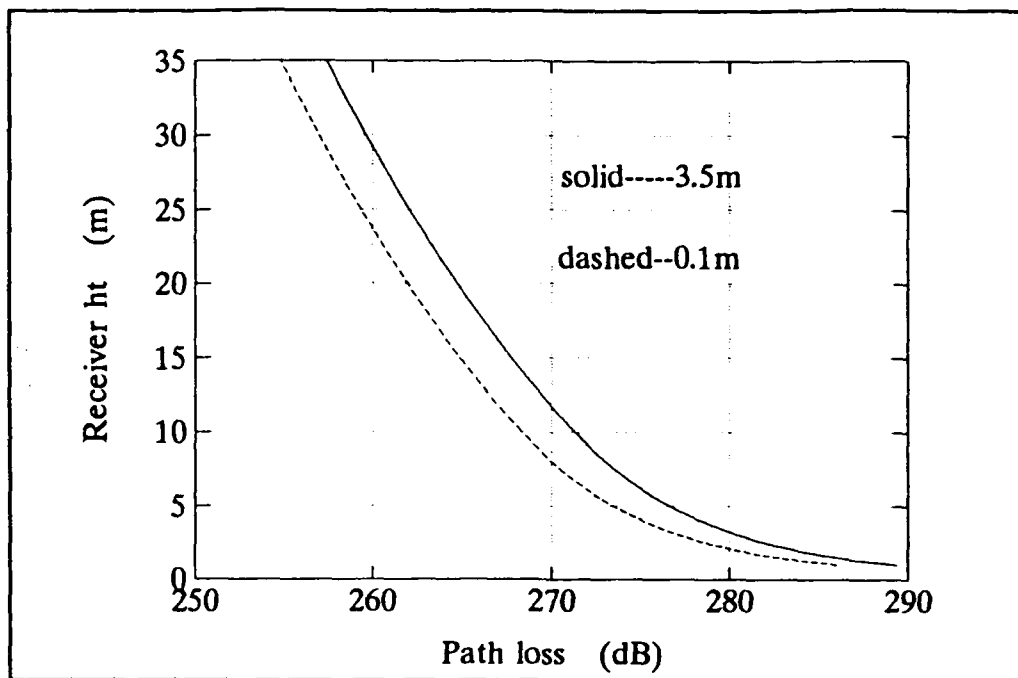


Figure 63. Path loss for 5-L-S, test points at 0.1 m and 3.5 m ( $f = 10$  GHz,  $r = 120$  km).

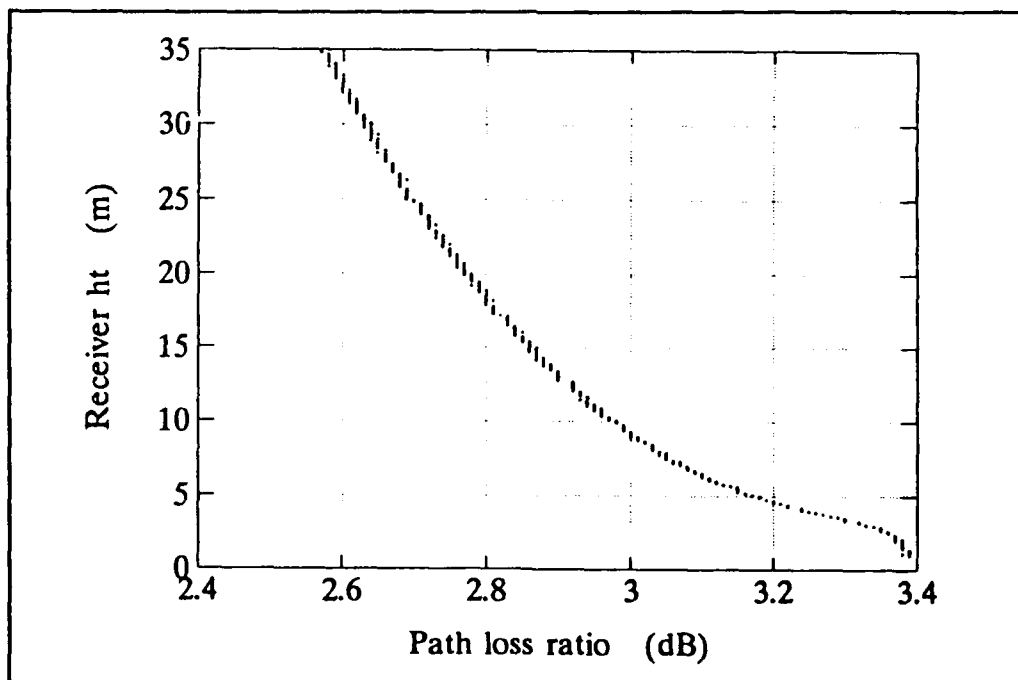


Figure 64. Path loss ratio.



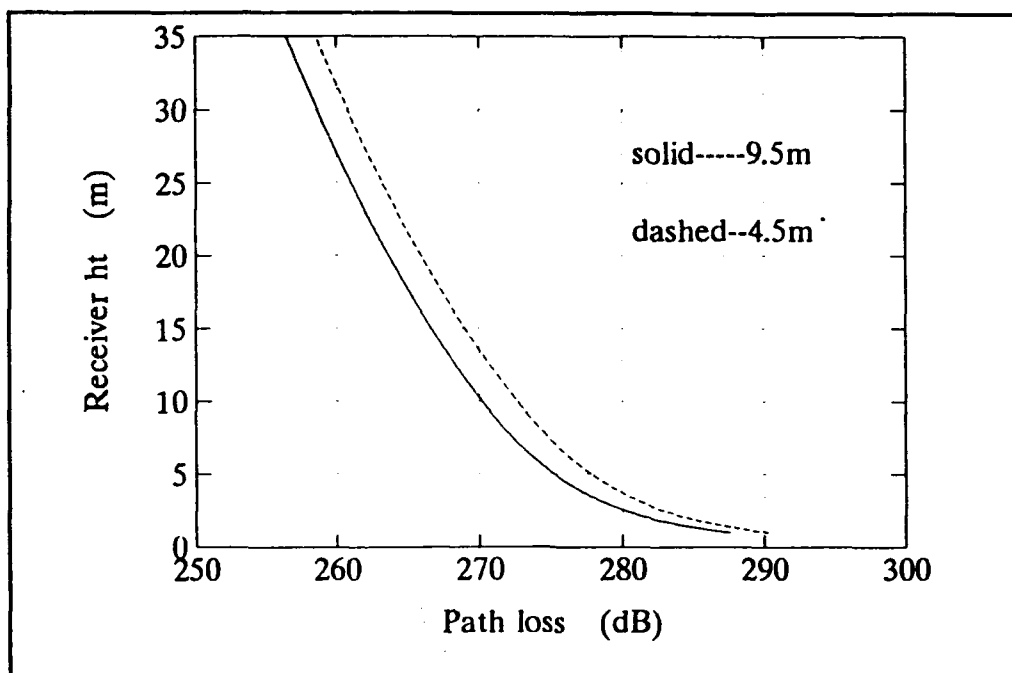


Figure 65. Path loss for 5-L-S, test points at 4.5 m and 9.5 m ( $f = 10$  GHz,  $r = 120$  km).

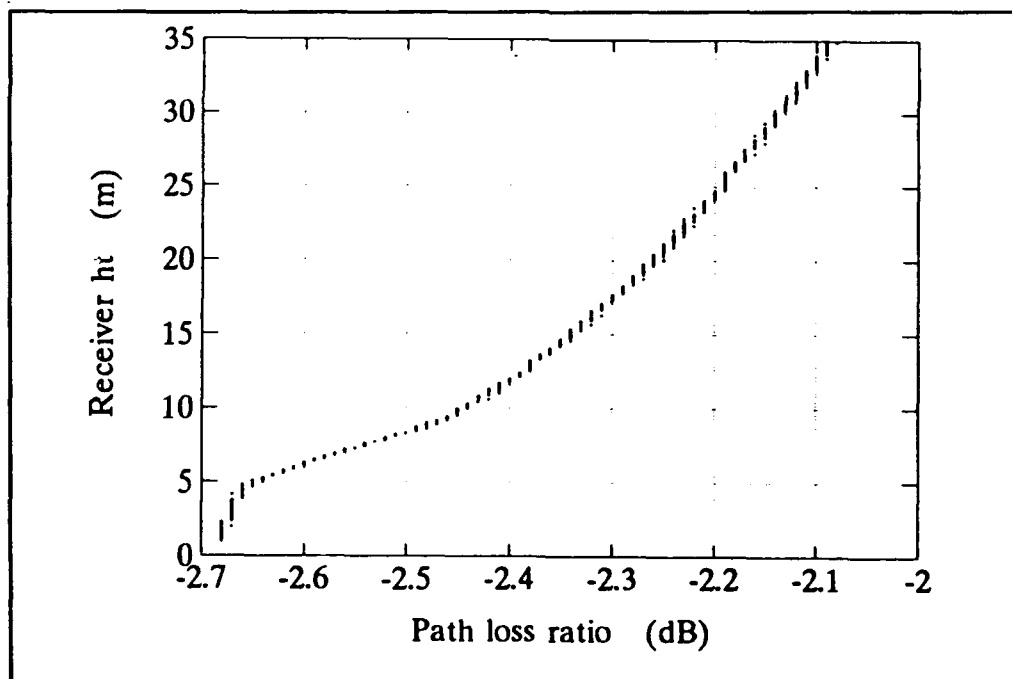


Figure 66. Path loss ratio.

When the test point is located at any of the four heights, the path loss for a 10 GHz signal is larger than that for a 15 GHz signal at every receiver height. This can be seen by comparing Fig. 47 with Fig. 59 and Fig. 49 with Fig. 61. It can, therefore, be concluded that the higher the propagation frequency, the greater the enhancement in the field strength by the duct.

When the test point is moved from 0.1 m to 3.5 m, the ratio of the path loss at these two test point heights changes from 1.61 dB, at 1 m receiver height, to 0.8 dB, at 35 m for 10 GHz propagation (see Fig. 60). For 15 GHz propagation, this ratio changes from 3.45 to 1.6 dB as shown in Fig. 48. It can be concluded from these figures that when the test point is moved from 0.1 m to 3.5 m the path loss ratio for 15 GHz propagation is greater than that for 10 GHz propagation at every receiver height. When the test point is moved from 4.5 m to 9.5 m, the path loss ratio for 15 GHz propagation is also greater than that for 10 GHz propagation. This can be seen by comparing Fig. 50 with Fig. 62. Consequently, when the test point is moved from 0.1 m to 3.5 m and from 4.5 m to 9.5 m, the sensitivity of the height-gain function at 10 GHz is lower than that at 15 GHz.

*b. Attenuation Rate Analysis*

Three modes are found with an attenuation rate lower than 5 dB/km (Figs. 67 and 68). The dominant mode is mode c. It has an attenuation rate smaller than those of the other two modes by at least 1.6 dB/km at every sampling height. With the test point sampled between 6 m and 7 m, the attenuation rate of mode c

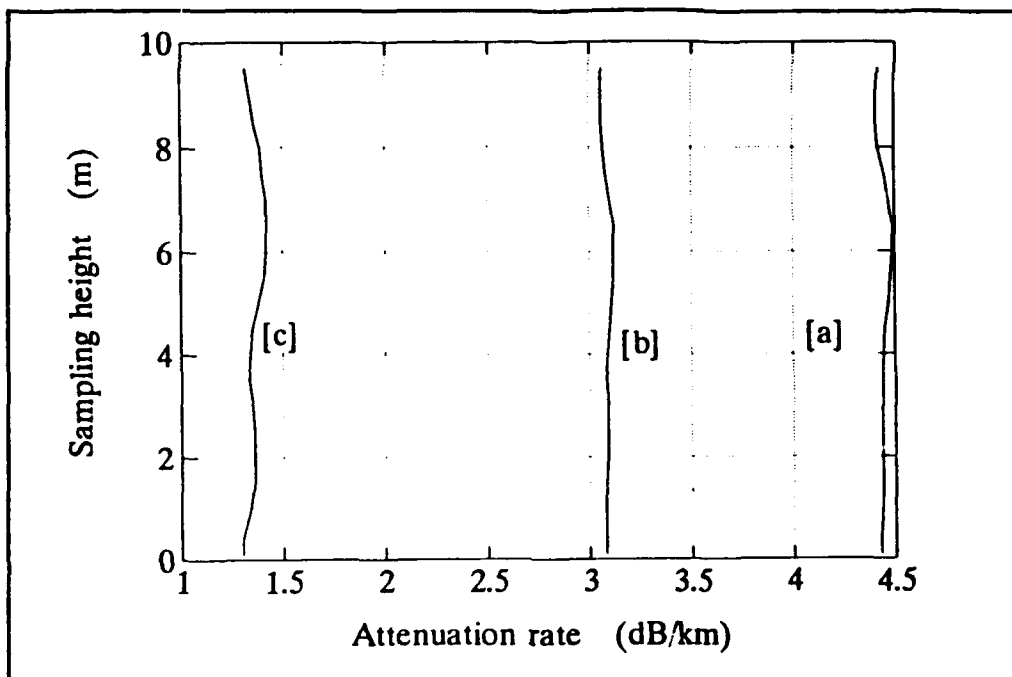


Figure 67. Modal attenuation rate for 5-L-S ( $f = 10$  GHz).

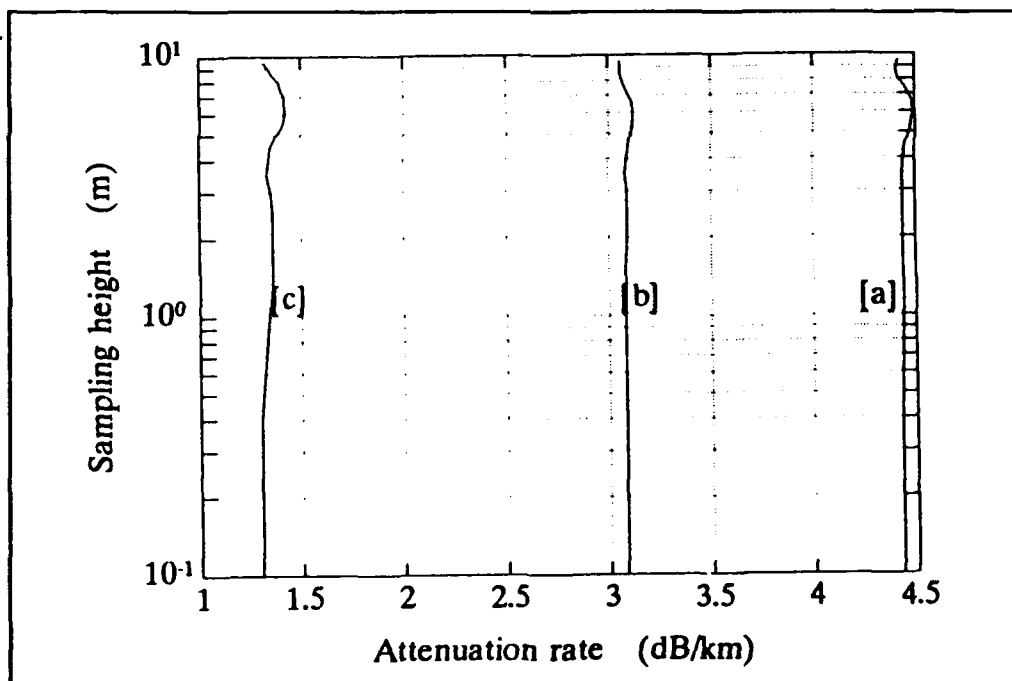


Figure 68. Modal attenuation rate for 5-L-S, sampling height in logarithmic scale ( $f = 10$  GHz).

reaches a maximum. The attenuation rate variation of the dominant mode *c* for *class two* is slightly greater than that of *class one*. Thus, for 10 GHz propagation, the field strength is more sensitive to a change of test point height in *class two* than in *class one*. This is different from 15 GHz propagation for which the field is more sensitive to test point variation in *class one*.

A comparison of the variation of the attenuation rate of the dominant modes for 10 GHz and 15 GHz propagation shows that the sensitivity of field strength to a change of test point height is higher for 15 GHz propagation.

### *c. Mode Location Analysis*

It can be seen from Fig. 69 that the imaginary part of mode *c* is the least negative of the three modes. This means that the field strength of mode *c* is the strongest. The modal attenuation rate increases from mode *c* to *b* to *a* for every sampling height (Figs. 67 and 68). The variation of mode *c* only is shown in Fig. 70.

From Fig. 70, it is seen that when the test point height is varied from 0.1 m to 3.5 m the imaginary part variation of this mode is a little smaller than when the test point height is varied from 4.5 m to 9.5 m. Thus, the sensitivity of the field strength is greater for *class two* than for *class one*. This is different from the situation at 15 GHz.

By comparing Fig. 57 with Fig. 69, it can be seen that between 15 GHz and 10 GHz the dominant mode location at the higher frequency is more sensitive to a change in test point height.

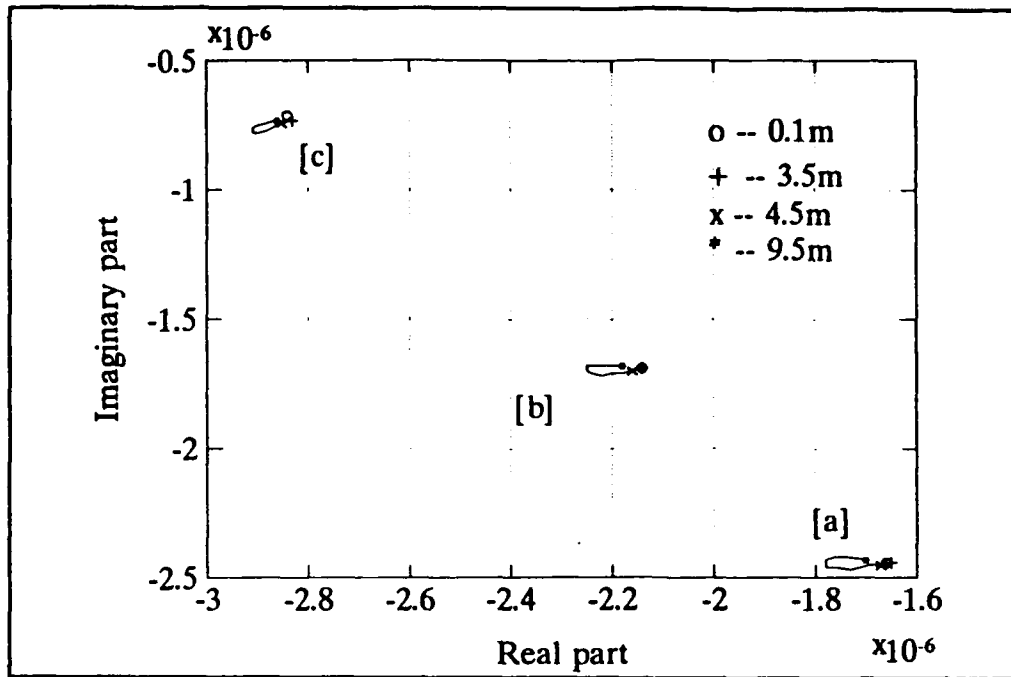


Figure 69. Mode location on the  $\beta-1$  complex plane for 5-L-S ( $f = 10$  GHz).

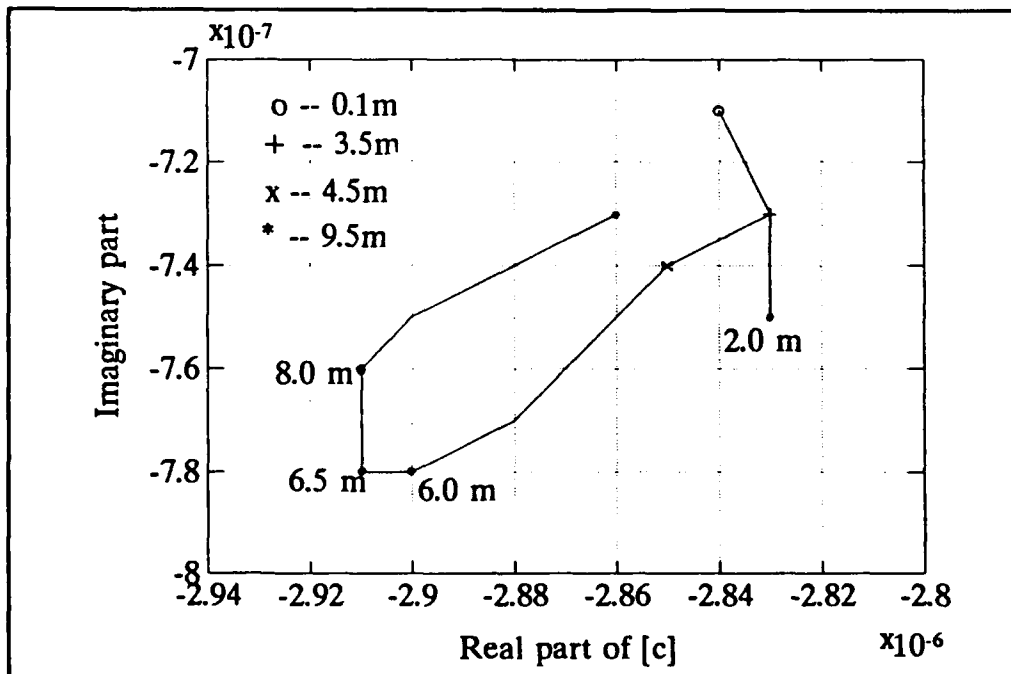


Figure 70. Dominant mode location on the  $\beta-1$  complex plane for 5-L-S ( $f = 10$  GHz).

### 3. 6 GHz

#### a. Path Loss Analysis

(1) *Class One.* In Figs. 71 and 72, the receiver range is fixed at 60 km; and in Figs. 73 and 74, the receiver range is fixed at 120 km. The path loss as a function of receiver height when the test point is located at 0.1 m and at 3.5 m is shown in Fig. 71. The path loss curves for 6 GHz propagation are similar to those of *class one* at 15 GHz. The only difference is that the two curves for 6 GHz propagation are closer to each other.

(2) *Class Two.* The path losses when the test point is selected at 4.5 and at 9.5 m are shown in Fig. 72. The path loss curves are similar to those for *class one* at 15 GHz propagation. Again, the difference is that the curves for 6 GHz propagation are closer. The path loss ratios for 6 GHz propagation are not plotted because they are too small to be presented accurately.

(3) *Discussion.* When the test point is selected at any of the four locations, the path loss for a 6 GHz signal is larger than that for a 10 GHz signal at every receiver height. This can be seen by comparing Fig. 59 with Fig. 71 and Fig. 61 with Fig. 72. Thus, the higher the propagation frequency, the greater the enhancement in field strength by the duct. This behavior is similar to those at 10 GHz and at 15 GHz discussed previously.

When the test point is moved from 0.1 m to 3.5 m, the path loss ratio for 6 GHz propagation varies from 1.61 dB at 1 m receiver height to 0.8 dB at

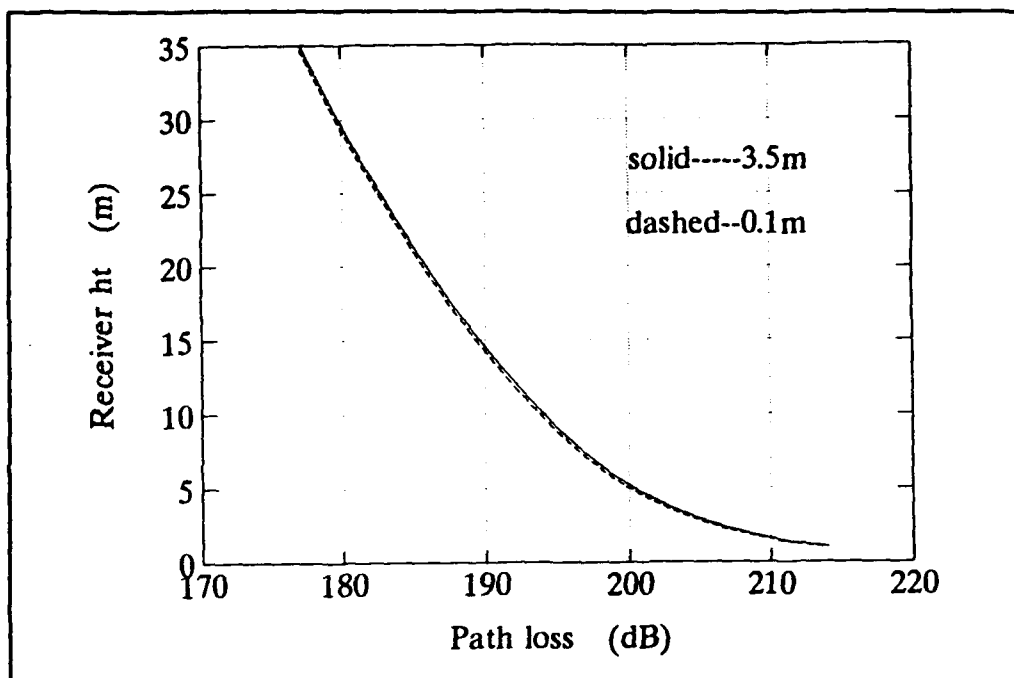


**Figure 71.** Path loss for 5-L-S, test points at 0.1 m and 3.5 m ( $f = 6$  GHz,  $r = 60$  km).

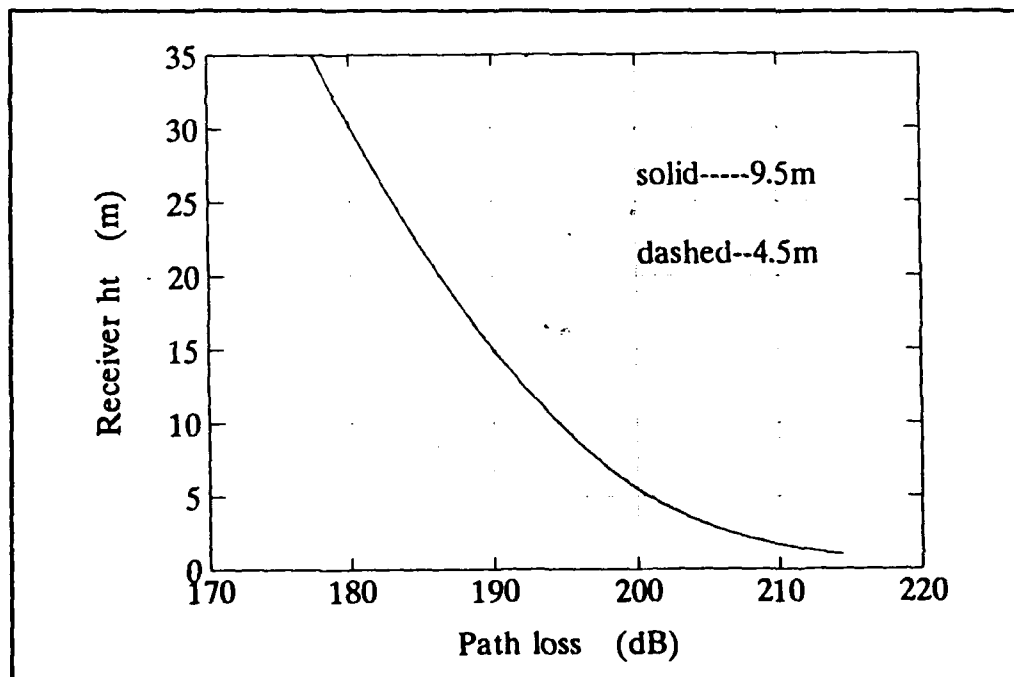


**Figure 72.** Path loss for 5-L-S, test points at 4.5 m and 9.5 m ( $f = 6$  GHz,  $r = 60$  km).

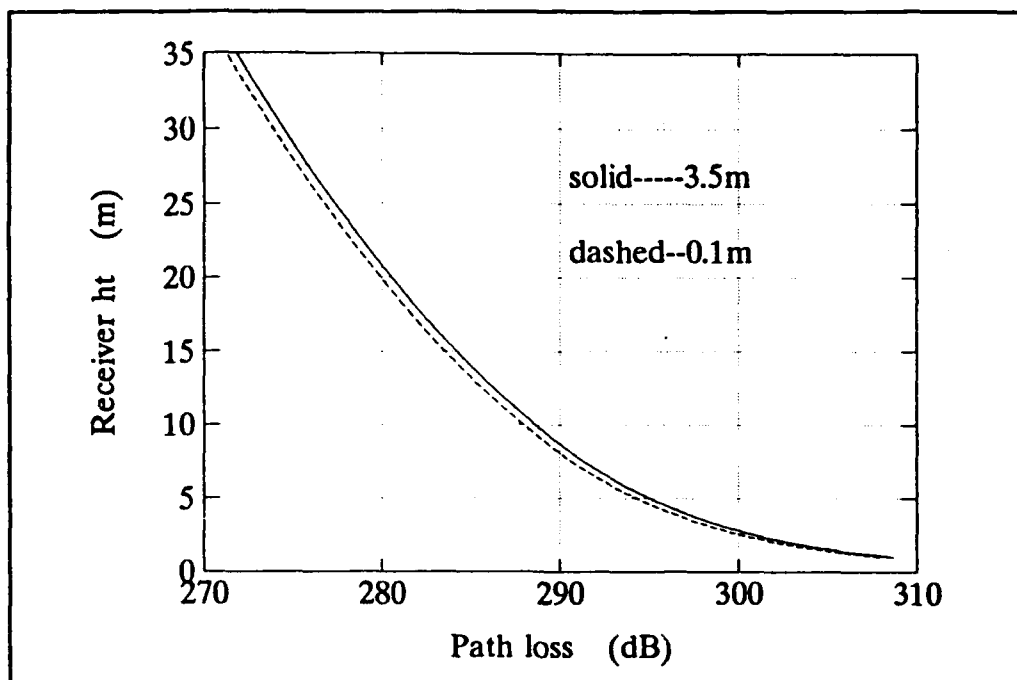


Figure 73. Path loss for 5-L-S, test points at 0.1 m and 3.5 m ( $f = 6$  GHz,  $r = 120$  km).

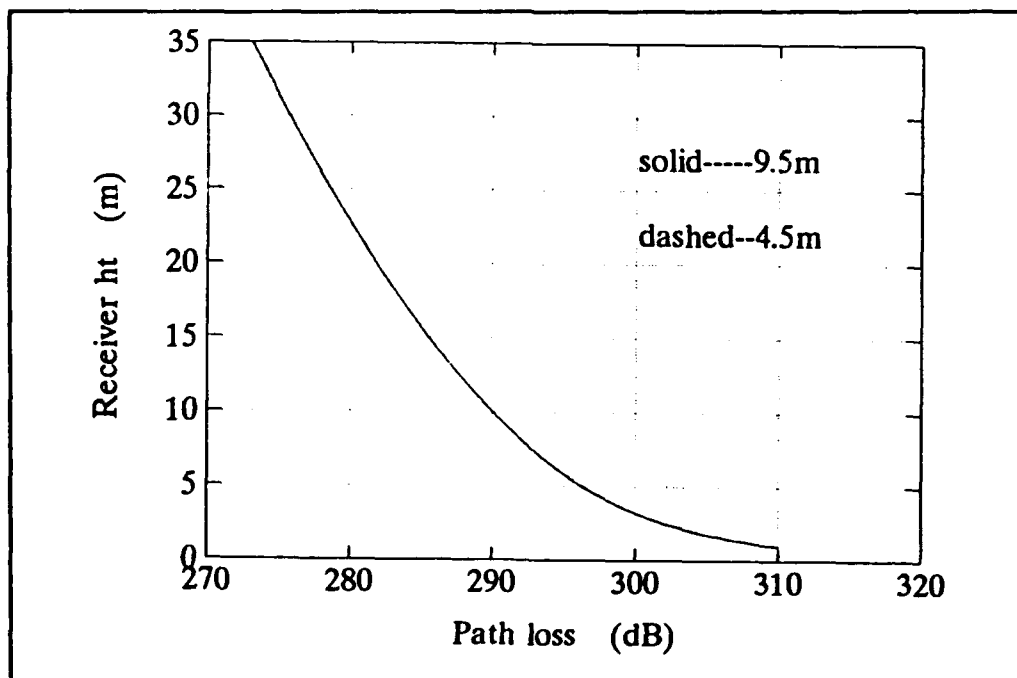


Figure 74. Path loss for 5-L-S, test points at 4.5 m and 9.5 m ( $f = 6$  GHz,  $r = 120$  km).



35 m. For 6 GHz propagation, this ratio varies less than 0.45 dB over the same range of receiver height. Therefore, the path loss ratio for 10 GHz propagation is greater than that for 6 GHz propagation. When the test point is moved from 4.5 m to 9.5 m, a similar result is obtained (Figs. 61 and 72). Consequently, when the test point is moved from 0.1 m to 3.5 m and from 4.5 m to 9.5 m, the sensitivity of the height-gain function for propagation at 6 GHz is smaller than that at 10 GHz.

***b. Attenuation Rate Analysis***

Four modes are found with attenuation rates lower than 5 dB/km (Figs. 75 and 76). The dominant mode is mode d. It has the smallest attenuation rate which is at least 1.2 dB/km smaller than any of the other modes at every sampling height. The attenuation rate of each mode deviates less than 0.1 dB/km between the two sampling classes. From the variation of the attenuation rate of mode b, it is observed that the field strength to a change of the test point is greater for *class two*. This behavior is different from that at 15 GHz.

A comparison of the variation of the attenuation rate of the dominant modes for 6 GHz and 10 GHz propagation shows that the sensitivity of field strength to a change of test point height is greater at the higher frequency.

***c. Mode Location Analysis***

As can be seen in Fig. 77, the imaginary part of mode d is the least negative of the four modes. This means that the field strength of mode d is the strongest. In increasing order the modal attenuation rate is mode d, c, b and then

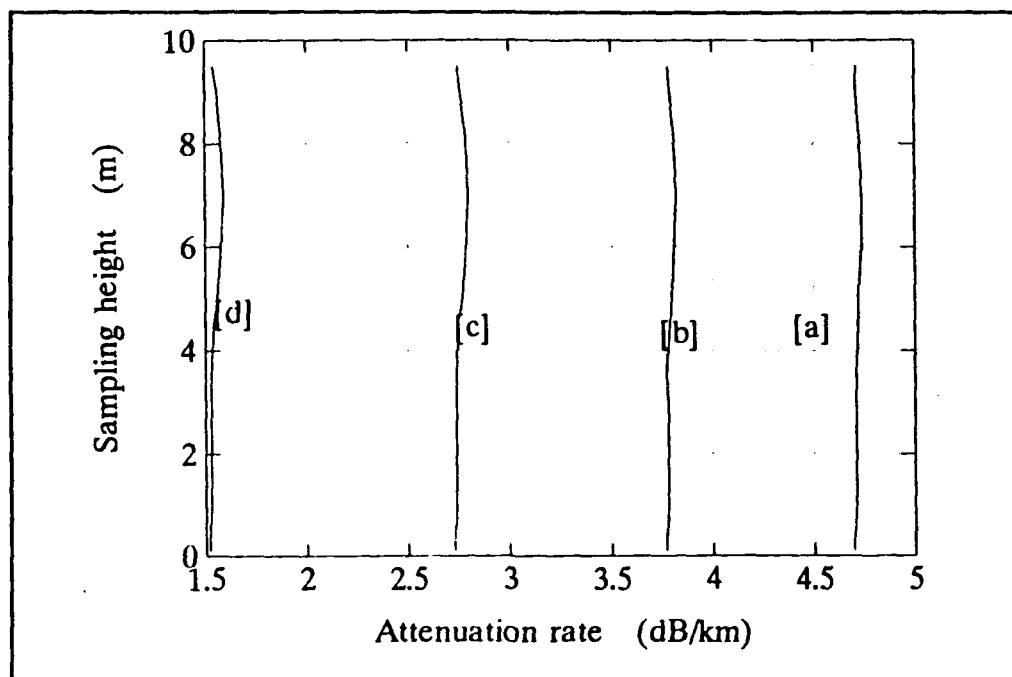


Figure 75. Modal attenuation rate for 5-L-S ( $f = 6$  GHz).

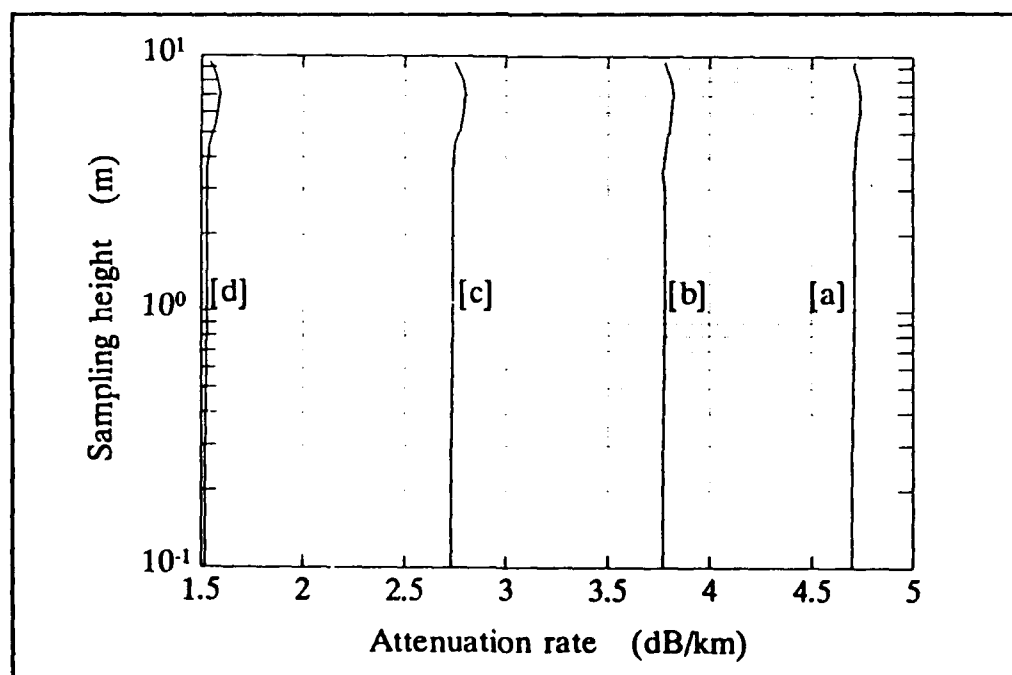


Figure 76. Modal attenuation rate for 5-L-S, sampling height in logarithmic scale ( $f = 6$  GHz).

a for every sampling height (Figs. 75 and 76). The variation of mode d alone is shown in Fig. 78.

By comparing Fig. 69 with Fig. 77, it can be seen that for 10 GHz propagation the variation of each mode location is greater than that at 6 GHz. Thus, the higher the propagation frequency, the higher the sensitivity of the mode location to a change of test point height.

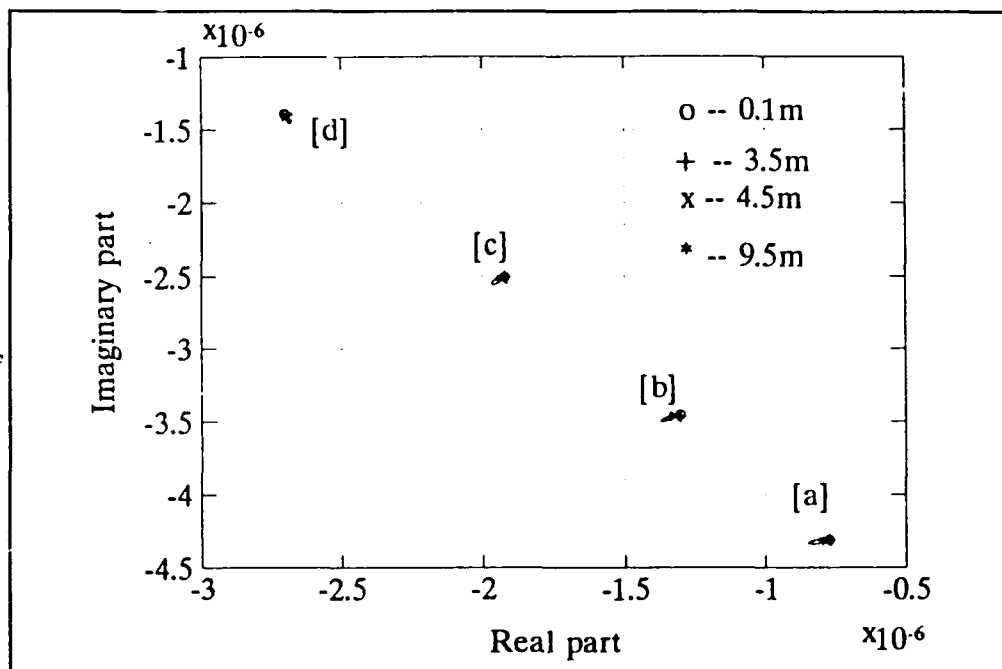


Figure 77. Mode location on the  $\beta-1$  complex plane for 5-L-S ( $f = 6$  GHz).

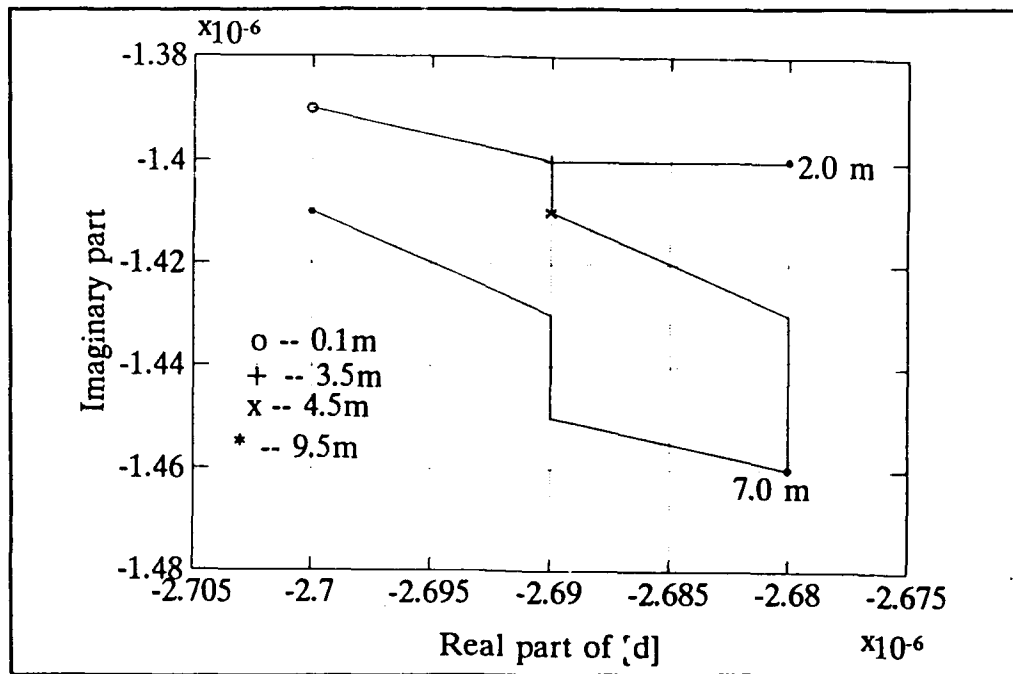


Figure 78. Dominant mode location on the  $\beta$ -1 complex plane for 5-L-S ( $f = 6$  GHz).

#### 4. 3 GHz

##### a. Path Loss Analysis

(1) *Class One.* In Figs. 79 and 80, the receiver range is fixed at 60 km; and in Figs. 81 and 82, the receiver range is fixed at 120 km. The path loss as a function of receiver height when the test point is located at 0.1 m and at 3.5 m is shown in Fig. 79. The path loss curves for 3 GHz propagation are similar to those for *class one* at 15 GHz. The two curves for 3 GHz propagation are extremely close to each other.

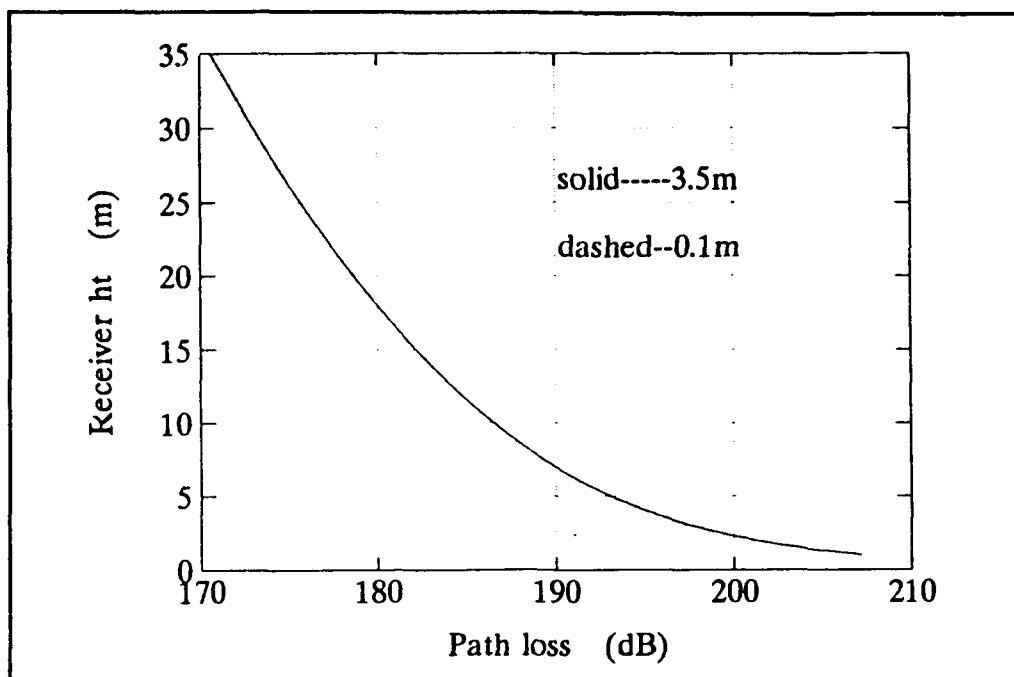


Figure 79. Path loss for 5-L-S, test points at 0.1 m and 3.5 m ( $f = 3$  GHz,  $r = 60$  km).

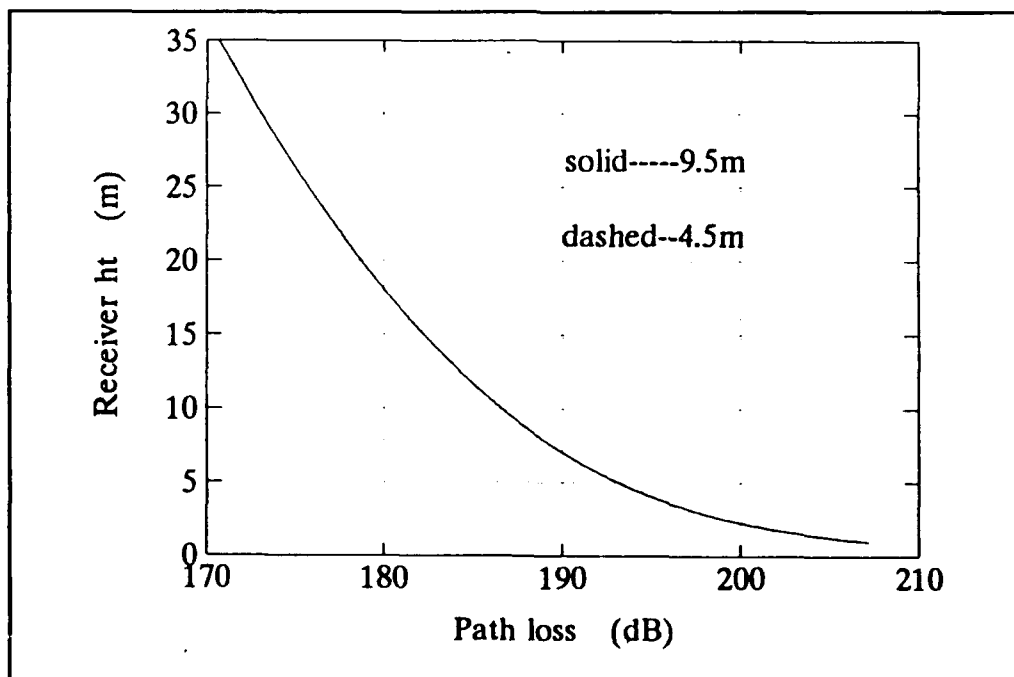


Figure 80. Path loss for 5-L-S, test points at 4.5 m and 9.5 m ( $f = 3$  GHz,  $r = 60$  km).

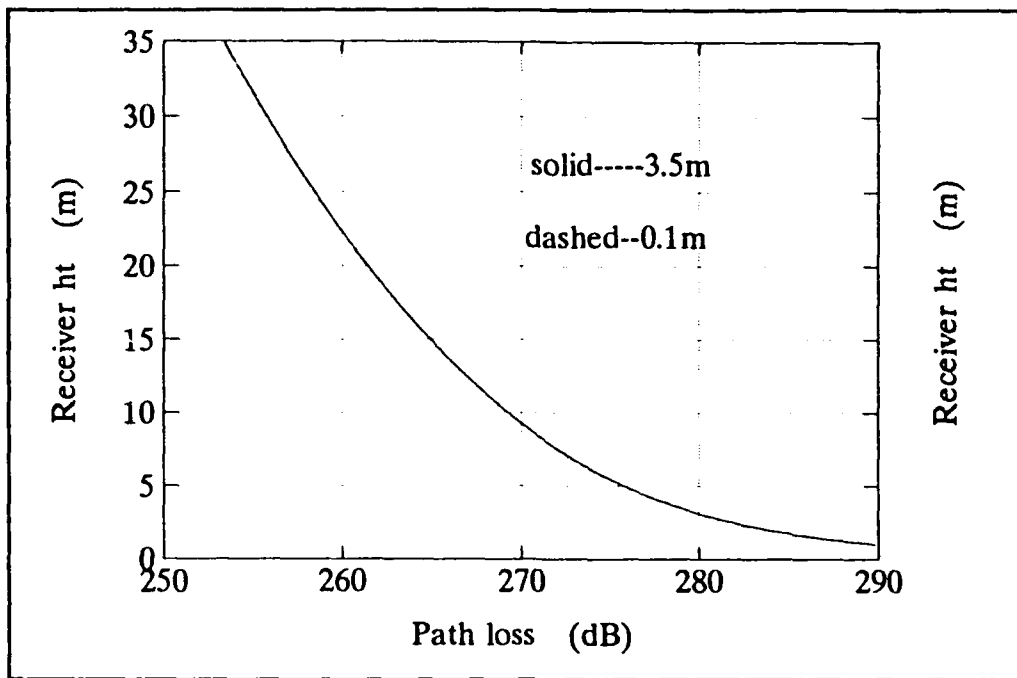


Figure 81. Path loss for 5-L-S, test points at 0.1 m and 3.5 m ( $f = 3$  GHz,  $r = 120$  km).

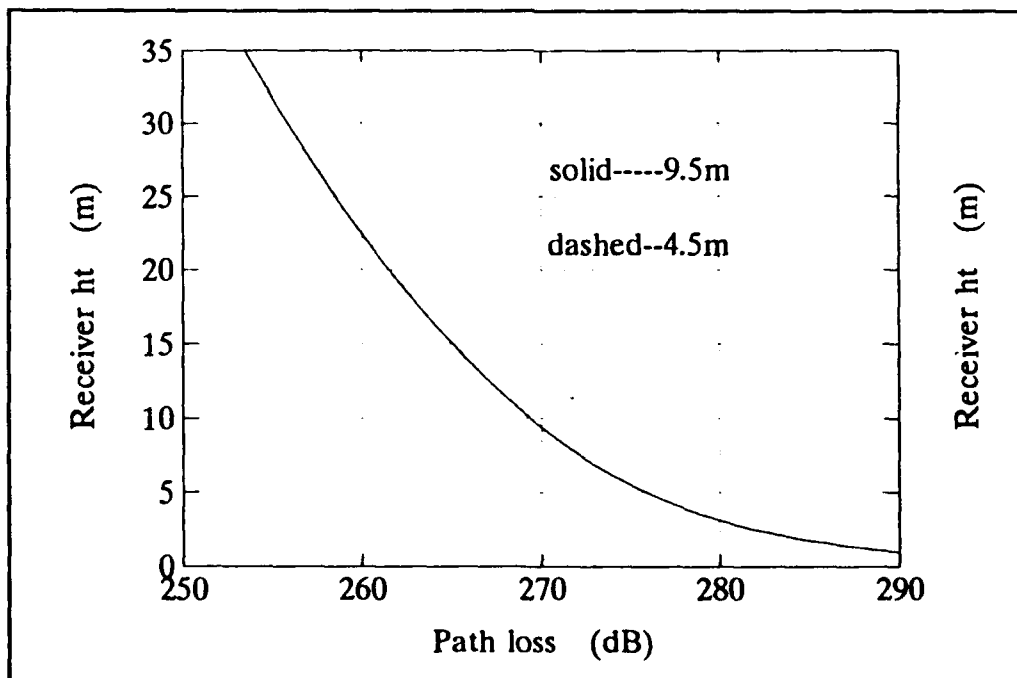


Figure 82. Path loss for 5-L-S, test points at 4.5 m and 9.5 m ( $f = 3$  GHz,  $r = 120$  km).

(2) *Class Two.* The path losses when the test point is selected at 4.5 m and at 9.5 m are shown in Fig. 80. The path loss curves have the same features as those for *class one* at 15 GHz propagation. Again, the difference is that the curves for 3 GHz propagation are fairly close to each other. The path loss ratios for 3 GHz propagation are not plotted because they are too small to be presented accurately.

(3) *Discussion.* When the test point is selected at any of the four locations, the path loss for a 6 GHz signal is larger than that for a 3 GHz signal at every receiver height. This can be seen by comparing Fig. 71 with Fig. 79 and Fig. 72 with Fig. 80. Thus, between 3 GHz and 6 GHz the lower the propagation frequency, the greater the enhancement in field strength by the duct. This is different from the case when the frequency is increased from 6 to 10 to 15 GHz. This behavior is explored further in Chapter III.

#### *b. Attenuation Rate Analysis*

Three modes are found with attenuation rates lower than 5 dB/km (Figs. 83 and 84). The dominant mode is mode c. It has an attenuation rate smaller than those of the other two modes by at least 1 dB/km at every sampling height. The attenuation rate of each mode varies less than 0.04 dB/km in both sampling classes. For 3 GHz propagation, the sensitivity of the field strength to a change of the test point height is negligible.

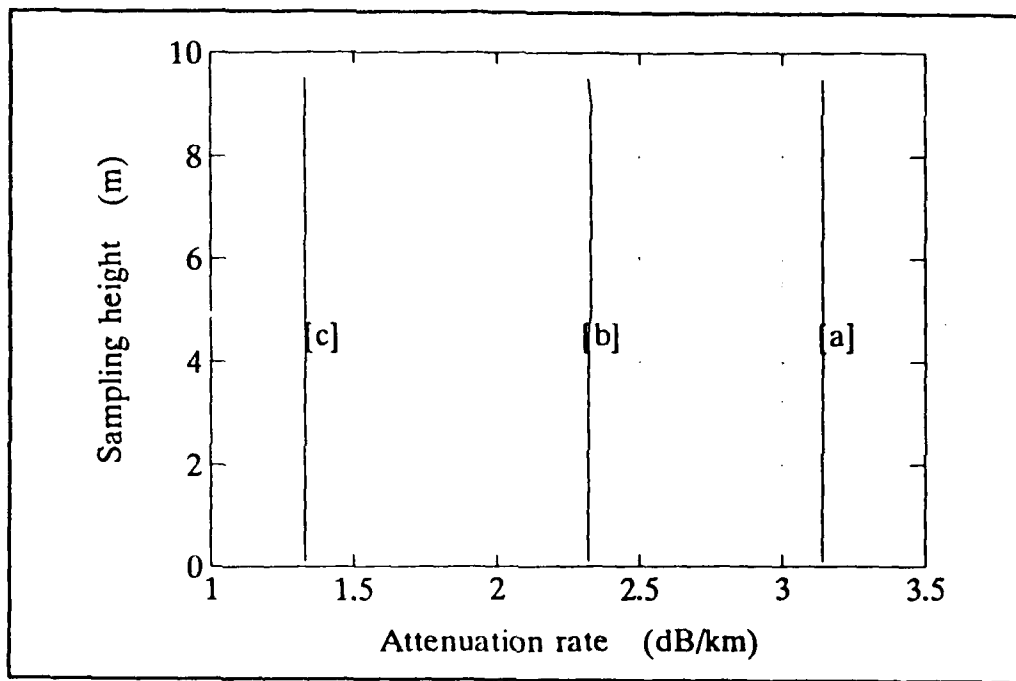


Figure 83. Modal attenuation rate for 5-L-S ( $f = 3$  GHz).

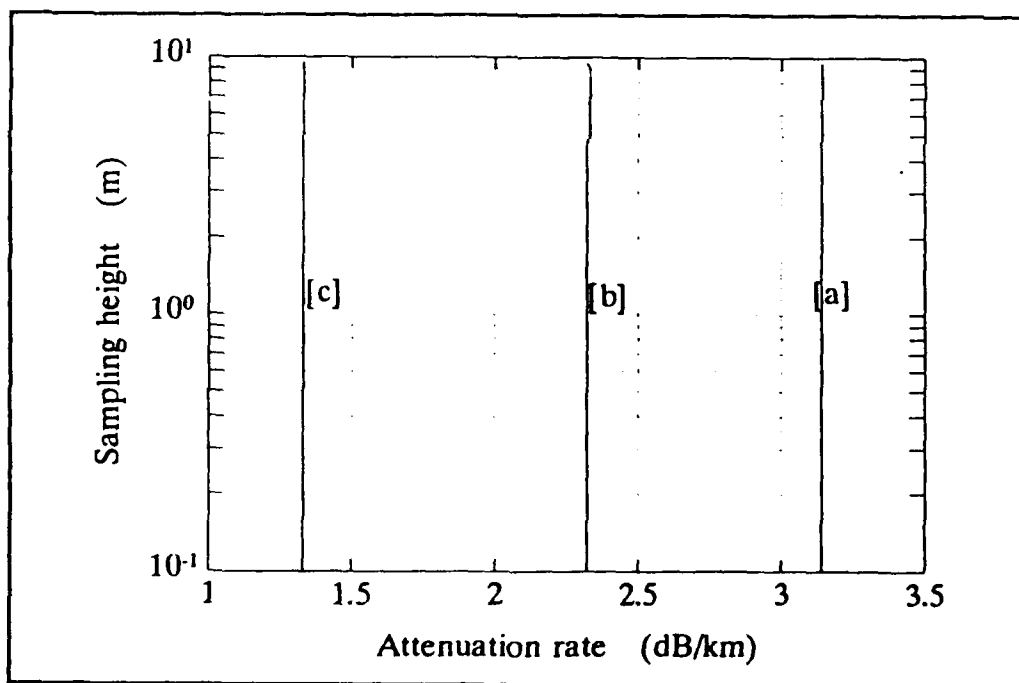


Figure 84. Modal attenuation rate for 5-L-S, sampling height in logarithmic scale ( $f = 3$  GHz).



A comparison of the variation of the attenuation rate of the dominant modes for 3 GHz and 6 GHz propagation shows that the sensitivity of field strength to a change of test point height is greater at the higher frequency.

*c. Mode Location Analysis*

It can be seen from Fig. 85 that the imaginary part of mode c is the least negative of the three modes. This means that the field strength of mode c is the strongest. The modal attenuation rate increases from mode c to b to a for every sampling height (see Figs. 83 and 84). The variation of mode c only is shown in Fig. 86.

By comparing Fig. 77 with Fig. 85, it can be seen that the variation of each mode location for 6 GHz propagation is greater than that at 3 GHz. Thus, the higher the propagation frequency, the higher the sensitivity of the mode location to a change of test point height. This behavior is similar to the comparison of 6 with 10 GHz and 10 with 15 GHz propagation.

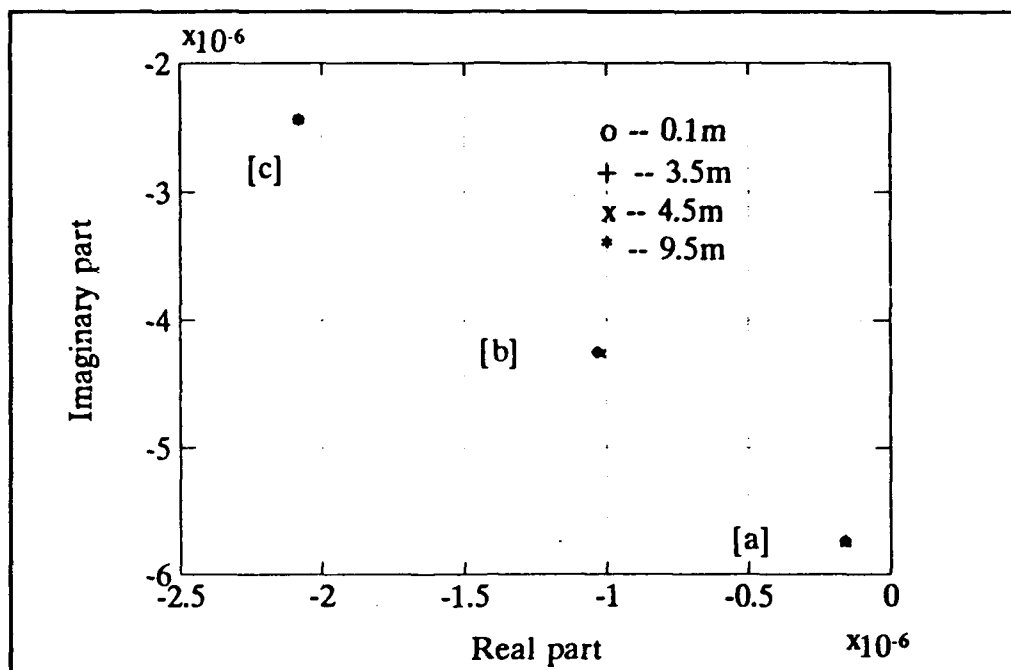


Figure 85. Mode location on the  $\beta-1$  complex plane for 5-L-S ( $f = 3$  GHz).

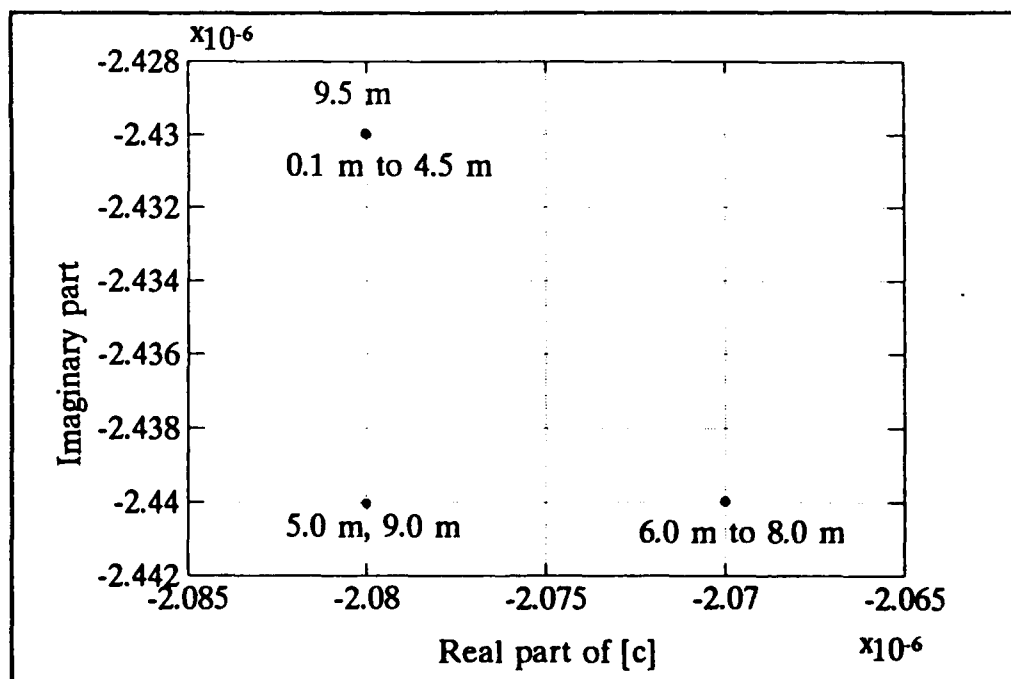


Figure 86. Dominant mode location on the  $\beta-1$  complex plane for 5-L-S ( $f = 3$  GHz).

### III. DISCUSSIONS AND SUGGESTIONS

The dependence of MLAYER predictions on the set of heights at which the refractive index values are sampled has been investigated carefully in Chapter II. Some interesting features which are broader in scope and deserve further considerations are discussed below.

#### A. FREQUENCY DEPENDENCE

It has been observed in Chapter II that the sensitivity of the attenuation rate to variations in test point height has a tendency to be weaker near 6 GHz. To investigate further, the four-linear-segment approximation to the reference profile with test point chosen at 0.5 m is utilized. In Fig. 87, the solid line represents the approximate *M*-profile used by MLAYER and the dashed line is the reference *M*-profile. The attenuation rate of each mode found by MLAYER having an attenuation rate below 5 dB/km over the 1 GHz to 25 GHz frequency range at 0.25 GHz increments is shown in Fig. 88. Four modes are found in two intervals: from 1 GHz to 7.25 GHz and from 10.5 GHz to 25 GHz. Between 7.25 GHz and 10.5 GHz, three modes are found. The maximum attenuation rate of the dominant mode is 1.52 dB/km at 5.75 GHz. It appears that this higher attenuation rate near 5.75 GHz helps reduce the sensitivity of the field strength to the variation of test point height.

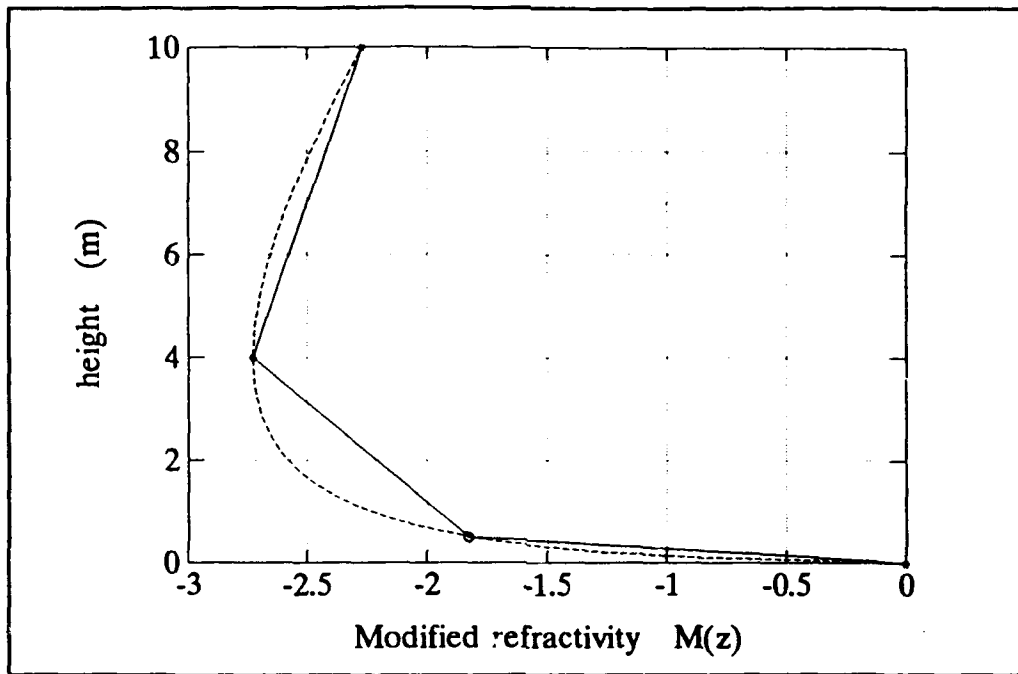


Figure 87. Approximate four-linear-segment profile, test point at 0.5 m.

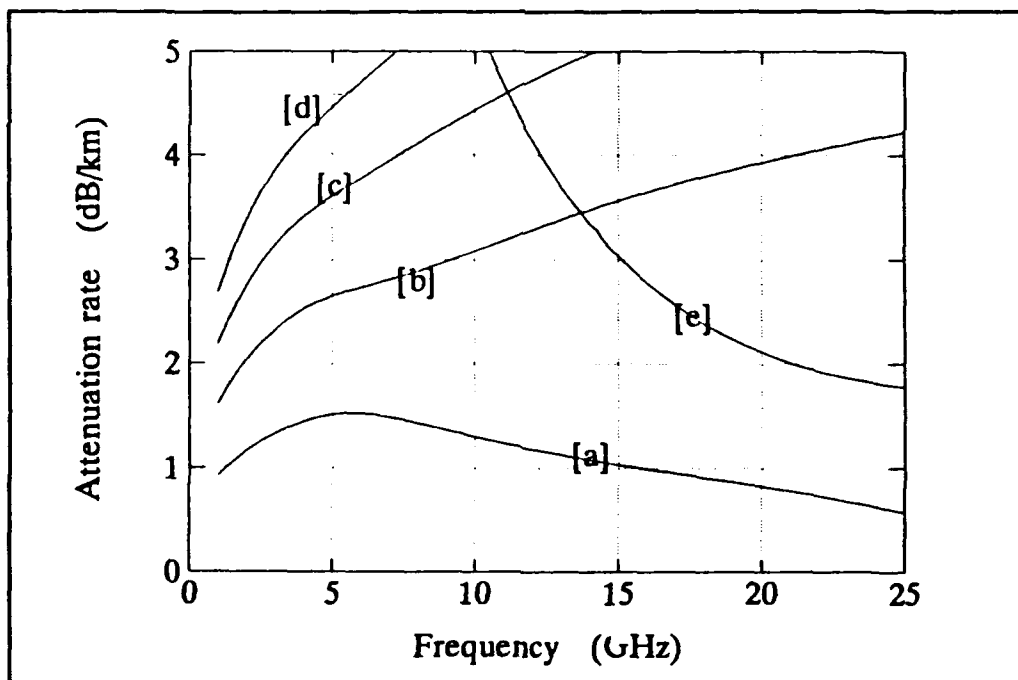


Figure 88. Modal attenuation rate for 4-L-S, test point at 0.5 m.

## B. REFRACTIVITY DEPENDENCE

Using a four-linear-segment approximate  $M$ -profile in general results in a lower attenuation rate than when a five-linear-segment approximation is used. The situation for the 15 GHz case is shown in Fig. 89. One explanation which applies in general to the direction of change in attenuation rate with a change in  $M$ -profile follows.

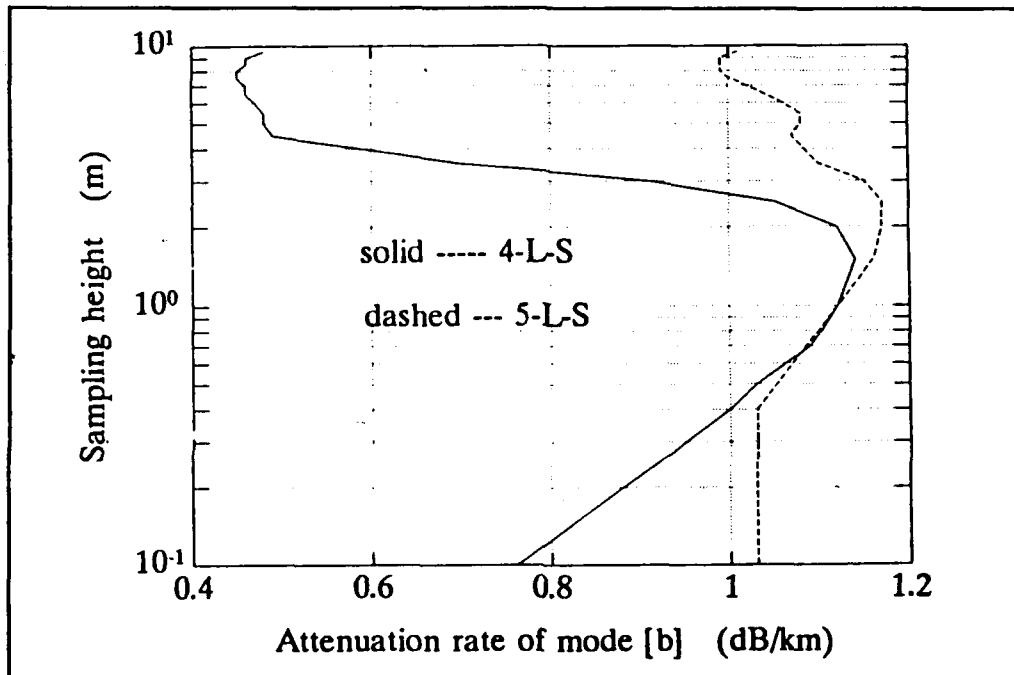


Figure 89. Modal attenuation rate for 4-L-S and 5-L-S, sampling height in logarithmic scale ( $f = 15$  GHz).

For microwave propagation, the variation in refractive index profile of the troposphere is very slight over a distance of many wavelengths. A wave can be considered as a plane wave locally, bent slowly as it moves within a layer and reflected and refracted at the boundary surfaces. Hence, its phase constant  $q$  and

attenuation rate  $s$  along the vertical direction in the  $i$ -th layer are slowly varying and are given approximately at the height  $z$  by:

$$q + j s = k [ m_i^2(z) - \beta^2 ]^{\frac{1}{2}}, \quad (15)$$

where  $k$  is the free space wave number and  $k\beta$  is the guide wavenumber of the earth-tropospheric waveguide. From Eq. (4) and the fact that the deviation of  $\beta$  from 1 is small:

$$\begin{aligned} q + j s &= k \sqrt{2} [ 10^{-6} M(z_i) - (\beta - 1) ]^{\frac{1}{2}}, \\ &= (b + j d)^{\frac{1}{2}}, \end{aligned} \quad (16)$$

where

$$q = 2 ( b + \sqrt{b^2 + d^2} )^{\frac{1}{2}}. \quad (17)$$

From Eq.(16), a reduction in  $M$  results in a reduction in  $b$ . If only  $b$  is reduced,  $q$  will be reduced according to Eq.(17). The phase of the wave on the  $i$ -th layer boundary will change and the boundary condition cannot be met. Hence, the change in  $b$  has to be accompanied with an increase in  $d$ , which is the negative of the imaginary part of  $\beta$ . This is the effect demonstrated in Fig. 89 in which the addition of an extra fixed point at 0.5 m on the reference profile almost always increases the attenuation rate. The exception occurs only when the height of the test point of the 4-L-S case is near 0.5 m. This should apply as a general rule of thumb for predicting change in range attenuation rate when the  $M$ -profile is changed slightly.

### **C. ROOT-FINDING**

Given a sufficiently long execution time, MLAYER appears capable of locating any specified number of modes of propagation. However, the smaller the imaginary part of a zero found by the Shellman-Morfitt root-finding routine, the smaller the range attenuation rate of the corresponding mode. The current root-finding algorithm often selects a zero of the smallest real part first. It is desirable to revise the algorithm to look for the mode which has the next smallest range attenuation rate. This will insure that whenever the root-finding routine stops that all the modes found are more important than those yet to be located.

## LIST OF REFERENCES

1. L.W. Yeoh, *An Analysis of M-layer*, Technical Report, NPS-62-90-009, June 1990.
2. C.L. Pekeris, "Accuracy of the earth-flattening approximation in the theory of microwave propagation", *Physical Review*, Vol. 70, No. 7 and 8, October 1946.
3. G.B. Baumgartner Jr, "XWVG : A waveguide program for trilinear tropospheric ducts", Technical Document 610, Naval Ocean Systems Center, San Diego, CA. 92152, June 1983.
4. R. Pappert, "Field strength and path loss in a multilayer tropospheric waveguide environment", Technical Note 1366, Naval Ocean Systems Center, San Diego, CA. 92152 June 1984.
5. D.E. Kerr, *Propagation of Short Radio Waves*, Peter Peregrinus Ltd, London, United Kingdom, 1987.
6. H.V. Hitney and R.A. Paulus, "Integrated refractive effects prediction system (IREPS), interim user's manual", Technical Document 238, Naval Ocean Systems Center, San Diego, CA. 92152, March 1979.
7. H.V. Hitney, A.E. Barrios, and G.E. Lindem, "Engineer's refractive effects prediction system (EREPS), revision 1.00 user's manual", Technical Document 1342, Naval Ocean Systems Center, San Diego, CA. 92152, July 1988.
8. M. Abramowitz and I.A. Stegun, *Handbook of Mathematical Functions*, Dover Publications, Inc., New York, NY, 10014, December 1972.
9. L.V. Blake, *Radar Range-Performance Analysis*, Artech House Inc., Norwood, MA. 02062, 1986.
10. Z. Schulten and D.G.M. Anderson, "An algorithm for the evaluation of the complex Airy functions", *Journal of Computational Physics*, Vol. 31, No. 60-75, 1979.
11. S. Marcus and W.D. Stuart, "A model to calculate EM fields in tropospheric duct environments at frequencies through SHF", Electromagnetic Compatibility Analysis Center Report ESD-TR-81-102, Annapolis, MD, 21402, September 1981.



12. A.V. Kukushkin and V.G. Sinitsin, "Rays and modes in a nonuniform troposphere", *Radio Science*, Vol. 18, No. 4, pp. 537-581, July 1983.
13. R.A. Pappert and C.L. Goodhart, "Case studies of beyond-the-horizon propagation in tropospheric ducting environments", *Radio Science*, Vol. 12, No. 1, pp. 75-87, January-February 1977.
14. J. Griffiths, *Radio Wave Propagation and Antennas*, Prentice-Hall International Ltd., Englewood Cliffs, NJ. 07632, 1987.
15. R.V. Churchill and J.W. Brown, *Complex Variables and Applications*, 5th ed., McGraw Hill, Inc., New York, NY. 10020, 1990.
16. R.A. Pappert and C.L. Goodhart, "Waveguide calculations of signal levels in tropospheric ducting environments", Technical Note 3129, Naval Electronics Laboratory Center, San Diego, CA. 92152, February 1976.
17. G.B. Baumgartner Jr., H.V. Hitney, and R.A. Pappert, "Duct propagation modelling for the integrated-refractive-effects prediction system (IREPS)", *IEEE Proceedings*, Vol. 130, Part F, No. 7, December 1983.